UiT The Arctic University of Norway

Faculty of Science and Technology, Department of Geosciences

Dynamically controlled hydrocarbon column heights in fault bounded traps of the Hammerfest Basin, SW Barents Sea

Fault valve theory applied to the Snøhvit field

Akos Kiss

Master thesis in Geology GEO-3900 November 2019

Abstract

During initial exploration efforts in the Barents Sea several gas prone and underfilled prospects were drilled which significantly dropped the interest in the area. The Hammerfest Basin however turned out to hold significant hydrocarbon volumes. Although still mostly underfilled, the discoveries here today make up the Snøhvit oil and gas field. The Hammerfest Basin is an overfilled petroleum basin, meaning that the several source intervals have produced enough hydrocarbons over time to fill all the traps. This, and the hydrocarbon shows below the hydrocarbon-water contacts inside the traps indicate that the reason behind underfilled structures is leakage. This means that the main exploration risk in the area is trap integrity.

Given the large amount of evidence for fault-assisted remigration, this thesis focuses on explaining the hydrocarbon column heights observed today in these structures with the help of fault valve theory. The theory suggests that a subset of faults oriented at the right angles to the stress field can control the pore pressures in a pressure compartment in a dynamic equilibrium. When pressure increases with hydrocarbon charge, or gas dissolution the effective stress drops which can reactivate the faults leading to the leakage of hydrocarbons from the trap.

In this study, the slip tendencies of faults around the Albatross, Snøhvit and Askeladd structures were calculated and plotted on the interpreted fault planes. This gave the critical pressure perturbations of the faults, i.e. the pressure increase needed to cause slip on them. Faults and fault segments with low critical pressure perturbations are regarded as areas of high risk of leakage. After identifying high risk segments, their intersection with the top reservoir was found and compared with the level of hydrocarbon-water contacts.

On Albatross Sør and Snøhvit Nord high risk faults and fault intersections intersect the top reservoir on the level of the gas-water contact. On Albatross and Snøhvit, both of which have leaked considerably, high risk faults were identified near the culmination of the trap. Askeladd, Askeladd Vest and Askeladd Gamma which are not as severely underfilled, the fault planes show higher critical pressure perturbations. Delta Vest, an empty structure also has higher pressure perturbations, however it has a fault intersection right at the culmination. Askeladd Beta, the second dry structure showed higher risk on a fault directly at the top of the structure.

Foreword

First, I would like to thank my supervisors at the Department of Geology at UiT Iver Martens and Amando Putra Ersaid Lasabuda for giving me the freedom to choose my research, while doing everything to support me with outside contacts, supportive criticisms and finding research material. A special thanks goes out to my external supervisors at Equinor in Harstad: Jan-Robert Eide, Gard Ole Wærum and Bjarne Rafaelsen. They never hesitated to take time out of their very busy schedule to help me. I really appreciate their help in the data application process and in connecting me with the right people to solve a very specific (as it turned out) research problem. I am also very grateful to Paul Brockbank from Equinor in Stavanger who travelled to Tromsø for a day to teach me how to use the software for this thesis. I would also like to thank Equinor for supplying seismic and well data for this study. Badley Geoscience supplied TrapTester software for modeling slip stabilities. I would like to mention Dave Quinn from Badley here, who was always extremely helpful when problems with TrapTester arised.

This thesis would have never been made without them. Thank you all!

Akos Kiss

Tromsø, 15th November 2019

Table of Contents

1. Introduction 7
1.1. Overview and objective 7
2. Geological background 11
2.1.1. Regional setting 11
2.1.2. Tectonic evolution 12
2.2. Hammerfest Basin 13
2.2.1. Hammerfest Basin's structural framework 13
2.2.2. Stratigraphic evolution of Hammerfest Basin 16
2.3. Petroleum geology of Hammerfest Basin 17
3. Theoretical background 18
3.1. The hydrocarbon trap 18
3.1.1. Nomenclature of a trap 18
3.1.2. Hydrocarbon filling 19
3.2. The fault valve theory 21
3.2.1. Static and dynamic permeability 21
3.2.2. The stress field 22
3.3. Failure processes 26
3.3.1. The Mohr diagram 26
3.3.2. 3D Mohr diagram 26
3.3.3. Fracture criteria 26
3.3.4. Modes of failure 28
3.4. 3D reflection seismic 31
4. Data and Methods 32
4.1. Data 32
4.1.1. Seismic 32
4.1.2. Well data 32
4.2. Methods 33
4.2.1. Seismic interpretation 33
4.2.2. Constraining the stress field 34
5. Results 41
5.1. Reservoir state of stress 41
5.1.1. Stress regime 41
5.1.2. Methods for estimating Shmin via xLOT 42
5.2. Reservoirs' state of stress and slip stabilities 45

6. Discussion 73
6.1. Failure mechanisms controlling HC columns 73
6.2. The effect of P_{pcrit} on HC column preservation 77
7. Conclusions 86
References 90

1. Introduction

1.1. Overview and objective

The Barents Sea is an intracratonic shelf area containing a mosaic of platforms, basins and structural highs (Doré (1995); (Gabrielsen et al., 1990). Surrounded by the Svalbard, Novaya Zemlya archipelagos, the Russian and Norwegian coasts, and the Atlantic margin; it is a target for hydrocarbon exploration. It is part of a circumpolar region with known petroleum basins, some of which contain giant fields (e.g. the Sthokman gas field situated in the Russian Barents Sea). This circumpolar region contains the largest unexplored prospective area in the world; and the majority of undiscovered resources are expected to occur in the offshore areas of it (Bird et al., 2008). In the Norwegian sector of the Barents Sea, however relatively small and gas prone fields dominate. The first blocks (altogether 7) in this area were awarded at the 5th licensing round in 1980; which were followed by five more in the 8th round in 1984 (Jakobsson, 2018). The first discoveries soon followed: Askeladd, Albatross and Snøvhit; all of which today belong to the Snøvhit field complex (Jakobsson, 2018). These gas-filled structures and the residual oil in traps near the Troms-Finnmark Fault Complex have proven that remigration from traps was common in the area; which caused the perceived prospectivity to drop.

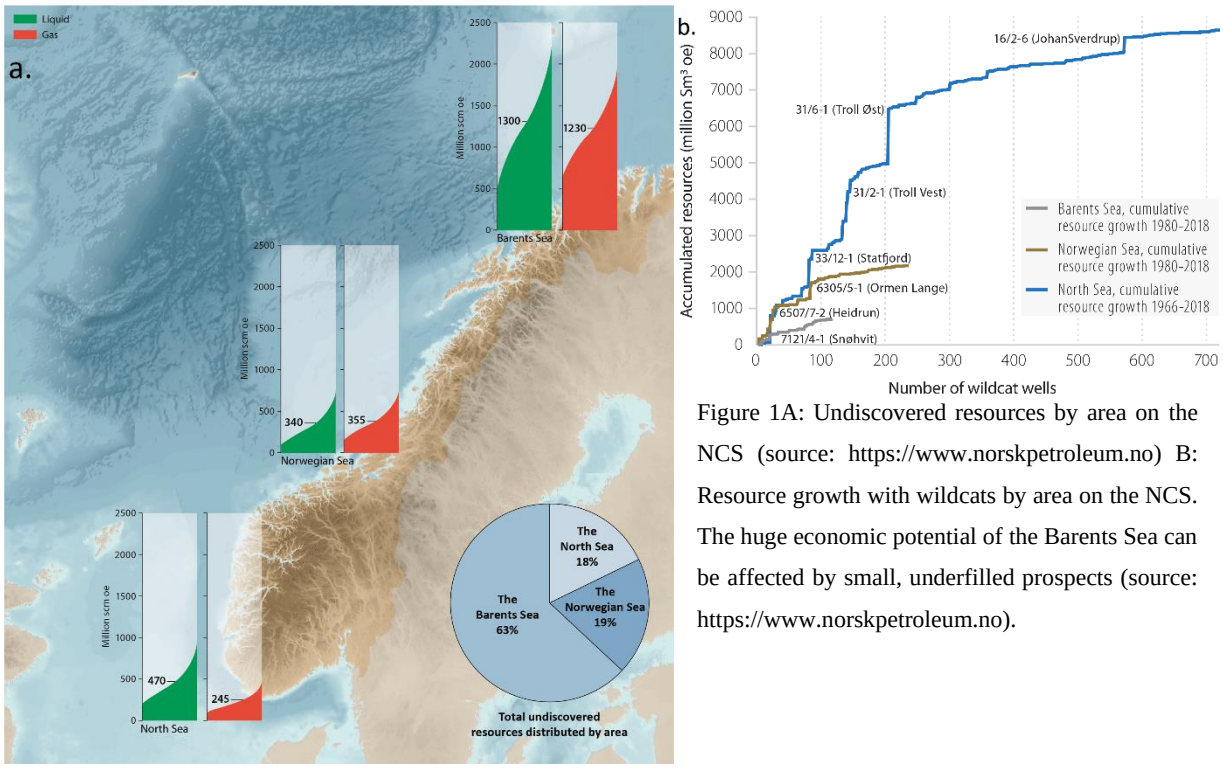

Figure 1A: Undiscovered resources by area on the NCS (source: https://www.norskpetroleum.no) B: Resource growth with wildcats by area on the NCS. The huge economic potential of the Barents Sea can be affected by small, underfilled prospects (source: https://www.norskpetroleum.no).

After the 1980's, interest in the Barents Sea remained low, with a steady amount of discoveries in different plays; but no commercially viable prospects. This negative trend was fortunately broken by the discovery of a commercial oil accumulation (Goliat) in 2000 and the more recent discoveries of Johan Castberg, and the Alta-Gohta fields (2011). However, after almost four decades since the first exploration well; the area still remains the most under-explored on the Norwegian Continental Shelf (NCS). By the end of 2018, more than 1100 wildcats had been drilled on the NCS, with 700 of those in the North Sea, about 250 in the Norwegian Sea and only about 120 in the Barents Sea (Figure 1B). However, the general increase in interest towards natural gas, and the fact that 60% of the undiscovered resources on the NCS are estimated to be found in the Barents Sea (Figure 1A); will definitely increase exploration activity in the area. Another vital part in the revitalization of the area is the new geological assessment from the Norwegian Petroleum Directorate containing large; still closed areas of the NE Barents Sea, increasing the estimate of total undiscovered resources by 40% compared to its previous assessment (NPD, 2018). Thus, it seems timely to reassess some of the available data to aid future exploration efforts.

The biggest geological reason for the relative low interest in the Barents Sea are underfilled and gas-prone structures. Several studies have focused on the possible leakage mechanisms and plumbing systems associated with these emptied traps (S. M.; Mohammedyasin et al., 2016), (Ostanin et al., 2017), (Ostanin et al., 2012), (Rodrigues Duran et al., 2013), (Tasianas et al., 2016), (Vaddakepuliyambatta et al., 2013). Two important points emphasized by all of these studies are the periods of uplift and erosion during the Cenozoic as a trigger for remigration; and the importance of fault planes as pathways for vertical fluid flow. Despite the obvious economic significance, there is little attempt at finding a relation between leakage mechanisms and the observed fluid contacts in these traps. The most extensive study that tries to explain the observed hydrocarbon column heights is done by Christian; Hermanrud et al. (2014), who looked at the underfilled fields of the western Hammerfest Basin. According to Christian; Hermanrud et al. (2014), from the 12 structures investigated in this study, only one is filled to its structural spillpoint (Alke Nord), while only one contains a thin oil leg (Snovhit). The emptying of the traps occurred via spilling and leakage.

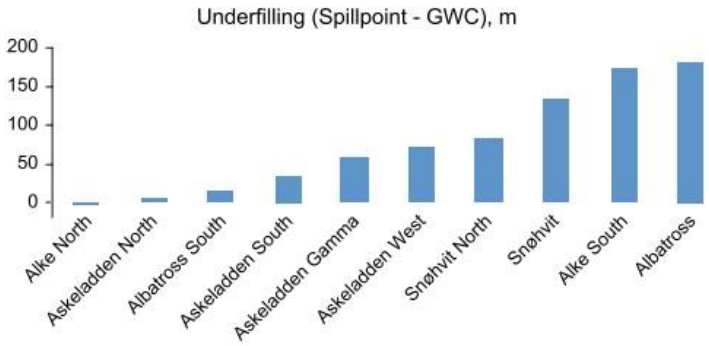

Figure 2: Vertical distance between hydrocarbon-water contacts (HWC) and spillpoints in the structures investigated by Christian; Hermanrud et al. (2014). Figure from Christian; Hermanrud et al. (2014).

Christian; Hermanrud et al. (2014) emphasized the importance of fault intersections as main conduits of fluid flow. They also explained the position of the fluid contacts with fault intersections, assuming a clear causation where these intersections and fluid contacts coincide (figure 3). The fault valve theory (introduced in chapter 3) however, adds nuance to the issue of fault permeability by showing a complex interplay between the stress field, fault orientations and reservoir pore pressure. Even less studies have investigated fault permeability in the Hammerfest Basin from this dynamic perspective, despite several studies emphasizing the role of pore pressure in leakage processes (Finkbeiner et al., 2001; Christian Hermanrud et al., 2005; Hillis & Nelson, 2005a; Mildren et al., 2005; Nordgard Bolas & Hermanrud, 2003; Sibson, 2000; Wiprut & Zoback, 2002).

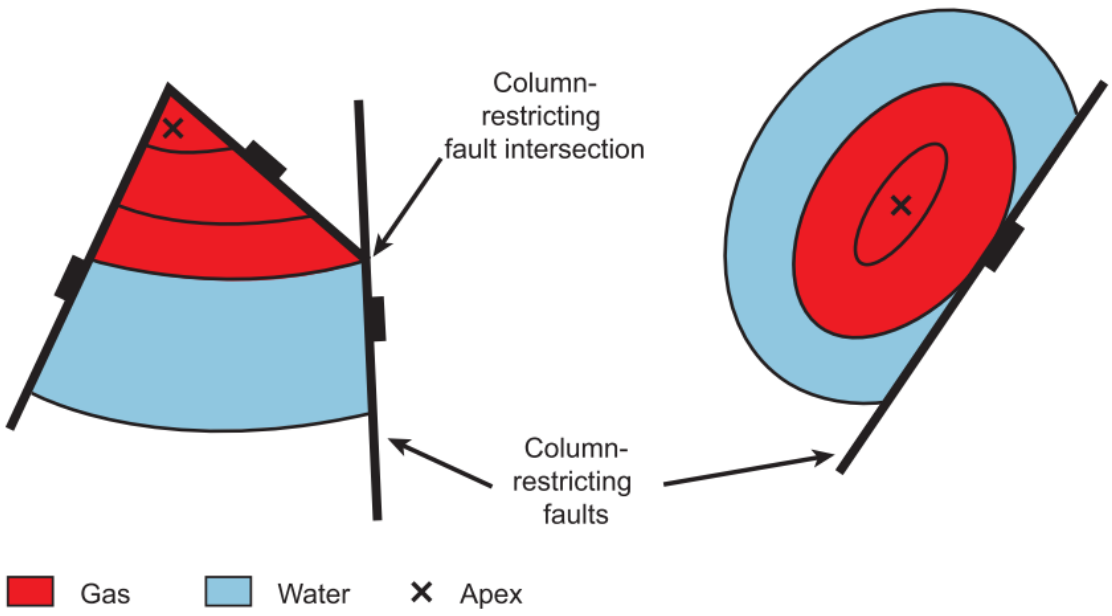

Figure 2. Leaky faults' spatial relation to hydrocarbon-water contact according to (Christian; Hermanrud et al., 2014). Figure from (Christian; Hermanrud et al., 2014)

In the Hammerfest Basin and the Barents Sea in general, the process that could have contributed to an increase in pore fluid pressures is the Cenozoic uplift causing the expansion of the gas caps, and the push out of oil legs (Henriksen et al., 2011). There is ample evidence, that subsequent leakage was fault-assisted, but some authors also propose the tensile failure of the cap rock as a possible dynamic controlling mechanism (Tasianas et al., 2016). Nordgard Bolas et al. (2005) and Christian Hermanrud et al. (2005) suggest however, that crustal flexuring caused by, for instance, the advancement and retreat of glaciers can perturb the stress field; resulting in a more anisotropic stress field, ultimately promoting shearing along fault planes instead of tensile failure. Where stresses remained more isotropic, chances are bigger for seal hydrofracturing. Hoshino (1972) warns for the development of the embrittlement zone, that makes cap rocks more vulnerable to hydrofracturing in uplifted basins. Deciding on which fracturing mode controls the hydrocarbon column heights can be ambiguous. Finkbeiner et al. (2001) attempted to determine the type of dynamic control in different pressure compartments by calculating the dynamic capacity of traps in the Gulf of Mexico.

There is considerable advantage in having knowledge about fault conductivity during the risking of prospects. This is especially true to the Hammerfest Basin, which is an overfilled petroleum basin (Ohm et al., 2008). This means that several source rock intervals exist in the stratigraphic column, that have expelled enough hydrocarbons during the basin's hiStøry to fill the investigated traps. The underfilled traps we see today are exclusively the result of spill and leakage. Hence, the most important risk factor during exploration is seal integrity. This is the characteristic of basins that underwent considerable uplift causing pressure redistribution, changes in seal rheology and stress perturbations. Having fault bounded

traps only adds to the risk, since the critical pressures for these traps are generally lower than those of non-faulted traps (Wiprut & Zoback, 2002). Faults can place dynamic controls on the amount of pressure that can be Støred in a compartment. This can be an aid in estimating hydrocarbon column heights and in place volumes (Figure 4).

(Wiprut & Zoback, 2002)

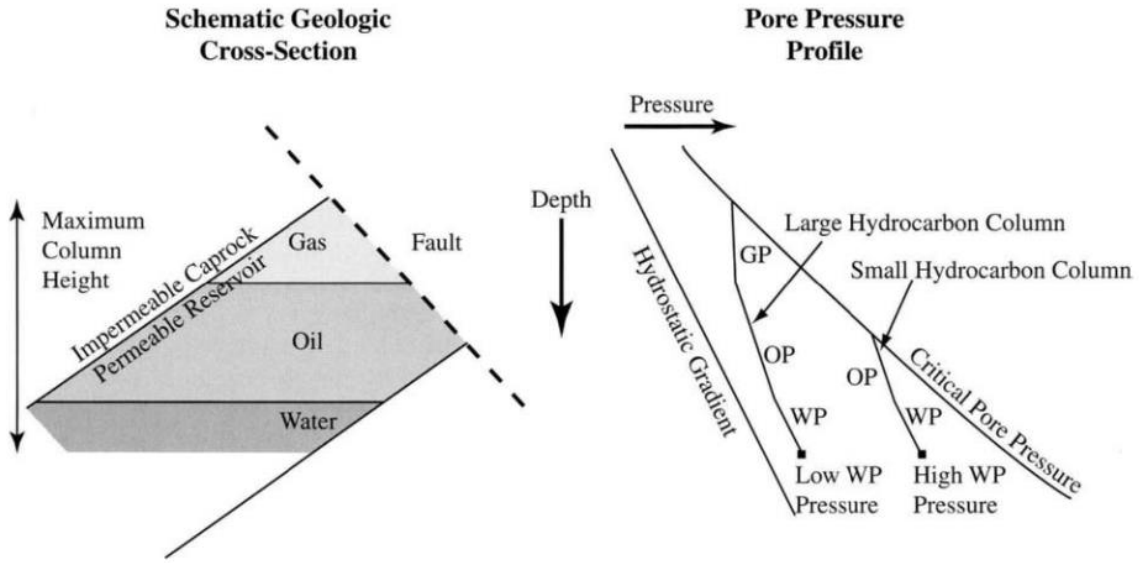

Figure 4. The effect of water phase pore pressure on hydrocarbon column heights. Figure from Wiprut and Zoback (2002)

The purpose of this thesis is to revisit some of the prospects investigated by Christian; Hermanrud et al. (2014) from a more dynamic perspective; estimating dynamic capacities of the traps, finding weak spots for leakage from them, and attempt to explain the level of hydrocarbon-water contacts by assuming a dynamic equilibrium.

2. Geological background

2.1.1. Regional setting

The hydrocarbon fields in this study are located in the Hammerfest Basin, SW Barents Sea. Presently, it is one of the largest continental shelf areas in the world and is part of the Northeast Atlantic passive margin. West of this margin, the Fram strait and the Lofoten Basin consisting of oceanic crust separates the Barents and the Greenland shelves (Figure 5.). The shelf consists of various subbasins, structural highs and fault zones of different ages (Figure 5.). The Western Barents Sea can be divided into two domains: to the north, the Svalbard Platform consists of a thin sedimentary cover; while between the Svalbard and the Troms-Finnmark platforms lies a depression consisting of a patchwork of sub-basins and highs where thick Mesozoic and Upper-Paleozoic sediments have been preserved (Berglund et al., 1986). The structural elements of the Western Barents Sea dip towards the west, and they are characterized by a westward thickening of the Jurassic-Cretaceous, while in the westernmost parts along

the continental margin a westward prograding Plio-PleiStøcene sedimentary wedge is preserved (Faleide et al., 1993).

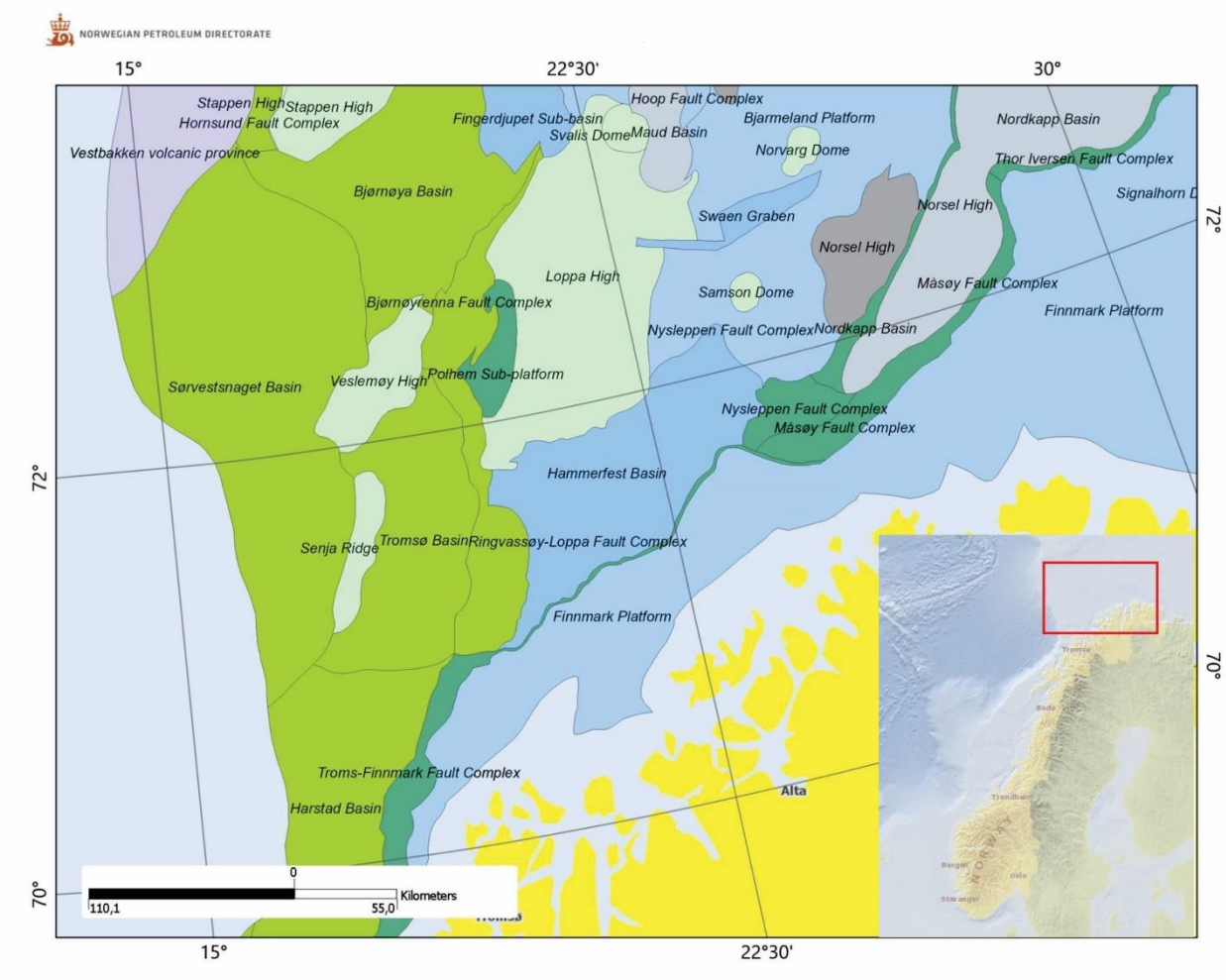

Figure 5. Major structural features around the Hammerfest Basin

The subbasins can be grouped into two geological provinces, based on their sedimentary infill: the Cretaceous/Lower Tertiary (Harstad, Tromsø, Sørvestsnaget Basins), and the Mesozoic (Hammerfest, Fingerdjupet) basins (Faleide et al., 1993). The latter basins are located further away from the continental margin to the east, and lack the pronounced Cretaceous-Tertiary subsidence that is characteristic of the former province (Figure 6). While the main tectonic event for the formation of these basins is the Late Jurassic-Early Cretaceous rifting (Cimmerian phase); earlier structural grains, and later reactivations of fault zones also had a profound effect on the divergent evolution of these basins (Berglund et al., 1986), (Brekke & Riis, 1987), (Gabrielsen, 1984), (Gernigon et al., 2014).

2.1.2. Tectonic evolution

In a tectonic sense the Barents shelf can be subdivided into two provinces: the eastern province was largely influenced by the Uralian orogeny; while the western Barents region's evolution was mainly shaped by post-Caledonian events (Faleide et al., 1993; Smelror et al., 2009; Worsley, 2008).

Basins in the SW Barents Sea were affected by previous structural grains. Major tectonic events influencing the structural evolution here include the Caledonian orogeny, the Kimmerian tectonic phase and the opening of the North Atlantic (Gabrielsen, 1984). It is suggested that the Carboniferous and Permian graben systems (related to the Caledonian orogeny) are situated in a similar NE-SW trend below the Mesozoic basins; defining an inherited structural grain (Gudlaugsson et al., 1998). After some minor tectonic events in the Early Triassic, the Middle and Late Triassic were both characterized by post-rift thermal subsidence (Gernigon et al., 2014). The Late Jurassic-Early Cretaceous Cimmerian phase mostly affected the western margin of the Barents Sea. This is also the time that the Hammerfest Basin was established as a separate depocenter from the Nordkapp Basin (Berglund et al., 1986). This tectonic phase has led to the characteristic E-W oriented horst-graben system in the northern parts of the basin (Figure 7.). Rifting continued well into the Cretaceous and Early Tertiary in the western margin along approximately N-S, NW-SE striking rotated fault blocks; creating the deep Cretaceous basins (Brekke & Riis, 1987), (Faleide et al., 1993), (Gabrielsen, 1984), (Gernigon et al., 2014). Renewed tectonic activity prior to the opening of the Norwegian-Greenland Sea saw the formation of the Spitsbergen orogenic belt (Worsley, 2008).

Lastly, Plio-PleiStøcene glaciations eroded the Barents shelf leading to isostatic uplift in the Hammerfest Basin. Vorren et al. (1991) estimates the average erosion in the southern Barents Sea to be around 420 m; while in the Hammerfest Basin it can reach up to 1000 m (Henriksen et al., 2011). The base of the glacial erosion is a well traceable reflector called the Upper Regional Unconformity (URU). The URU progressively deepens towards the shelf edge at the west; where ice streams deposited large mouth-fans such as the Sørvestsnaget fan.

This glacial episode is important since it could have affected the preservation of hydrocarbons in a number of ways: (1) the transition between net uplift and net deposition (hinge line) tilted the traps towards the west, altering the closure (Henriksen et al., 2011); (2) at the hinge line crustal flexuring under excess sediment load can locally perturb the stress field (Nordgard Bolas et al., 2005); (3) the cyclic loading-unloading caused by advancing and retreating ice sheets cause similarly cyclic pressure changes within the reservoirs (Ostanin et al., 2017); (4) the final uplift has also led to a pressure increase in the reservoirs via gas cap expansion.

2.2. Hammerfest Basin

In the following, a more detailed look is taken on the structural and stratigraphic setting of the Hammerfest Basin. Important aspects of the geological framework with relation to petroleum geology will be highlighted.

2.2.1. Hammerfest Basin's structural framework

The Hammerfest Basin is an elongated (70 km wide and 150 km long) asymmetrical basin striking NE-SW to NNE-SSW and dipping to the west (Figure 5). Neighboring structures include the Loppa High

to the north, the Tromsø Basin to the west, the Troms-Finnmark Platform to the south and the Nordkapp Basin to the east (Figure 6.). Major fault complexes defining the basin are the Asterias FC towards the Loppa High, the Ringavassoy-Loppa FC (RLFC) towards the Tromsø Basin and the Troms-Finnmark FC (TFFC) towards the Troms-Finnmark Platform (Figure 6).

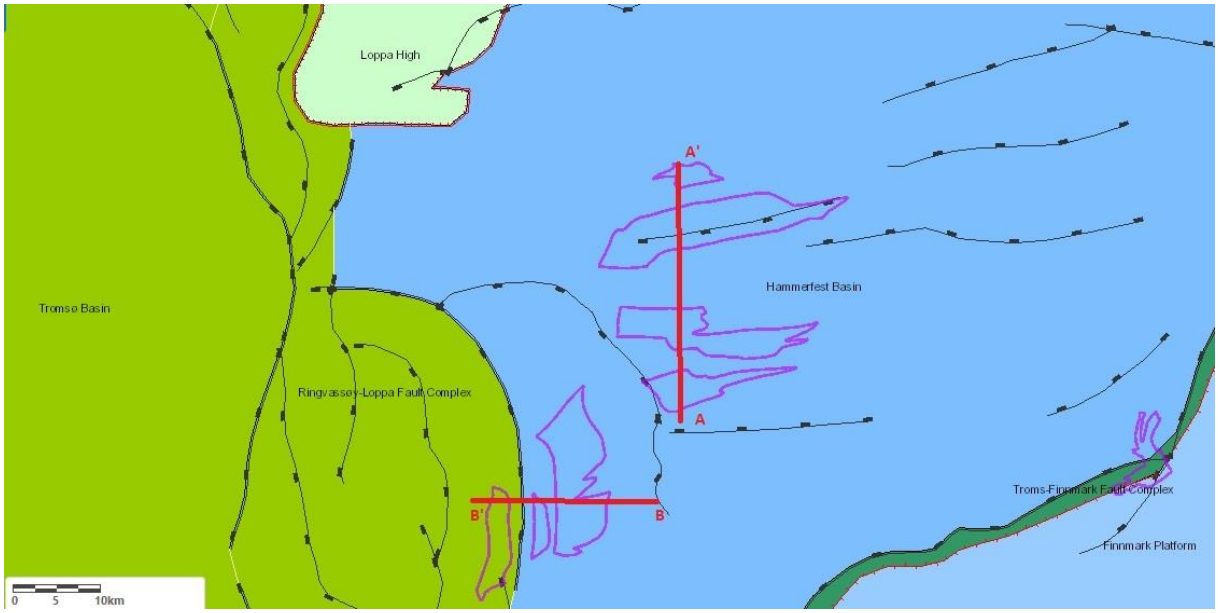

Figure 6. Characteristic strike of major faults in the study area. Red lines indicate the positions of the sections in Figure 7. and 8.

The TFFC separates the shelf's sedimentary sequences from the Scandinavian mainland mostly consisting of crystalline bedrock. According to Gabrielsen (1984) faults of this complex originate in the crystalline basement, meaning that this lineament has probably been active for most of the post Caledonian evolution of the basin. The zone strikes roughly NE-SW, with a characteristic dog-leg pattern, having E-W striking segments between the main NE-SW trends (Berglund et al., 1986). It is associated with basinward listric normal faults, often featuring rollover anticlines in the hanging wall. The RLFC separating the Tromsø and Hammerfest basins consists of NNE-SSW striking rotated, detached normal faults dipping towards the Tromsø Basin (Gabrielsen, 1984). Intersections of these faults often result in rhomb-shaped terraces containing some hydrocarbon accumulations (Figure 8). The ESE-WSW trending Asterias Fault Complex separating the Hammerfest Basin from the Loppa High to the north features complex cross-cutting normal faulting often involving antithetic faults (Berglund et al., 1986).

All the fault complexes mentioned above delineate the Hammerfest Basin, while also affecting the fault patterns inside the basin, especially towards the marginal areas. However, the basin itself has a characteristic fault pattern as well termed as the Hammerfest Basin Fault System (HBFS) by Gabrielsen (1984). The HBFS mainly consists of E-W trending normal faults resulting in horst-graben structures (Figure 7). They have been connected to the Late Jurassic Cimmerian tectonic phase, and run oblique

to the axis of the basin defined by the TFFC. This has led Gabrielsen (1984) to suggest that while the main trend of the basin represents an older Caledonian grain; the HBFS is the manifestation of a younger Jurassic stress field. As such, these faults are not rooted in the basement contrary to the fault zones described above.

Berglund et al. (1986) uses a classification system that contains five different types of faults to distinguish the fault systems within the Hammerfest Basin. Types 1, 2 and 3 correspond to faults of the TFFC, the RLFC and Asterias FC, respectively. Types 4 and 5 are part of the HBFS, but the latter type contains shallow faults that do not penetrate the Triassic succession.

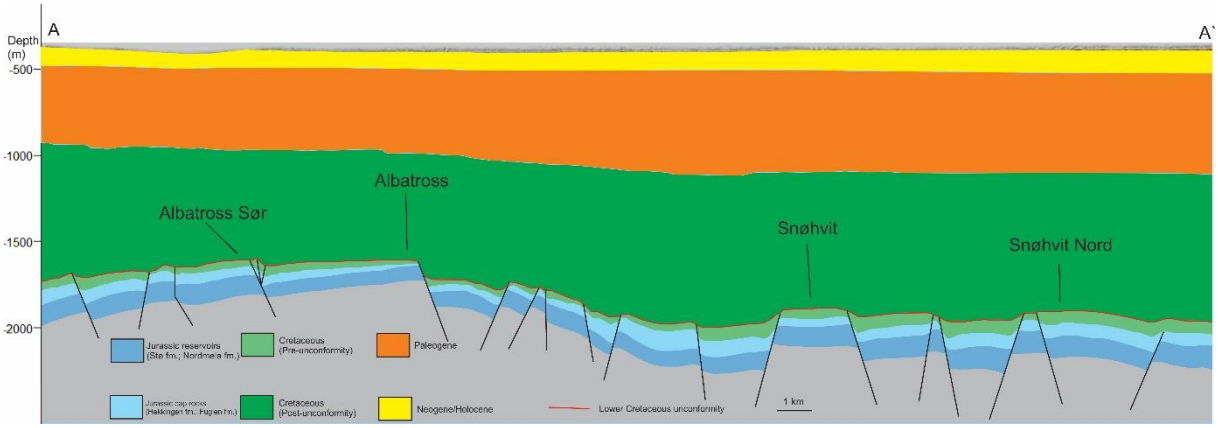

Figure 7. Schematic section of the Hammerfest Basin along line AA'

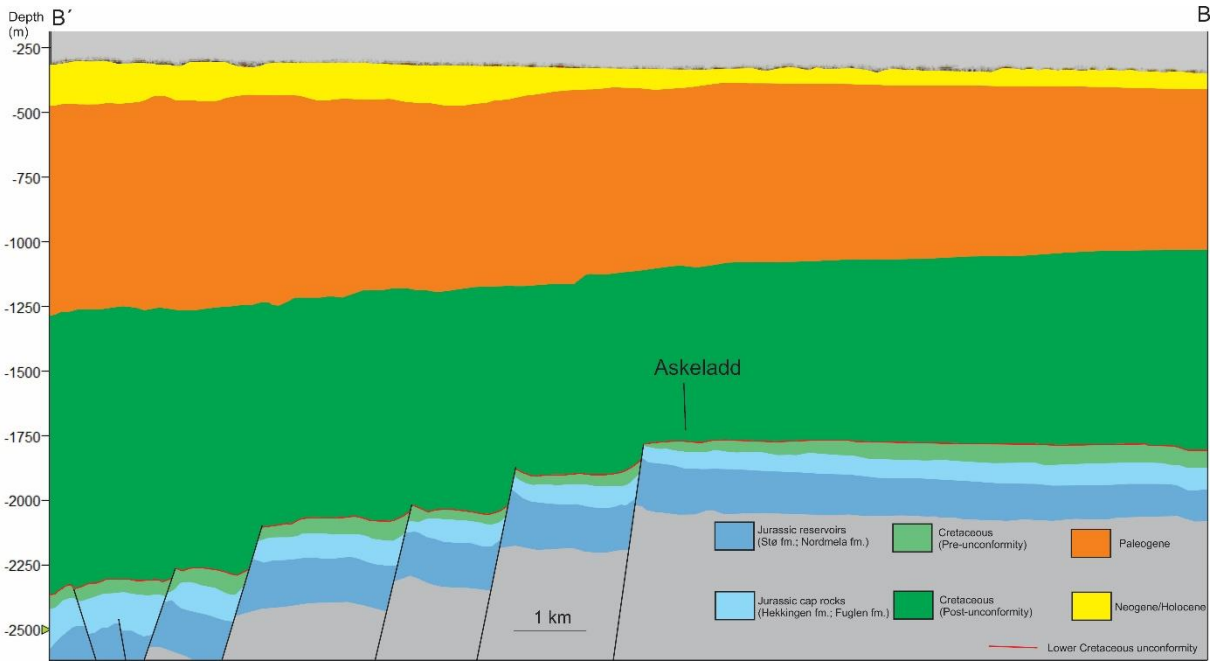

Figure 8. Schematic section of the Hammerfest Basin along line BB'

2.2.2. Stratigraphic evolution of Hammerfest Basin

Deposition inside the present-day Hammerfest Basin started as early as the Carboniferous, but the basin did not become an independent depocenter until the Late Jurassic Cimmerian event. Therefor it makes sense to investigate the stratigraphic evolution separately as pre, and post Cimmerian phases.

Pre-Cimmerian phase

The evolution of the Hammerfest Basin can be traced back to Upper Paleozoic times. The sediments from this period were accumulated in the hinterland basins of the Caledonides and are associated with post-Caledonian orogenic collapse (Gernigon et al., 2014). At this time, the Hammerfest Basin made up a single structure with the Nordkapp Basin (Berglund et al., 1986). In the Carboniferous, carbonate platform sedimentation dominated the area, while evaporitic sequences were deposited inside the graben systems. The Upper Permian is characterized by general basin wide subsidence, and clastic deposition which formed in response to the Uralian Orogeny (Brekke & Riis, 1987; S. M.; Mohammedyasin et al., 2016). Fine grained clastic sedimentation continued into the Early Triassic in the form of westerly-prograding clinoforms. From Late Triassic to Middle Jurassic a cyclic alteration of continental and shallow marine sediments can be observed in the Hammerfest Basin. From the Middle Jurassic another general rise in sea level took place initially leading to the deposition of marine sandStønes, then calcareous shales as the nearby sediment source drowned.

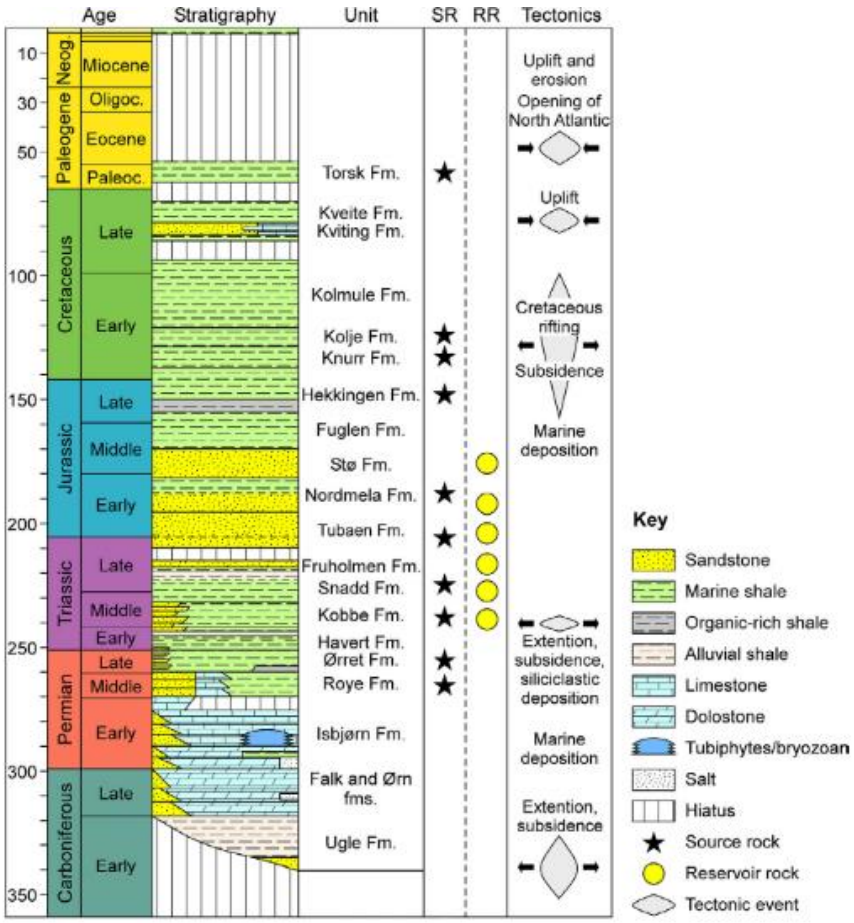

Figure 9. Stratigraphy, and tectonic evolution of the Hammerfest Basin (S. M.; Mohammedyasin et al., 2016)

Post-Cimmerian phase

The Late Jurassic faulting has led to the creation of deep anoxic basins where organic material was deposited and resulted in a shale event not only in the Barents Sea, but in

the Norwegian and North Seas as well. This Cimmerian faulting phase has established the Hammerfest Basin as an independent entity from the Early Cretaceous onwards. The characteristic E-W, NW-SE and NE-SW oriented normal faults of the HBFS developed during this time. The Cretaceous contains open marine sediments, with some with periodic restricted bottom circulation (Faleide et al., 1993). The thickness of the sequence is mainly controlled by fault of the HBFS and the RLFC. Cretaceous faulting in the HBFS caused a structural high in the basin axis, where the Cretaceous sequence thins out. Meanwhile, the RLFC showed intensive reactivation during this time. As a result, the Cretaceous sediments thicken away from the basin axis and towards the west, before they onlap to the Loppa High and the Troms-Finnmark Platforms (Faleide et al., 1993). Paleogene sediments consisting mostly of clayStønes and interbedded siltStønes from a marine shelf environment sit unconformably on the Cretaceous, and span in age from Upper Paleocene to Lower/Middle Eocene (Berglund et al., 1986; Faleide et al., 1993). The Paleogene succession thickens and contains progressively younger sediments towards the west. From the Eocene into the Oligocene a western progradation can be seen. From Middle Oligocene times, the areas east of the now developed passive margin experienced erosion, while a large sediment influx came into basins on the margin. The Neogene/Quaternary in the Hammerfest Basin is represented by a thin sediment cover sitting unconformably on the Paleogene (Berglund et al., 1986).

2.3. Petroleum geology of Hammerfest Basin

One the most important hydrocarbon plays (and the only one considered by Christian; Hermanrud et al. (2014) and this study), in the Hammerfest Basin is the Middle Jurassic associated with the pre-rift sandStønes of the Nordmela and Stø Formations; deposited in coastal-plain and shallow marine environments (Christian; Hermanrud et al., 2014). Source rocks in the area range in age from Carboniferous to Tertiary shales (Sund et al., 1986), however in the Hammerfest basin only the Upper Triassic-Lower Jurassic coal sequences (Kobbe and Snadd Formations), and the Upper Jurassic shales (Hekkingen Formation) have contributed significantly to current hydrocarbon volumes (S. M. Mohammedyasin, 2017; Sund et al., 1986). Generation of hydrocarbons from the Kobbe started in Late Triassic, in the Snadd from Early Cretaceous and in the Hekkingen from Late Cretaceous times, but accumulation in the Middle Jurassic play only started from the Paleocene; by which time all three source rocks have entered into the gas window mainly in the northwestern edge of the basin (Rodrigues Duran et al., 2013). After expulsion, hydrocarbons from the Kobbe and Snadd Formations have reached the pre-rift reservoirs via fault assisted vertical migration. The same vertical migration from the Hekkingen shale mostly charged the Cretacous Knurr Formation (S. M. Mohammedyasin, 2017).

The Middle Jurassic play is located in fault blocks. The cap rocks are the Fuglen and Hekkingen Formations, which are followed by 1-3 km thick mostly Cretaceous and Paleogene overburden. The preservation of hydrocarbons in this system was strongly affected several phases of uplift and erosion. Earlier Oligocene uplift resulted in gas expansion and the total or partial lateral spill of oil legs; while

the vertical leakage of gas through fault planes is mainly associated with stress and pore pressure perturbations during Neogene glacial erosion (Rodrigues Duran et al., 2013).

3. Theoretical background

This chapter aims to provide an overview of some basic concepts of petroleum geology that bear relevance to this thesis. The most important concepts include dynamic trapping mechanisms, the influence of stress regimes and pore pressure on trapping mechanisms; and the different processes that can lead to leakage from a dynamically constrained trap. To understand these concepts, an introduction to the petroleum system, and some of its elements is needed. After defining traps and dynamic traps as well, stress regimes will be discussed. Finally, this chapter will close off with a brief introduction to seismic surveys.

3.1. The hydrocarbon trap

A hydrocarbon trap is a place where "oil and gas are barred from further movement"(Selley & Sonnenberg, 2015). There are a number of different classification schemes for traps, but on the most basic level structural and stratigraphic traps are commonly distinguished. The former consists of traps that are defined by secondary structures; most commonly anticlinal and fault related traps. On the other hand stratigraphic traps are delineated by changes in lithology that can either be syn, or post depositional. Typical syn-depositional traps include sand bars, sand barriers and channels that can form pinchout structures; or carbonate reefs. Post-depositional traps can be diagenetic traps, or traps related to unconformities.

3.1.1. Nomenclature of a trap

The highest point of a trap is called culmination. The lowest point of the trap is the point from where an extra drop of hydrocarbon would migrate in a different updip direction. This point is called the spill point. The vertical distance between the culmination and the spill point is the closure of the trap (Figure 10). In hydrocarbon filled traps the different phases separate from each other: gas being the most buoyant creates a gas cap at the top, which can be followed by an oil leg and formation water below the oil. The contacts between these phases are called gas-oil (GOC), oil-water (OWC) and gas-water contacts (GWC). In a hydrocarbon filled trap the vertical distance between the culmination and any

hydrocarbon-water contact (HWC) is called the hydrocarbon column height. If the hydrocarbon column height equals the closure, the trap is said to be filled-to-spill; otherwise it is underfilled.

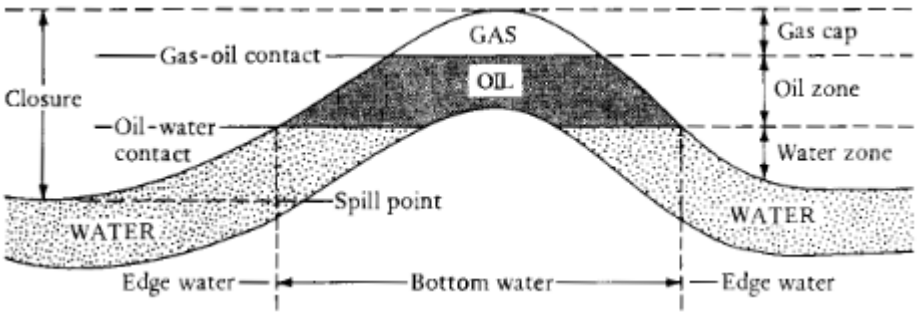

Figure 10. Nomenclature of a trap illustrated by a simple anticlinal trap. Figure from Selley and Sonnenberg (2015).

3.1.2. Hydrocarbon filling

Both oil and gas are more buoyant than water, which means that the first drop of hydrocarbon in a water filled closure migrate updip all the way to the culmination of the trap. Subsequent droplets of hydrocarbons will be replacing the formation water below this uppermost drop; gradually pushing the HWC down in the trap, creating a continuous hydrocarbon column. This process can continue until an equilibrium state (one drop in, one drop out) is reached. The equilibrium state imposes an upper limit on the hydrocarbon column height; and can be controlled by different factors (Figure 11).

3.1.2.1. Structural controls

If the column heights are controlled by structural factors, then the traps can fill up to the spill point (given that there is sufficient amount of hydrocarbons), since it's the structural configuration of the trap that determines the position of the spillpoint. The spillpoint can be the lowest hinge point in the case of an anticlinal trap; or the highest point of a reservoir-reservoir juxtaposition across a non-sealing fault plane. Structural controls prevail, when none of the dynamic controls discussed in the next section affect hydrocarbon column heights.

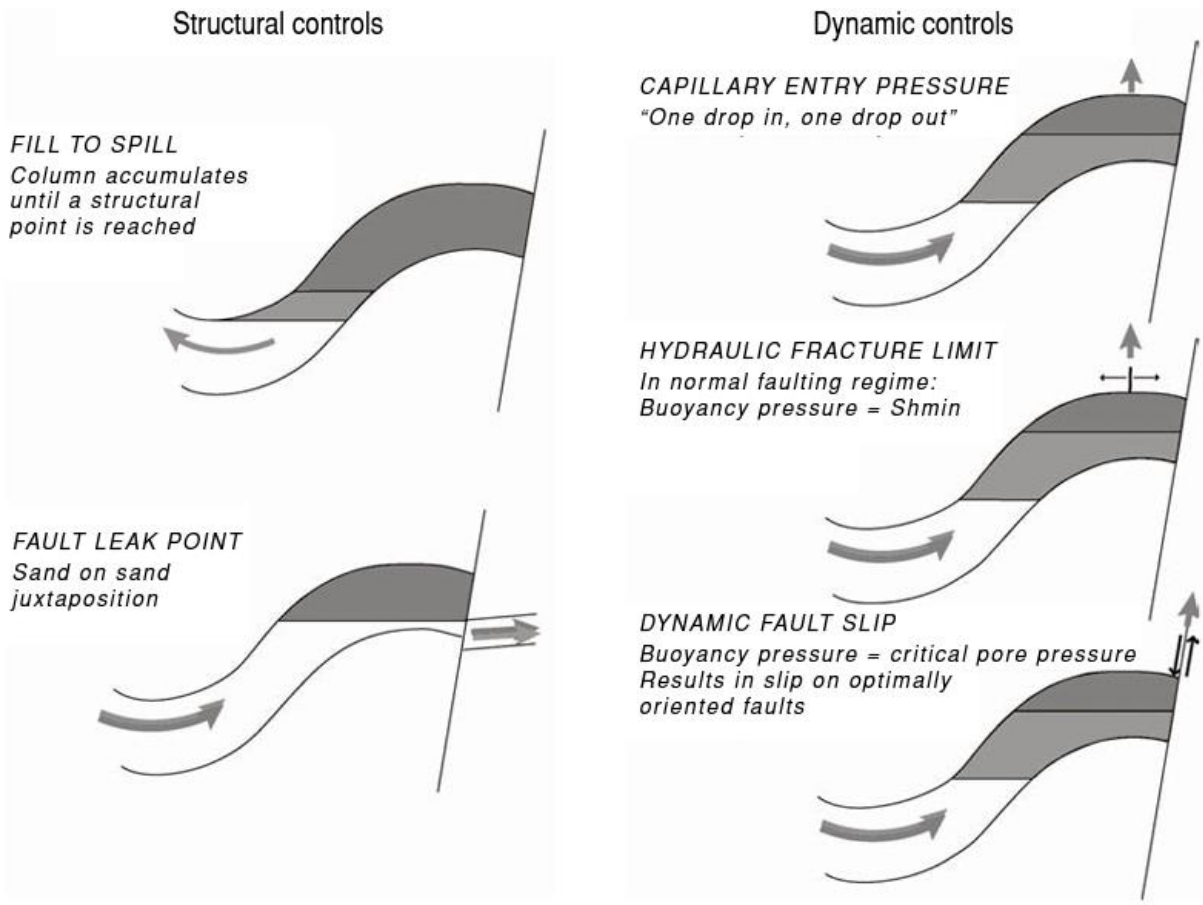

Figure 11. Different controls on hydrocarbon column heights in traps. Figure from (M. D. Zoback, 2007)

3.1.2.2. Dynamic controls

A dynamic equilibrium can occur when the reservoir pore fluid pressure reaches either the pore throat entry pressure of the seal, the fracture pressure of the seal, or a pressure high enough to cause slip on a fault intersecting the reservoir. This dynamic equilibrium can result in a HWC that is higher than the spillpoint, hence the trap can be underfilled. In this case "the maximum column the reservoir can support depends on (1) the initial water-phase pressure in the reservoir, (2) the mechanism by which fluids migrate out of the trap, and (3) the density of the hydrocarbon phase" (Finkbeiner et al., 2001). The second point will be explored more in the following sections.

Capillary entry pressure

Hydrocarbon traps are sealed off in updip direction by a seal. Sealing lithologies are low permeability rocks that owe their good sealing characteristics to their large capillary entry pressure. The capillary entry pressure is the force that a buoyant hydrocarbon column has to overcome in order to enter the pores:

$$P_{ce} < (\rho_w - \rho_{hc})g_h$$

where P_{ce} is the capillary entry pressure, ρ_w is water density, ρ_{hc} is hydrocarbon density, g is gravitational acceleration, and h is the hydrocarbon column height. P_{ce} is dependent on the largest pore throat radius of the seal.

Hydraulic fracture limit

The other characteristic that makes a good seal is its propensity to ductile deformation. Certain conditions however can promote the development of "shale embrittlement", where fractures open up enhancing permeability (Hoshino, 1972). Seal failure is often associated with the hydraulic fracture limit, which is reached when the reservoir pore pressure is as high as the minimum effective principal stress (see section 3.4.4.). In case of a seal failure, an amount of hydrocarbons that is proportional to the amount pressure causing the failure can leak out of the trap.

Dynamic fault slip

Traps bounded by critically stressed faults (see section 3.4.3.1.) can be vulnerable to hydrocarbon leakage in the fault plane; when the fault is reactivated. In this case the height of the HC column is controlled by a critical pressure that relates to a number of variables including fault plane orientation with respect to stress field, frictional coefficient and cohesive strength of the fault, and stress anisotropy. Similarly to hydraulic fracture limit; a reactivated fault plane can act as an open valve for hydrocarbons, promoting leakage out of the trap. This behavior is discussed in more detail in the following section.

3.2. The fault valve theory

The fault valve theory is the main principle behind this research. The theory of fault-controlled hydrocarbon prospects is based on the static and dynamic properties of faults. This theory suggests that faults have a differential role in fluid flow when active and inactive-an idea that forms the basis for dynamic fault slip, and fault controlled hydrocarbon columns.

3.2.1. Static and dynamic permeability

A large number of publications is concerned with the static properties of fault planes((Fristad et al., 1997; Gartrell et al., 2003; Harper & Lundin, 1997; Knipe et al., 1997; Sverdrup & Bjorlykke, 1997; Welbon et al., 1997)). These all emphasize the importance of reservoir-seal juxtaposition, fault core lithologies, clay smearing, fault intersections, diagenesis etc. when it comes to fault permeability. It is generally accepted that static fault conductivity is a complex issue, with many variables; and it is hard to come up with a general rule to determine it. An exception from this rule could be the fault valve theory, suggesting that faults which are oriented for failure in a given stress regime (i.e. potentially active); are the most likely to conduct fluids. (Linjordet & Skarpnes, 1992) used borehole breakout data to determine principal stress orientations, and to explain an acoustic masking zone interpreted as a gas column at the western perimeter of the Snovhit discovery (Linjordet & Grung Olsen, 1992). (Wiprut & Zoback, 2002) calculated the leakage potential on the surface of a fault plane intersecting the Visund

field in the North Sea; based on the orientation of the fault plane to the stress field. They were able to demonstrate, that a large gas column appears over the section of the fault where it starts striking for failure at present stress field. (Sibson, 2000) describes a so called fault valve mechanism, where well-oriented faults would fail after a buildup of excess pressure in their compartments; thus functioning as a pressure release valve.

It can thus be seen, that the issue of fault permeability can be broken down into static and dynamic permeability. The former is concerned with faults that emplace a structural control on hydrocarbon column heights, while the latter investigates the dynamic controls that active faults emplace through the critical pore pressure.

3.2.2. The stress field

When discussing the dynamic permeability of faults, and the controls they emplace on hydrocarbon column heights; a basic understanding of the stress field is needed. Both the absolute, and the relative magnitudes of principal stresses affect fault permeability. More specifically; it's the effective stress magnitudes that are important to the fault valve theory. Effective stress is the difference between stress and pore pressure. As a result, pore pressure also becomes central when describing the state of stress in a reservoir.

"Stress is a tenSør which describes the density of forces acting on all surfaces passing through a given point" (M. D. Zoback, 2007). Contrary to pressure, a stress field can be anisotropic (which is mostly the case in the crust), so an ellipsoid is commonly used to visualize it. The 3 axes of the ellipsoid correspond to the three principal axes of the stress field; these are poles to the planes on which no shear stresses act. The symbols for these from largest to lowest are S_1, S_2 and S_3.

The surface of the crust is always in contact with a fluid unable to support shear stresses. Hence one of the principal stresses in the crust is always perpendicular to the surface, with the remaining two axes being horizontal, and perpendicular to each other. The vertical axis is the weight of the overburden, and is commonly denoted as S_v. The horizontal stresses are made up of several factors such as the horizontal elastic deformation of rocks, and tectonic stresses. The largest horizontal principal stress is commonly written as S_{hmax}, while the smallest S_{hmin}.

The vertical principal stress

The vertical principal stress (S_v) corresponds to the weight of the overburden, so it is most commonly simply calculated by integrating density logs from several wells and taking an average value to account for the small differences between wells (Nordgard Bolas & Hermanrud, 2002). The gradient of S_v is commonly referred to as the lithostatic gradient, and for simpler calculations an average rock density of 2.3 g/cm^3 is usually assumed; resulting in a lithostatic gradient of 23 MPa/km.

Least horizontal stress

The least horizontal stress (S_{hmin}) is the least principal stress (S3) in both normal and strike-slip faulting regimes. Nordgard Bolas and Hermanrud (2002) warns based on the World Stress Map database; that assuming a normal faulting regime in most of the World's sedimentary basins is a faulty preconception. Even so, the Shmin=S3 assumption would work in approximately two-thirds of the basins. The only exception would be reverse faulting regimes where S_v=S_3.

Where S_{hmin}=S3; the least horizontal stress gradient becomes an important boundary for both exploration and well operations. If the wellbore fluid pressure reaches the level of S_{hmin}, loss of circulation can occur. Also, a pore pressure increase in the reservoir reaching S_{hmin} is associated with seal failure and a leakage of hydrocarbons. The cause behind these processes is hydrofracturing; the opening of tensile fractures oriented perpendicular to the direction of S3 via an increase in pore pressure. Since rocks generally have little or no tensile strength; hydrofracturing will occur when the pore pressure reaches the value of S3.

This makes it suitable to use controlled hydrofracturing in wellbores (called as leak-off tests-LOT) to constrain S_{hmin} gradients. Plotting the leak-off pressures (LOP) from several wells and from different depths in a given basin will provide the S_{hmin} gradient in the area. LOP's close to S_v can either indicate a reverse faulting regime, or a close to isotropic stress field.

Maximum principal stress

There is no direct measurement for the maximum principal stress. However assuming that S3 will equal S_{hmax}; then S3 may be calculated from the occurrence of borehole breakouts (Nordgard Bolas & Hermanrud, 2002). Wellbore breakouts are wellbore enlargements caused by stress-induced failure of a well occurring 180 degrees apart (M. D. Zoback, 2007). In a vertical well; the azimuth of breakouts correspond with the orientation of S_{hmin}, while drilling induced tensile fractures (situated 90 degrees away from breakouts around the wellbore) correspond with S_{hmax}. Thus, the elliptical shape of a vertical wellbore mirrors the anisotropy of the horizontal stress components. Through more complex calculations borehole breakouts can give absolute stress magnitudes, relative stress magnitudes; while in the simplest case, the orientation of the horizontal stress components.

Linjordet & Skarpnes, (1992) used breakout orientations inferred from caliper logs to risk fault bounded prospects with regards to fault seal effectiveness. The theory is that prospects bounded by faults that strike parallel with S_{hmax} will have higher exploration risks associated with them, since these faults will be more open and permeable; due to the fact that they have the lowest possible normal stresses resolved on their surfaces.

Pore pressure

Pore pressure is simply the pressure of any fluid occupying the pore space in a rock. The pressure of a water column that can be found in interconnected pores all the way to the surface, and is not sealed off

from communication with atmospheric pressure is called hydrostatic pressure; while its gradient is the hydrostatic gradient. The hydrostatic gradient is approximately 10 MPa/km coming from the density of water. Pore pressures higher than hydrostatic are called overpressures, while formations with pressures plotting below the hydrostatic gradient are said to be underpressured.

Pressure measurements in porous formations are commonly done by the Repeat Formation Tester (RFT) wireline tool. Pressure samples from different depths in a reservoir can be plotted in a pressure vs depth space. The obtained pressure gradients can be useful in separating fluid columns with different densities inside the reservoir. Fluids with lower densities than water will always result in pore pressures deviated from hydrostatic conditions; but the values that are much more telling about the reservoir's initial pressure characteristic is the water-phase pressure. The horizontal distance between the water-phase gradient and the hydrostatic gradient gives the initial magnitude of overpressure-this would ultimately affect the hydrocarbon column height as well. In a hydrocarbon filled reservoir pore pressures measured in the gas or oil columns will reflect the added effect of their lower densities.

Stress regimes and stress provinces

When we are discussing stress in the crust, the relative magnitudes of S_v, S_{hmax} and S_{hmin} has a large significance. Depending on how they relate to S1, S2 and S3 Anderson distinguished at least three different stress regimes (Figure 12). He also theorized what styles of faulting would be active in each of these stress regimes. With the help of this classification scheme a basic description of the state of stress in any given location can be done by giving the stress regime and the orientation of one of the horizontal principal stresses (usually S_{hmax}).

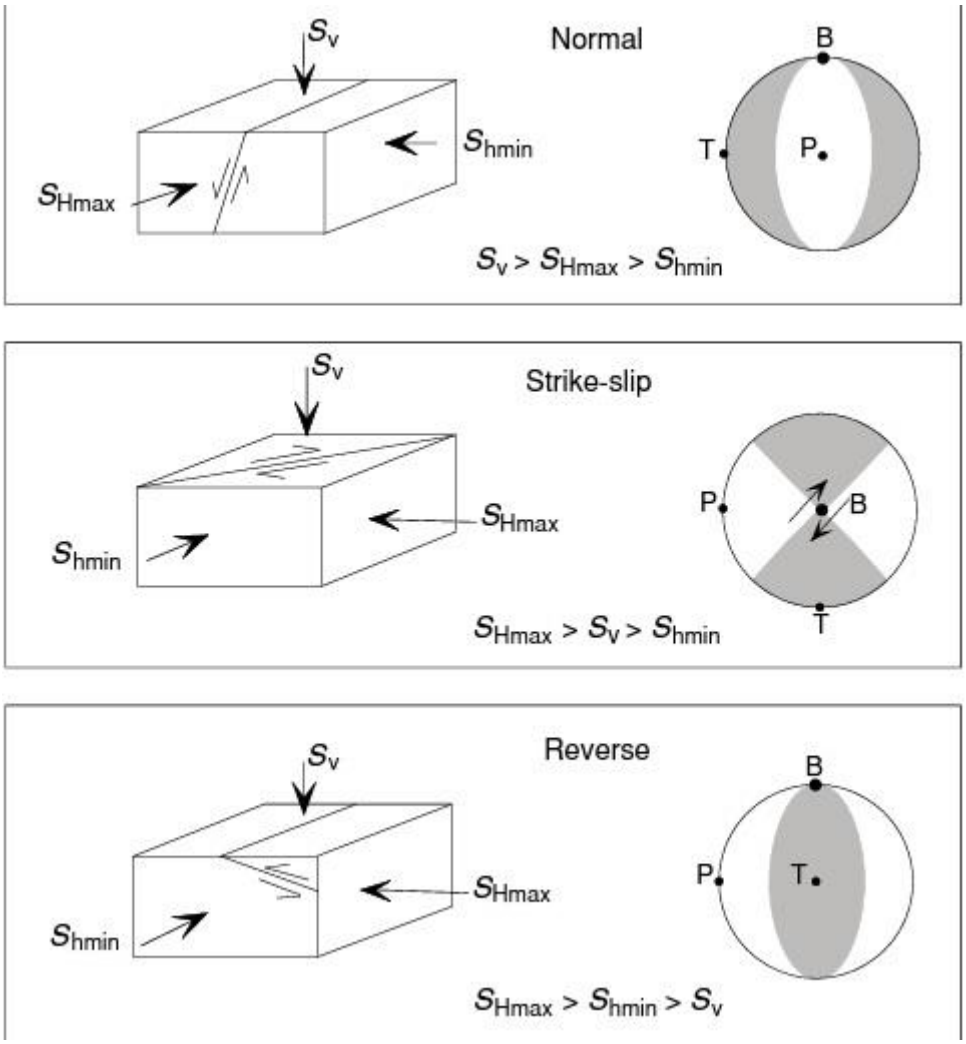

Figure 12. Anderson's classification of different types of faulting, and how they relate to stress regimes. Source: (M. D. Zoback, 2007)

M. L. Zoback et al. (1989) has noted that in situ stress measurements at different locations have shown that stress regimes and the orientations of principal stresses can show large continuity over extensive geographical areas. Such areas with more or less uniform stress magnitudes and orientations are called stress provinces. It is worth noting that stress provinces are not only spatial but also temporal concepts; meaning stress regimes change over geological time. Fault populations that were introduced in a given stress regime can stay dormant afterwards, or possibly get reactivated in a different stress regime.

3.3. Failure processes

This section will briefly discuss the method behind determining the dynamic capacity of a trap in a given stress field. Afterwards an overview is given on how fracture criteria for failure processes is incorporated in a Mohr space.

3.3.1. The Mohr diagram

The Mohr diagram is used to get the amount of shear and normal stress on a plane with a given orientation to the stress field (Figure 13.). It is very useful in assessing the possibility of failure.

3.3.2. 3D Mohr diagram

The 3D diagram shows all three principal stresses, and contains three Mohr circles (Figure 13.). It is able to display the shear and normal stresses of all the planes with regards to their orientations to the stress field. The planes are represented by points found in the area between the two smaller and the largest Mohr circles. To define one plane, we need its Θ angle to at least two of the principal stresses.

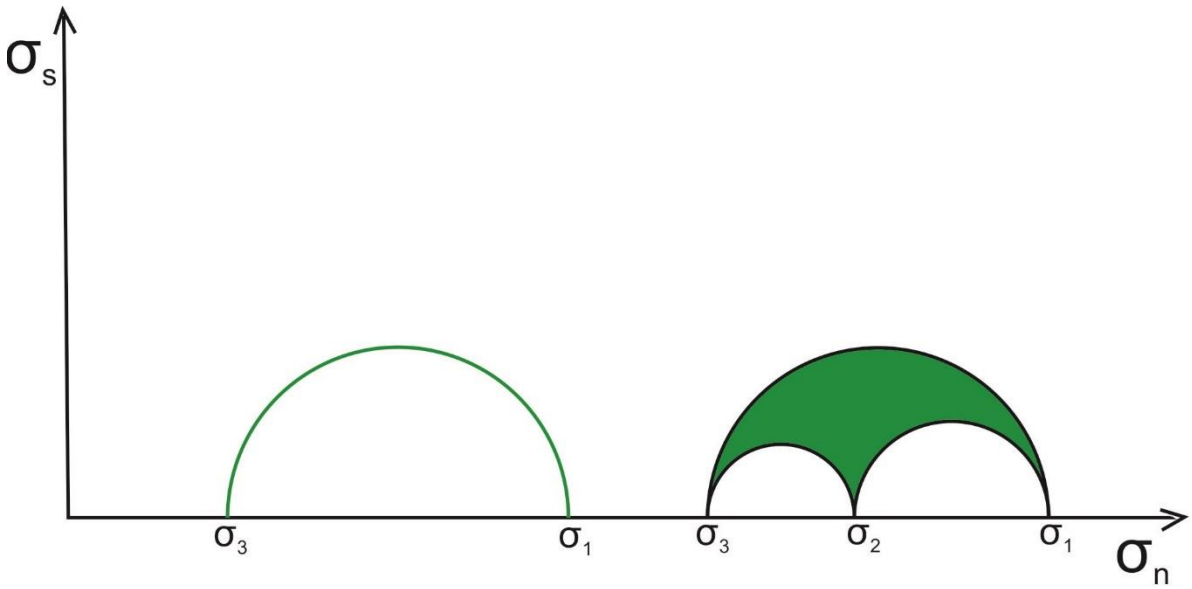

Figure 13. Representation of a 2D and 3D Mohr circle. Green color shows the possible stress configurations of planes. The vertical axis shows effective shear stress and the horizontal axis shows effective normal stress.

3.3.3. Fracture criteria

Certain configurations of stresses and pore pressures can give rise to the failure of rocks. The states of stresses that can lead to failure in the crust are represented by the so-called failure envelope in the Mohr diagram. Failure envelopes in the Mohr space represent the different combinations of shear and normal stresses that would cause a given type of rock to fail. The envelopes are commonly determined experimentally, and they can be differing depending on the type of rock, whether it is intact or not, or the mode of failure involved.

The geometric relation of a Mohr circle to the failure envelope defines different states of stress: in a stable state the Mohr circle does not touch the failure envelope (Figure 14.). All the states of stress, where the Mohr circle is intersecting the envelope are unstable. Unstable states of stress are theoretical, but do not exist in the nature, because as soon as the Mohr circle touches the envelope; failure occurs followed by a stress release; causing the state of stress to revert to stable state. The state of stress where the Mohr circle touches the failure envelope is referred to as critical. In this state, an incrementally small increase in stress anisotropy, or a decrease in effective stress would cause imminent failure.

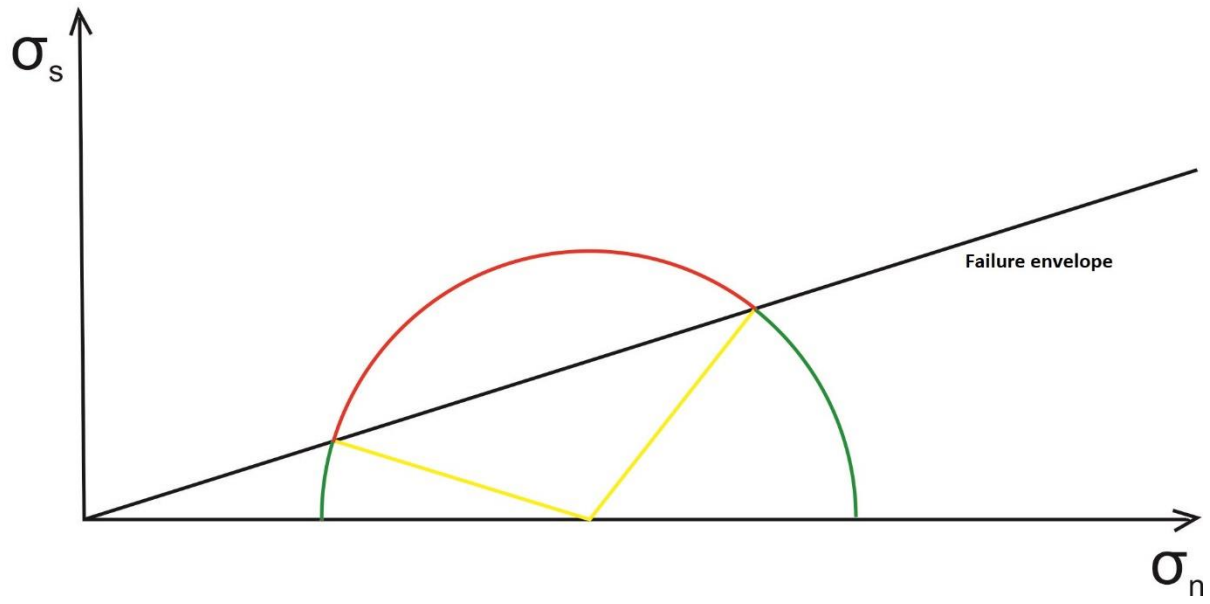

Figure 140. Relation of a Mohr circle to the failure envelope: green points represent planes with stable stress configurations, while the red ones are unstable. The two yellow planes are critically stressed.

3.3.3.1. Critically stressed faults

When the resolved shear and normal stresses on a fault's surface allow slip (shear failure) to occur on the surface (or in other words the Mohr circle is touching the fault's failure envelope), the fault is said to be critically stressed. In a natural crustal setting, critically stressed faults would be a subset of faults in the crust, that are oriented according to Anderson's faulting theory in any given stress regime. Critically stressed faults have a huge importance since in a dynamically controlled pressure compartment these faults are the weakest; and so it is the dynamic properties of these faults and their relationships to the prevailing stress field that will put constrains on the pore pressure inside the compartment.

3.3.3.2. Causes of failure

There are two broad processes by which failure can occur: increase in stress anisotropy and decrease in effective stress. The former can be caused by the accumulation of tectonic stress, or stress perturbations from the differential loading of crust. The increase in differential stress means that the diameter of the Mohr circle increases, until it touches the failure envelope.

The decrease in effective stress happens through an increase in pore pressure. In this case all of the effective principle stresses decrease by the same amount, shifting the Mohr circle to the left in the diagram while keeping the differential stress constant. Again, this will lead to an eventual failure as the Mohr circle touches the failure envelope.

The pore pressure induced failure of critically stressed faults is one of the most important natural regulator of hydrocarbon column heights in dynamically controlled compartments.

3.3.4. Modes of failure

Shear failure is a type of failure, that involves considerable movement parallel with the surface of the fracture. Shearing occurs on surfaces over which the shear stresses are relatively high compared to normal stresses. The shear strength of different media is defined by the Mohr-Coulomb failure envelope. The shear strengths of cohesionless fault surfaces are for example commonly represented by a Mohr-Coulomb envelope starting from the center of the diagram with a steepness that corresponds to a frictional coefficient of 0.6.

Extensional (Mode I) fractures form with low shear stresses on the fracture surface. The bulk of the movement is perpendicular to the fracture walls, and they open up perpendicular to the least principle stress. This means that with the exception of a reverse faulting regime these fractures will always be vertical. If we want to include the formation of extensional fractures into our model; then the Griffith-Coulomb failure envelope represents a more realistic behavior of rocks. Instead of a straight line all the way, this failure criteria becomes parabolic towards low confining pressures (Figure 15).

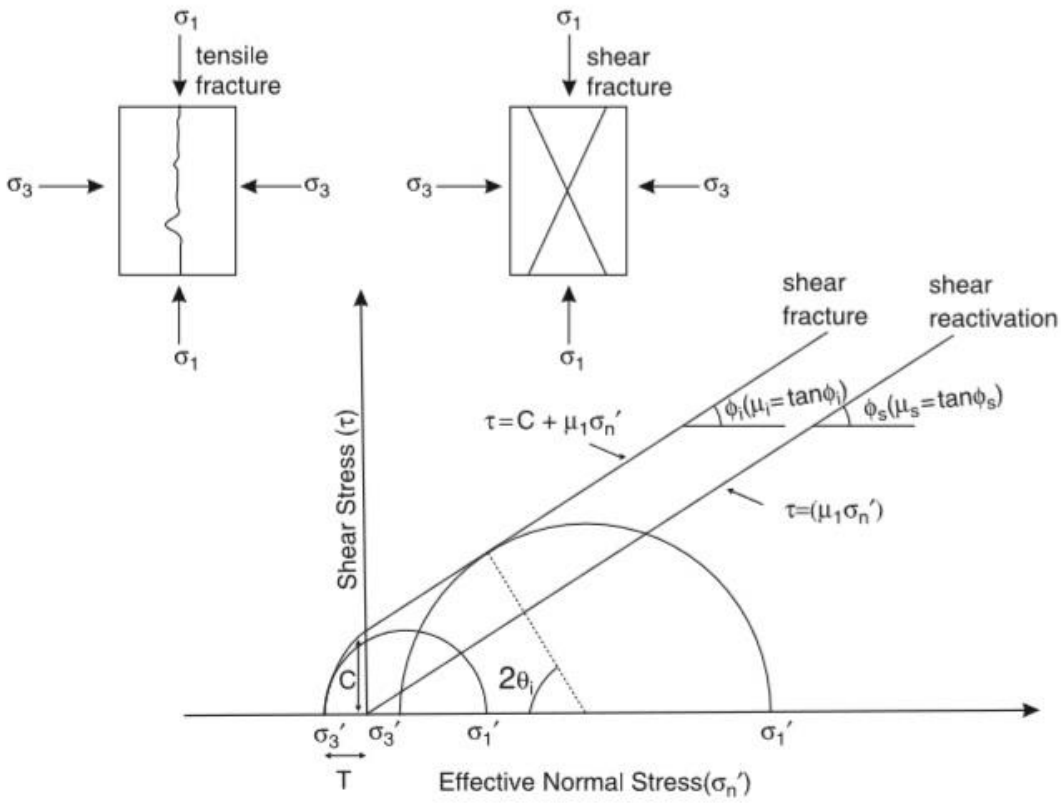

Figure 15. (Previous page) Geomechanical parameters for fracture related seal breach. A Mohr-Coulumb envelope (starting from the center) only allows for the modelling of shear failure. The Griffith envelope gives a more realistic interpretation with the possibility of tensile failure at low differential stresses. Figure from Mildren et al. (2005)

As mentioned above, there many approaches to the determination of the critical pressure in a dynamically controlled trap depending on modes of failure, petrophysical characteristics etc. As a consequence there are a number different parameters that can be used to quantify and asses dynamic trap risk (Figure 16.).

Gaarenstroom et al. (1993) introduced retention capacity (RC) as the difference between pore pressure and the minimum principal stress (minimum principal effective stress) to assess the risk of seal related failure on prospects of the Central Graben in the North Sea. This approach assumes tensile fracturing of a seal without tensile strength as the main control on hydrocarbon column heights. A low retention capacity can either be indicative of a dynamically underfilled trap (with a pore pressure lower than dynamic equlibrium); or a trap in dynamic equlibrium but with a different mode of failure active (Mildren et al., 2005). RC can only be a measure of true dynamic capacity where the cap rock has no tensile strenght, and there are no well-oriented cohesionless faults in the rock (Sibson, 1996). In most of the cases however, real rocks are far from intact and have faults going through them in every direction; making a fault-shear reactivation more realistic (M. D. Zoback, 2007). In recognition of this; other parameters were commonly used including slip-tendency (Morris et al., 1996), the Coulomb failure function and the critical pressure perturbation (Wiprut & Zoback, 2002). None of

these techniques incorporate the tensile and cohesive strength of the faults, and the tensile and cohesive strength of intact cap rock.

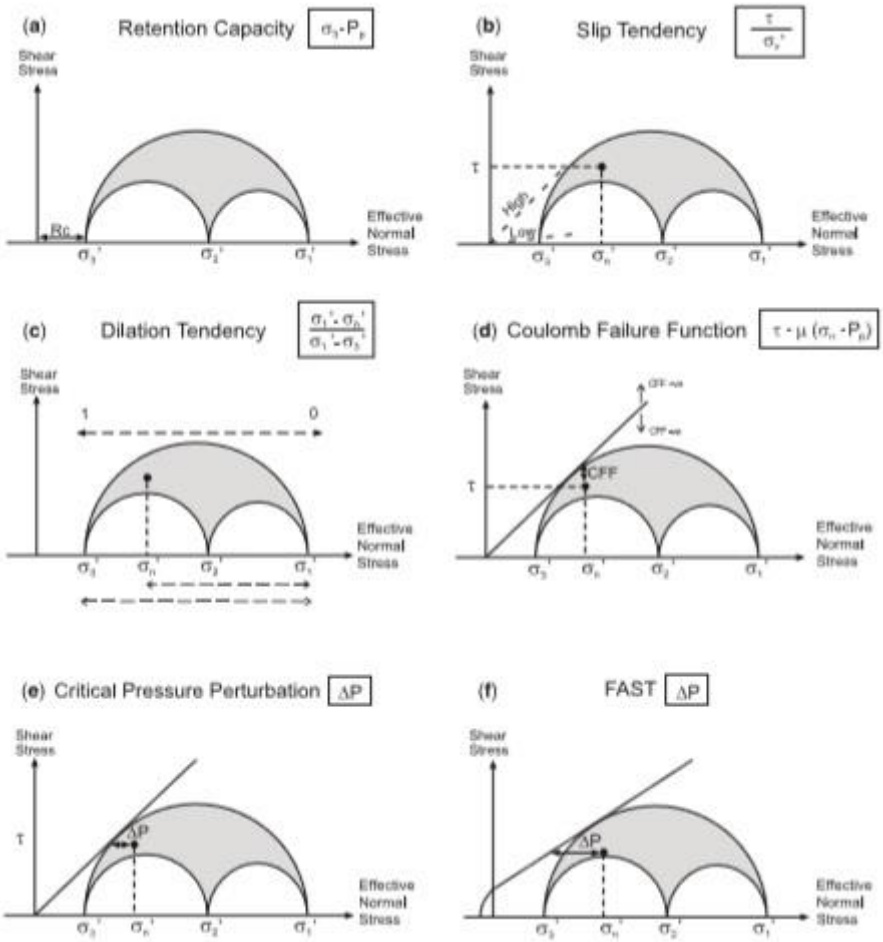

Figure 16. The different methods for assessing dynamic capacity. Figure from (Mildren et al., 2005)

The Fault Analysis Seal Technology (FAST) technique developed by (Mildren et al., 2005) and used by (Hillis & Nelson, 2005b) in the North Sea gives an opportunity to model a wide range of failure mechanisms. This method allows for the incorporation of cohesive and tensile strength of fault rocks together with intact cap rocks. In most cases the cap rock is assumed to be stronger, however according to (Hillis & Nelson, 2005b) this does not need to be the case all the time. This is the most comprehensive geomechanical analysis so far since it allows for a seal breach via for different cases: shear reactivation of faults, extensional reactivation of faults, shear failure of cap rock and extensional failure of cap rock (Figure 17.).

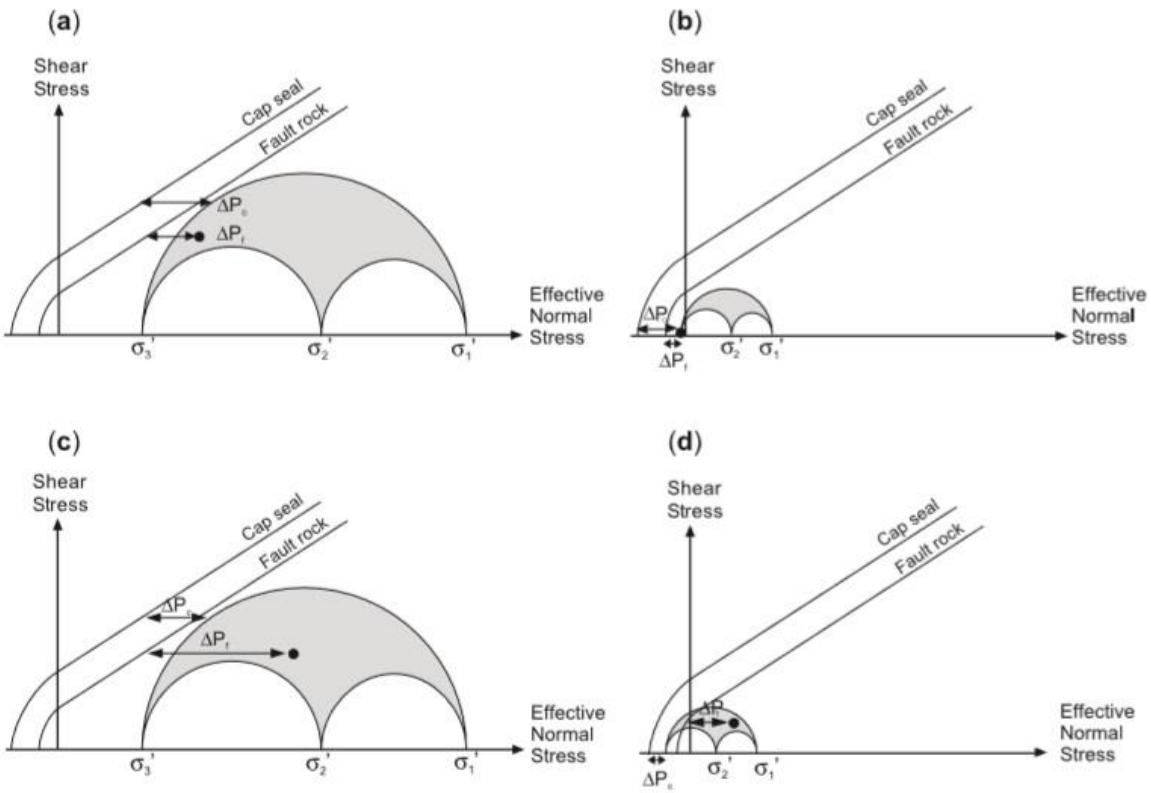

Figure 17. The 4 basic modes of seal breach: shear failure of fault (a), tensile failure of fault (b), shear failure of cap rock (c), tensile failure of cap rock (d) Figure from Mildren et al. (2005)

3.4. 3D reflection seismic

Reflection seismic is one of the most commonly used geophysical tools in exploration and field development alike. It uses the measured travel time of sound waves reflected from geophysical boundaries to construct a geological model. At sea, sound waves are usually generated using air guns, while an array of geophones detect the waves. Energy gets reflected every timethe incident wave arrives at a surface with different acoustic impedances across it. The acoustic impedance of a material is given by the seismic velocity times the density of that material. Thus surfaces with acoustic impedance constrasts can be layers in a sedimentary sequence.Hence, the most common surfaces appearing on sesimic data are sedimentary layers, unconformities and fluid contacts.

The reflection coefficient tells us what percentage of an incident wave energy gets reflected from a given surface of acoustic impedance contrast. The larger the acoustic impedance contrast, the more energy gets reflected from it, resulting in a more pronounced sign. On seismic data this will manifest itself as bigger amplitude waves.

As a rule of thumb, acoustic impedance will increase with depth. In some cases however a downward penetrating wave can reach layers associated with a decrease in impedance. This will result reverse phase reflection in contrast to a normal phase wave that is produced by an increase in acoustic impedance. A common form of reverse phase waves is the so-called bright spots. Bright spots are

reverse phase wavelets with increased amplitudes, that is commonly associated with gas charged sediments.

4. Data and Methods

4.1. Data

4.1.1. Seismic

The seismic dataset used in this study was ST15M04, a 3D depth-coverted seismic cube provided by Equinor. The seabed produces a normal polarity, zero-phase wavelet. It covers the Snøhvit, Albatross and Askeladd fields; in addition with two dry structures (Askeladd Beta, Delta Vest) (Figure 18.) that were originally investigated by Christian; Hermanrud et al. (2014).

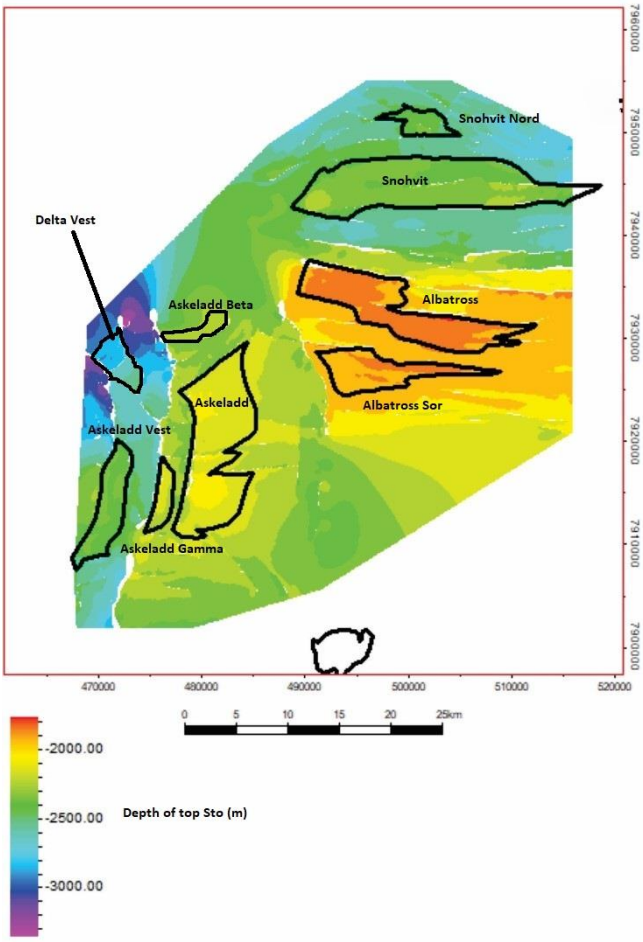

Figure 18: Depth map of top Stø interpretation over the survey area.

4.1.2. Well data

Well tops were used during seismic interpretation to correlate reflections with formation tops. Well correlation was especially important in this particular survey area, where the heavily faulted nature of the reservoir level often makes interpretation between fault blocks ambigous. Well data was also utilized during the stress field modeling. Calculations of overburden stresses were done by the help of density logs. Caliper logs documenting borehole breakout orientations were unfortunately unavailable

to this study, so determining horizontal stress orientations was done via studies that did contain this information. A description of these studies will follow in the next chapter.

RFT pressure measurements were an integral part of determining the pressure profile and the degree of overpressure in the reservoirs. Pressure profiles were also utilized when determining the initial fluid contact levels in the traps. For simplicity's sake, the same fluid contact level was assumed in each trap; meaning that the possibility of reservoir compartmentalization was ignored during this study. RFT pressure points and other important well parameters (water depth, kelly bushing height) were obtained from well completion reports publicly available on NPD's website. At each of the traps information from the discovery wellbore, (or from the first wellbore in the case of no discovery) were used as reference for that entire trap.

Leak off tests (xLOT) were used form wells and provided by Equinor. The data from these tests was used to approximate S3 of the stress field. With the help of xLOTs and and overburden calculations from density logs; a realistic approximation for S_{hmin} and S_v was achieved, which helped constraining the final principle stress (S_{hmax}). This will be elaborated further in the following section.

4.2. Methods

The workflow for this study can be divided into two main parts: seismic interpretation involving horizon and fault interpretation; and constraining and building the stress model. The structure of this chapter reflects this two phase workflow.

4.2.1. Seismic interpretation

The seismic interpretation was done with Schlumberger's Petrel software. Several seismic horizons were picked and interpreted using seeded 3D autotracking, or more crude interpretation methods where the seismic signals were deterioated. The Hekkingen and Fuglen formations were chosen as cap rocks, and the Stø and Nordmela as main reservoirs (Figure 19/A.). Faults were interpreted in and around of known discoveries and prospects. On the shallower western parts of the survey variance volume attribute was used to aid fault interpretation. In the deeper parts of the survey (around the Askeladd fields) the seismic signal was too deterioted for variance aided interpretation. Through dip-linkage these faults often link up vertically with deeper (Paleozoic) and shallower (Cainozoic) fault segments alike. Interpretations however were kept mainly on the Jurassic level never going shallower than the Upper Jurassic unconformity; or deeper than the top of Fruholmen Formation (Figure 19/B). The reasons for this include: a rapidly deterioating seismic signal below the Jurassic sequence, dip separation seems to be concenrtrated around the Jurassic reservoirs and the fact that the Upper Jurassic unconformity provides a good approximation as the top of the traps. This way, trap geometry can be defined as an intersection between the top Hekkingen and fault surfaces.

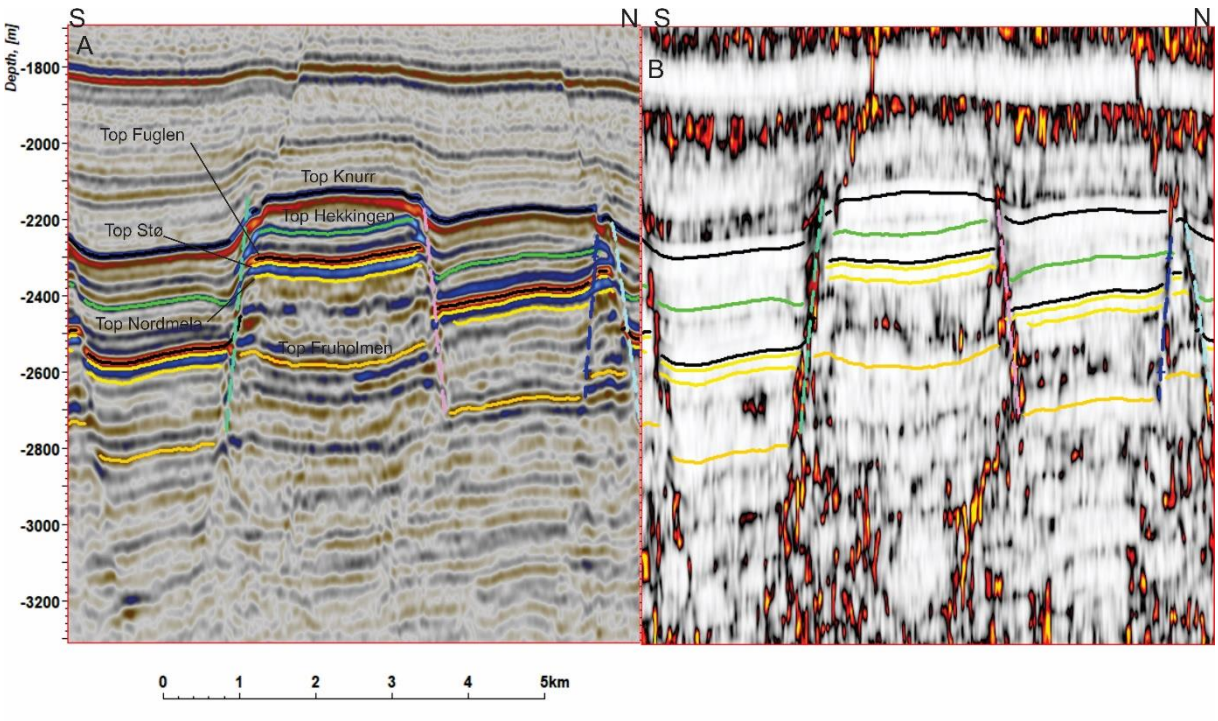

Figure 19. A: N-S seismic section through Snøhvit, showing the interpreted horizons around the reservoir. Yellow horizons belong to the reservoir, green is source rock, while the black ones are cap rocks. B: The same section in variance attribute view: fault planes light up as areas of higher variance (red-yellow colors) between the fault blocks. Mapping of fault planes were kept between top Knurr, and top Fruholmen surfaces.

4.2.2. Constraining the stress field

In order to incorporate the influence of the stress field in fault permeability evaluations; the following important points must be addressed:

1. A model for the local stress field is required. The simplest way to define a stress field (also used in this thesis) is by estimating the magnitude of the three principal stresses; and the orientation of the horizontal principal stresses
2. An understanding of the pore pressure within the reservoir is required
3. And finally, a geomechanical model for the failure process thought to be in "dynamic control" is needed.

This section will go through these points following the order above; detailing the workflow and discussing the weakspots of each of the methods.

4.2.2.1. Determining the stress field

*In the following section would like to introduce the process of building a geomechanical model. Since the stress field profoundly influences the final results of this research, this is a crucial step with regards to the validity of any findings presented about fault permeability. The geomechanical model was mainly based on well data (density logs, caliper logs, xLOTs).

The World Stress Map project was a worldwide cooperation between research institutes to gather information about the large scale stress fields. The project put a big emphasis on tectonically less active intraplate areas where earthquake focal mechanism data are scarce and other techniques are required to get a grip on the active stress field. The techniques used to collect data for this project are still relevant today; and form the basis for stress measurements. M. L. Zoback et al. (1989) gave a good overview of these methods. Below a short description follows of the ones that are relevant to this thesis.

S_v from density logs

The vertical stress S_v is purely derived from the weight of the overburden and is the only principal stress not affected by tectonic forces. Because of this it is also the easiest to estimate. It is commonly calculated by multiplying the densities from a density log with the height and the gravitational constant. If density logs are not available, an average density of around 2.3 g/cm3 is commonly used; however a more precise way to calculate S_v is to integrate on the densities of a well log by calculating the weight of small intervals for the whole length of the survied borehole and then adding them up:

$$S_v = \int \rho g \, dh \, ;$$

where ρ is density, g is the gravity constant and h is the height.

This will give the weight of the overburden over the length of the borehole where density logging was done. With the knowledge of this length the overburden gradient can easily be calculated.

It is important to mention that with this method, the overburden gradient is slightly overestimated since the less compacted and lighter sediments in the shallower parts of the borehole are not accounted since logging is usually not carried out in the first couple 100 meters of the well.

Methods for estimating S_{hmin} via xLOT

Hydrofractures are MODE I (extensional) fractures that develop when the pore pressure (or in the case of a wellbore the drilling mud pressure) is greater than the least principle stress (M. D. Zoback, 2007). The criteria for forming hydrofractures is that the fluid pressure must overcome the compressive stresses and the tensile strength on a given plane. The basis for using them as an indicator for S3 comes from the work of Hubbert and Willis (1957). According to that study, hydrofractures always propagate perpendicular to S3 (since this is the least energy configuration) with the same strike and dip. Additionally, naturally occurring rocks have tensile strength close to zero; meaning that the pressure at which they open only correlates with the in-situ least principle stress.

Leak-off tests (LOT) are the most common type of method for determining the minimum principal stress via the creation of hydrofractures. These tests are usually preformed in the earliest stages of a new well section; after they drilled through the casing shoe and the cement of the previous section. The determination of S3 is done via the interpretation of pressure vs time plots of LOT tests. Technical terms related to these plots include the leak-off pressure (LOP), formation breakdown pressure (FBP), fracture propagation pressure (FPP), instantaneous shut-in pressure (ISIP) and fracture closure pressure (FCP) (Figure 20). The number of studies concerned with different ways of interpreting these plots is extensive; however there seems to be an agreement that in the most simple case S3 can be approximated by LOP and ISIP. According to Raaen et al. (2006) the only reliable pressure value that is directly connected to S3 is the fracture closing pressure.

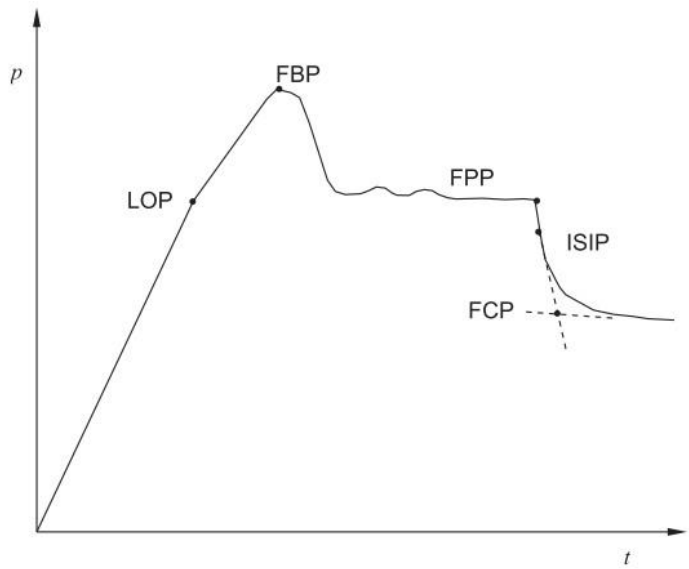

Figure 20. A typical pressure vs time curve from an LOT. Figure from Raaen et al. (2006)

Leak-off tests provide the drilling mud density and the depth at which ISIP occurred. This gives a good basis for estimating the gradient of the least principle stress. Moreover; the tensile failure occurring during hydrofracturing can also help constraining relative stress magnitudes (see next section).

Determining relative stress magnitudes and constraining S_{hmax}

S_{hmax} is the most difficult principle stress to determine, since there are no direct measurements that could be used for this purpose (M. D. Zoback, 2007). Instead, the most common way to estimate, it is to put constraints on the possible values based on knowledge about relative stress magnitudes; and borehole breakouts.

Relative stress magnitudes have a basic influence on the type of active faulting within a stress regime. For the description of these regimes based on Anderson's faulting theory, the reader is referred to section 3.3.2. Based on this theory several assumptions can be made about the stress field by only knowing the overburden stress and the minimum principle stress. If these two coincide, that could be

an indication of a strike-slip/normal or a reverse faulting regime. When the least principle stress is smaller than the overburden that either points to a pure normal faulting or a pure strike-slip regime. In each of these faulting regimes, differential stress cannot accumulate indefinitely; since failure would occur at some point limiting the growth of it. According to frictional failure equilibrium theory discussed in section 3.4.3.1.; the most likely type of failure limiting stress accumulation is by shear failure along well-oriented zones of weakness with a coefficient of friction of around 0.6. With this in mind, stress polygons can be constructed; showing the possible range of values for the horizontal principle stresses given that the overburden gradient is known. In normal and strike-slip faulting regimes this makes it possible to assign a theoretical minimum and maximum value to S_{hmax} given that S_{hmin} and S_v are known.

Wellbore breakouts and drilling induced tensile fractures (DITF) are fractures formed around a wellbore due to the diStørtion in stress trajectories caused by the wellbore itself. It should be noted that these can also be used to constrain S_{hmax}: the width of wellbore breakouts depends on the differential stress involved; while plotting the failure criteria for DITFs on the stress polygon can also narrow down the possible range of values (Figure 21).

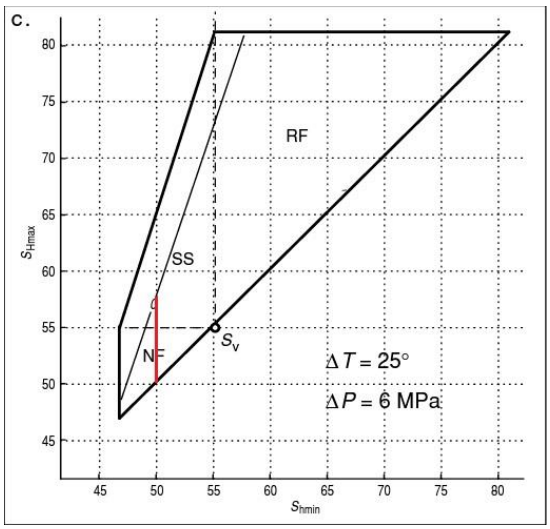

Figure 21: Example of constraining Shmax with a stress polygon. Dashed lines represent the limit between Anderson's faulting regimes. The outer boundaries of the polygon are determined based on frictional failure equilibrium theory assuming a frictional coefficient of 0.6. The 0 line is the failure criteria for DITF if the temperature difference between the mud and the formation is 25° with an excess mud pressure of 6 MPa. If S_{hmin} is also known to be 50 MPa at this depth, this gives a possible range for S_{hmax} highlighted by the red line. Figure modified from (M. D. Zoback, 2007).

Orientation of wellbore breakouts

Wellbore breakouts are fractures formed around the wellbore by compressive failure that locally give an increase to wellbore diameter. They occur in pairs on opposite sides of a wellbore; often resulting in a distinct elliptical shape. These compressive fractures form; where stress trajectories become "squeezed" around the wellbore resulting in a local increase in hoop stress (the stress around the wellbore). In a vertical well these areas of locally increased hoop stress can be found 90 degrees away from S_{hmax}; or at the azimuth of S_{hmin}. The azimuth of breakouts were earlier commonly measured with caliper log; nowadays FMI tool is standard.

A few previous studies have looked at caliper logs from wells in and around the Snøhvit field in order to determine S_{hmax} azimuths in the area. The findings of these papers were incorporated into the stress model used in this study. That process is further detailed in the Results chapter.

Reservoir pore pressure

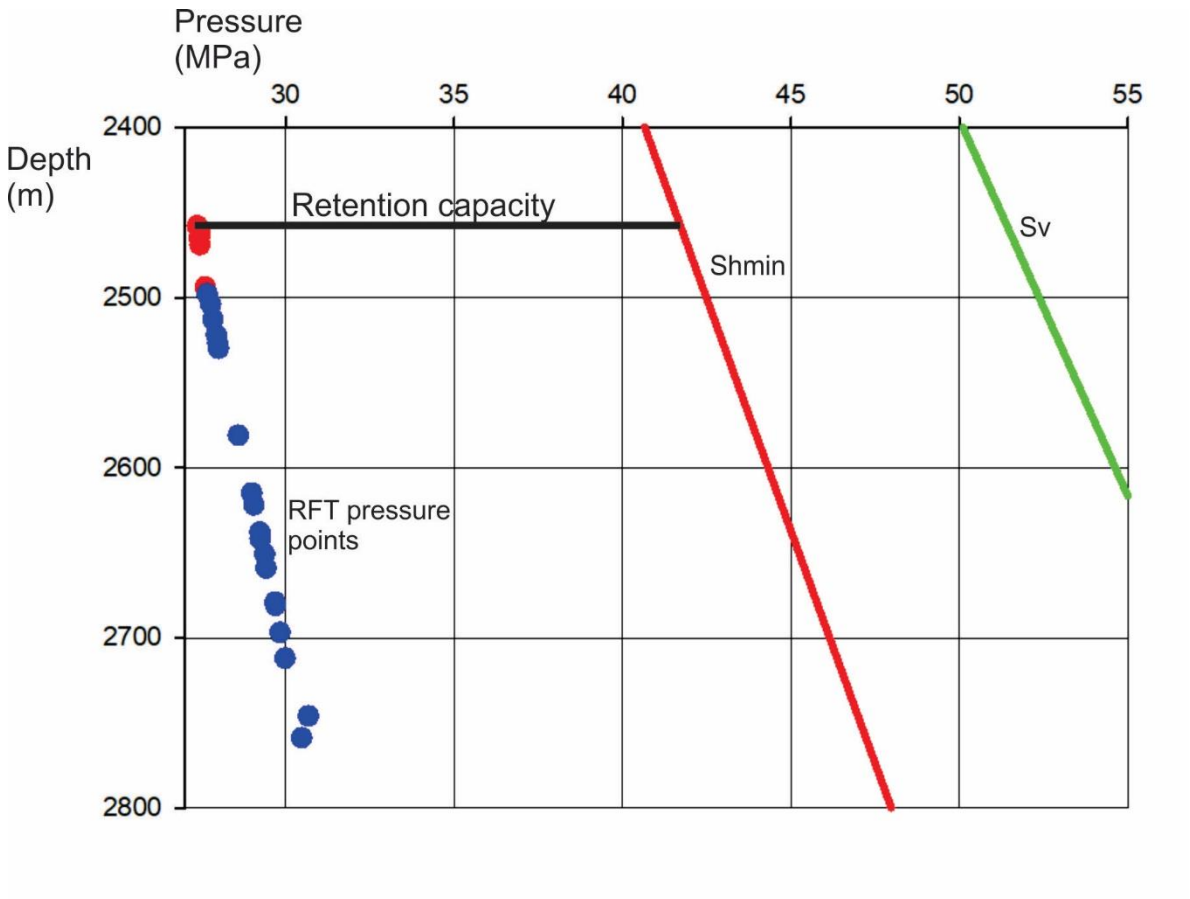

Figure 22: Retention capacity is a commonly used parameter to measure a trap's dynamic capacity. It assumes that the controlling mechanism is hydrofracturing.

A dynamically constrained reservoir's ability to trap hydrocarbons is mainly influenced by an interplay between the regional stress patterns and the reservoir's pore pressure. Therefor it is very common to display a reservoir's state of stress using a diagram showing the stress gradients and the pore pressure together in a depth vs pressure space. This is very useful for both exploration and drilling operations;

since the initial water phase pore pressure of the reservoir, and a critical stress gradient (commonly taken as S3 or S_{hmin}) defines a pressure window. This pressure window is the amount of overpressure the trap can accommodate before failure.

When talking about dynamically constraiend traps, most commonly the critical pressure (the pressure the trap can tolerate before failure) is taken to be the minimum principal stress. This assumption however heavily relies on a number of factors, and can lead to erroneous interpreatations of the dynamic capacity of the trap; if not used cautiously. The minimum prinicpal effective stress equals the amount of pressure needed to open the weakest fractures perpendicular to S3. In other words, it assumes that the primary leakage mechanism out of a dynamically controlled trap would be by hydrofracturing (extensional failure) of preexisting, cohesionless fractures (Figure 22).

Since other fracture mechanisms can result in lower critical pressure gradients than S3; this thesis considers other critical pressures as well. In the pressure vs depth plots presented in the results chapter, two critical pressure gradients are displayed: one by assuming the shear failure of a cohesionless fracture with a frictional coefficient of 0.6; while the other also assuming shear failure of a fracture with the same frictional coefficient but with a cohesion of 3 MPa. The distance of the maximum recorded pressure to the former gradient is referred to as critical pressure (P_{pcrit}) in this work.

Pressure vs depth plots provide an overview of the different controlling mechanisms, and the possible hydrocarbon column heights; but does not contain spatial information e.g. the stress orientations. They are perfect for presenting retention capacities which take a single pressure value from the crest of the trap (Hillis & Nelson, 2005b); but are not suitable for the determination of critical pore pressure variations along a fault plane. Hence, when it comes determining the distance to failure on every point of a fault plane, the calculations and visualizations were done by Badley's TrapTester software by getting the distance (critical pressure perturbations (Figure 16.)) to the failure envelope from different points of the fault surfaces and plotting them on the faults.

As mentioned earlier, RFT pressure plots were also used to determine the fluid contacts in a trap. Since different fluids have different densities, the depth of fluid contacts are easily identifiable on RFT plots as a shift in the steepness of the curve. In the example below (Figure 23), a gas-water contact is defined on a seismic section of Snøhvit Nord with the help of a superimposed RFT plot created from measurements in the discovery wellbore.

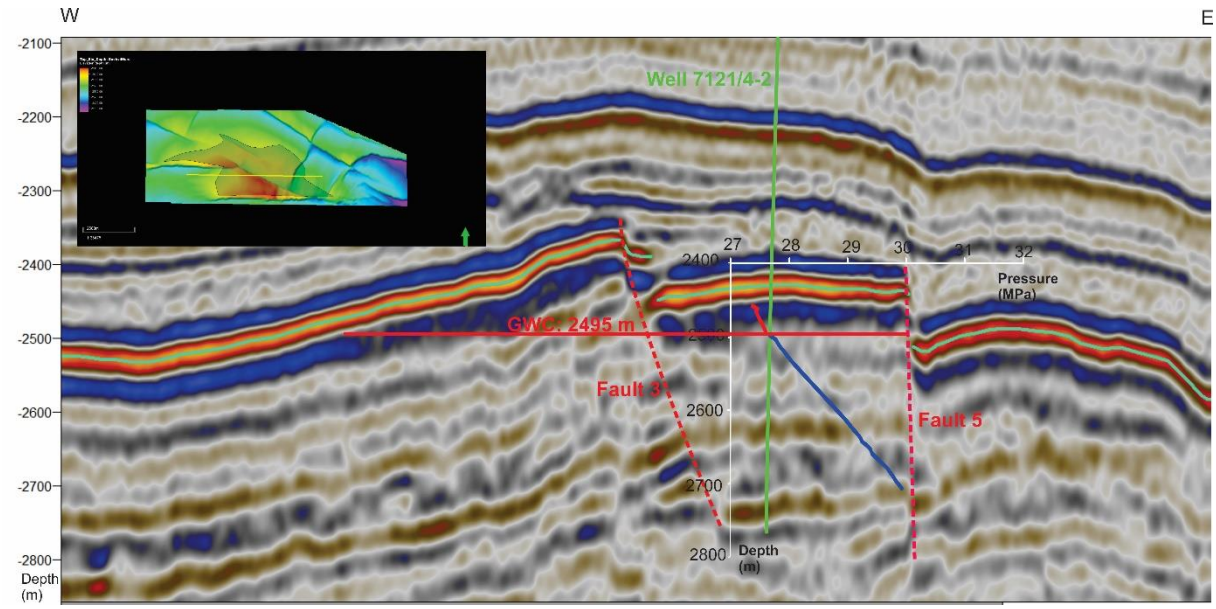

Figure 23: Method of determining initial fluid contacts from RFT logs. Example from Snøhvit Nord: RFT pressure log from well 7121/4-2 is superimposed on a seismic section of the trap.

Visualization of critical pressure perturbation on fault planes

The critical pressure perturbation (Ppcrit) is the amount of stress needed in a given stress field to induce slip on a fault surface of a given orientation. This parameter was visualized on fault planes with the help Badley's TrapTester. After interpretation in Petrel, the fault surfaces were exported into T7, where after specifying the stress field and pore pressure; Ppcrit was plotted on the fault surfaces with a color code. Two basic stress field models were created for the survey area with distinct pressure gradients: one for the shallower eastern parts (used for the Albatross, Albatross Sør, Snøhvit, Snøhvit Nord structures) (Table 1.); while another one for the deeper western parts (used at Albatross, Albatross Gamma, Albatross Vest, Albatross Beta and Delta Vest) (Table 2.). Due to the relatively low certainty with which the stress field can be determined; the faults at each of the structures were tested for 6 different stress scenarios (Table 1&2.). These scenarios were needed to cover the uncertainty of S_{Hmax} magnitude and orientation. In order to obtain a correct value of effective stress at reservoir level; the gradients within each of these scenarios had to be adjusted with sea depth, and overpressure. These two values were obtained from well completion reports of the discovery wellbore at each of the structures.

After specifying the stress field; T7 computes pressure vs depth profiles for each of the fields. From this; the Mohr diagrams for any given depth can be constructed. In our case the Mohr diagrams represent the state of stress at the top reservoir of the discovery wellbore. The following strep was defining a slip gradient. With that defined, the Mohr space could be color coded based on how far away is each point from the failure line. Here warm colors were chosen to represent closeness to failure, i.e. low Ppcrit or dynamic capacity. After importing the fault planes into T7, the software assigns points to the surfaces.

These points are then plotted on the Mohr diagram, from where the Ppcrit can be determined for each of these points. Lastly, with the help of the color code; Ppcrit values can be visualized on the interpreted surfaces and locations with higher risk of leakage can be identified.

5. Results

5.1. Reservoir state of stress

Determining the state of stress in a reservoir (stress orientations and magnitudes, pore pressure) is the most important step when investigating the dynamic capacities of traps. Scarcity of relevant available data from the area of investigation is an issue here. As a result, this thesis also relies on the small number of studies conducted in the Barents Sea that make estimations on the stress regime in the area. Generalizations were made on the stress regime, with the introduction of the regional stress regime concept. In the regional stress regime model data from the whole of the Hammerfest Basin was used to establish stress orientations and magnitudes on a broader regional scale; to which pore pressure data from the individual prospects can be compared. Based on previous studies, two regional stress models seem to be reasonable. The two base regional stress models are called Snøhvit (Table 1) and Askeladd (Table 2). The former was used for the two Albatross and two Snøhvit structures, while the latter is for the Askeladd structures and Delta Vest in the Western part of the study area. Within these two base models different stress scenarios were created to account for the uncertainty of S_{Hmax} magnitude and orientation. All of these scenarios were applied to the individual structures. Reservoir state of stress were calculated at each structure for each stress scenario by applying the base stress model's gradients to reservoir depth, pore pressure and water depth.

After determining the stress field, pressure points from the reservoirs were plotted along with the principal stress gradients and some failure gradients. The process of establishing these gradients for the stress models is detailed in the next two sections.

5.1.1. Stress regime

An important aspect of any stress regime is the type of active faulting involved (faulting regime). A low degree of seismicity in the Barents Sea region makes it difficult to determine the current faulting regime through the usual analysis of earthquake focal mechanisms. However, most of the studies assume a normal faulting regime similar to other parts of the Norwegian shelf (L. Chiaramonte et al., 2011). This is reasonable, based on the relative low stress anisotropy observed in the area. L. Chiaramonte et al. (2011) assumes a normal-fault/strike slip regime to account for a relatively large S_{Hmax}.

In a SS/NF stress regime the orientation of S_{hmax} is decisive in the question of fault permeability. Gölke and Brudy (1996) have reported that on a regional scale, the E-W orientation observable in the North Sea undergoes a progressive clockwise rotation into a N-S orientation at the Barents Sea. The main cause of this N-S oriented S_{hmax} is thought to be ridge push from the Nansen Ridge to the north. This means, that this stress regime is a direct result of the opening of the Atlantic Ocean, thus it is assumed

that it started no later than Oligocene times. Some studies however, including that of Linjordet and Grung Olsen (1992) who used observations of borehole breakouts in Snøhvit wells, have noted that local variations (especially around active faults) in orientations and magnitudes can be observed.

Lastly, regional stress gradients were determined and placed into this model. The largest stress gradient in this model is the vertical stress (overburden). In this analysis, the regional S_v gradient of 23.1 MPa/km is going to be used for the Snøhvit base model, and 23.7 MPa/km for the Askeladd base model. The former is from the density log of well 7120/9-1; while the latter is derived from the same log of well 7120/8-2.

5.1.2. Methods for estimating Shmin via xLOT

Leak-off tests (LOT) are the most common type of method for determining the minimum principal stress. These tests are usually preformed in the earliest stages of a new well section; after they drilled through the casing shoe and the cement of the previous section. The determination of S3 is done via the interpretation of pressure vs time plots of LOT tests. Technical terms related to these plots include the leak-off pressure (LOP), formation breakdown pressure (FBP), fracture propagation pressure (FPP), instantaneous shut-in pressure (ISIP) and fracture closure pressure (FCP). The number of studies concerned with different ways of interpreting these plots is extensive; however there seems to be an agreement that in the most simple case S3 can be approximated by LOP and ISIP. According to Raaen et al. (2006) the only reliable pressure value that is directly connected to S3 is the fracture closing pressure.

Two S_{hmin} gradients needed to be determined for the two base stress models. For the Snøhvit base models an xLOT from a Snøhvit injection well (7121/4-F-2H) was used. This gave a regional S_{hmin} gradient of 15.6 MPa/km. Similarly, the S_{hmin} gradient of 16.5 MPa/km for the Askeladd base model was obtained from xLOT data of well 7120/8-4.

A critical pressure related to fault reactivation (P_{pcrit}) is also plotted. For this, I assumed a cohesionless fracture with no tensile strength and with a frictional coefficient of 0.6. A failure envelope for this hypothetical fracture was plotted in Mohr space together with S_{hmin} and S_v corresponding to different crustal depths with the gradients given above. After this a pore pressure induced failure of the fracture was simulated by shifting the Mohr circle towards the envelope until it touches it (Figure 24). This exercise was done at several depths with the stress gradients of both base models. The result is two P_{pcrit} gradients for the two base models that in theory represent the failure line of a cohesionless fault surface with a coefficient of friction of 0.6. This gradient is 12 MPa/km in the Snøhvit, and 13.1 MPa/km in the Askeladd base model.

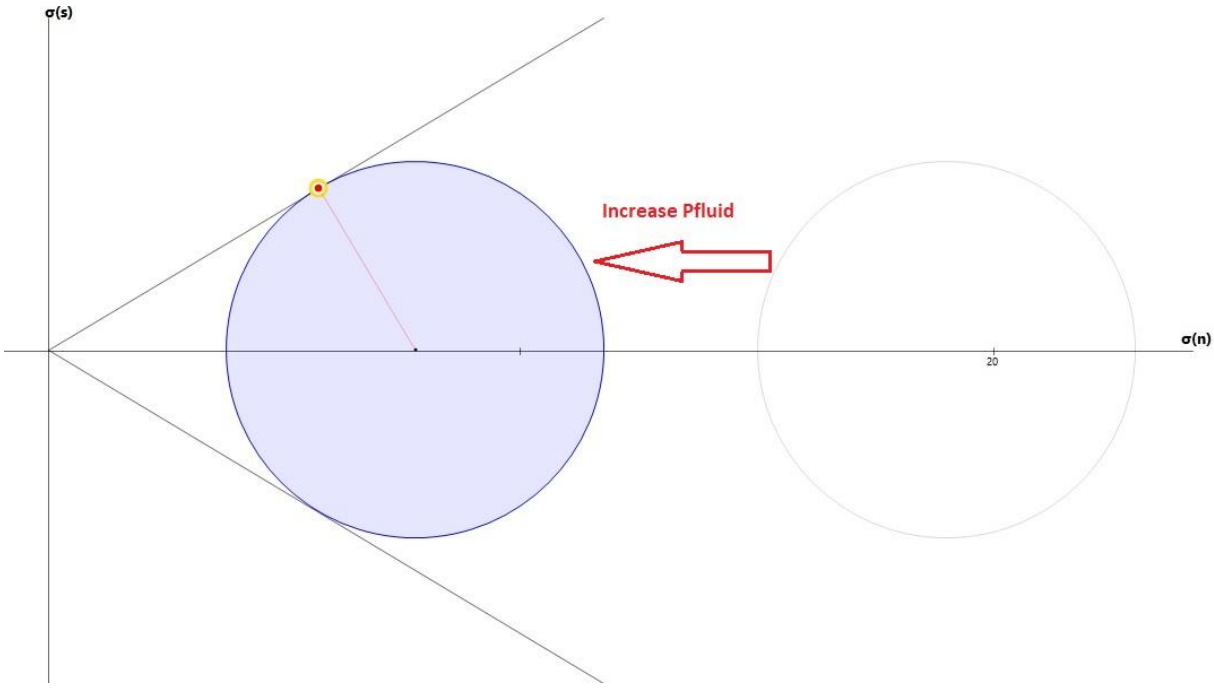

Figure 24: (previous page) Increasing the fluid pressure until the Mohr circle touches the failure envelope determines the failure gradient for the given type of failure in a given stress field.

A failure line for faults with 3 MPa cohesion and 0.6 coefficient of friction was also plotted on the individual stress diagrams of the fields. Instead of determining a regional gradient, the failure line was only determined at the level of the reservoirs by bringing a Mohr circle representative of the state of stress at reservoir level to failure with an envelope of said cohesion and friction. This is because for this

Askeladd base stress model (Ppcrit: 13.1 MPa/km)	Shmin (MPa/km)	SHmax (MPa/km)	Sv (MPa/km)	SHmax orientation
SH160_Sh	16.5	16.5	23.7	160°
SH160_12	16.5	19.8	23.7	160°
SH160_Sv	16.5	23.7	23.7	160°
SH160_SHmax	16.5	51.2	23.7	160°
SH180_Sh	16.5	16.5	23.7	180°
SH180_12	16.5	19.8	23.7	180°
SH180_Sv	16.5	23.7	23.7	180°
SH180_SHmax	16.5	51.2	23.7	180°

type of failure it is not possible to determine a linear gradient for all depths; since the Griffith failure envelope itself is not linear at lower stresses (shallow depths).

Table 1: (Previous page) Askeladd base stress model and the stress scenarios

The individual pressure profiles of the investigated prospects were then plotted on this regional stress model. The data used here were RFT pressure measurements from the discovery wells. All of the points were taken from the hydrocarbon charged parts, or from the main Middle Jurassic reservoirs. Plotting of the RFT measurements resulted in pressure profiles from the reservoir levels. Table 1 and 2 below summarize the stress gradients used in the two base stress models and the different stress scenarios. Table 3 is the summary of the reservoirs' state of stress.

Snøhvit base stress model (Ppcrit: 12 MPa/km)	Shmin (MPa/km)	SHmax (MPa/km)	Sv (MPa/km)	SHmax orientation
SH160_Sh	15.6	15.6	23.1	160°
SH160_12	15.6	18.7	23.1	160°
SH160_Sv	15.6	23.1	23.1	160°
SH160_SHmax	15.6	48.4	23.1	160°
SH180_Sh	15.6	15.6	23.1	180°
SH180_12	15.6	18.7	23.1	180°
SH180_Sv	15.6	23.1	23.1	180°
SH180_SHmax	15.6	48.4	23.1	180°

Table 2. Snøhvit stress model with the different stress scenarios

	Pressure	Overpressure	SHmin	RC	OpF	Ppcrit	Delta Ppcrit
Albatross	20.35	2.5	26.55	6.2	0.28	21	0.65
Albatross Sør	21	2.8	27.2	6.2	0.31	21.7	0.7
Snøhvit	26.52	3.6	33.94	7.42	0.25	26.64	
Snøhvit Nord	27.37	2.8	35.7	8.3	0.25	28.9	1.5
Askeladd	23.4	2.8	32.3	9	0.24	26.2	2.8
Askeladd Gamma	24.15	3	33.5	9.3	0.24	27.1	3
Askeladd Vest	26.6	2.8	37.8	11.2	0.2	30.5	4
Delta Vest	31.5	2.8	45.6	14.1	0.165	36.75	5.25
Askeladd Beta	27	4.5	35.2	8.2	0.35	28.5	1.5

Table 3. Summary of reservoir state of stress

5.2. Reservoirs' state of stress and slip stabilities

In the following section a short description of each of the structures are followed by a summary of the reservoir's state of stress and dynamic capacities. Slip stabilities in the different stress scenarios are also presented here.

Albatross

Albatross is a gas discovery located at the edge of an Upper Jurassic platform that trends roughly E-W within the Hammerfest Basin. The northernmost edge of Albatross is delineated by an E-W trending, N dipping normal fault that considerably deepens the basin towards the north, creating a closure in the Middle Jurassic reservoirs (Figure 25). The southern edge is bordered by south dipping normal faults with similar strikes. At the western edge of the discovery, a zone of acoustic masking can be observed.

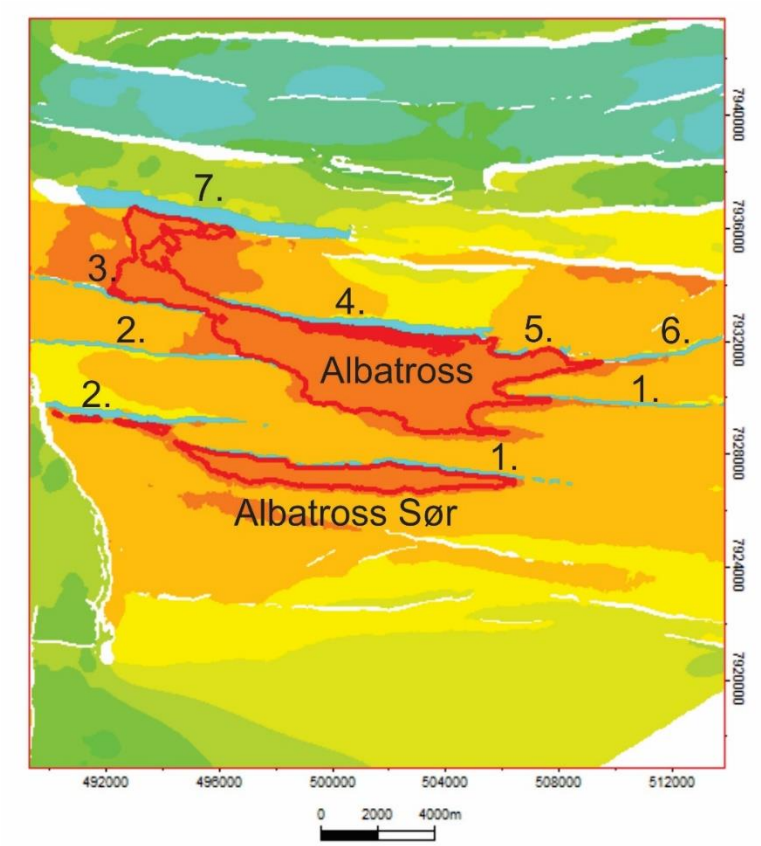

Figure 25: Faults and GWC of Albatross and Albatross Sør. GWC is shown by red line. See figure 18 for the color bar.

Discovery well 7120/9-1 hit the structure in the center. The hydrocarbon zone was hit at a depth of 1817 m below sea level, while the GWC at 1881 m. Pressure profiles derived from RFT data show a gas gradient of 0.084 psi/ft corresponding to 1.90 MPa/km (Figure 26). Pressure at the top of the gas column in the well reaches 20.35 MPa, while in the water zone just below the GWC it is 20.58 MPa. Overpressure at the top of the gas column is around 2.5 MPa. Given the regional gradient of S_{hmin} of

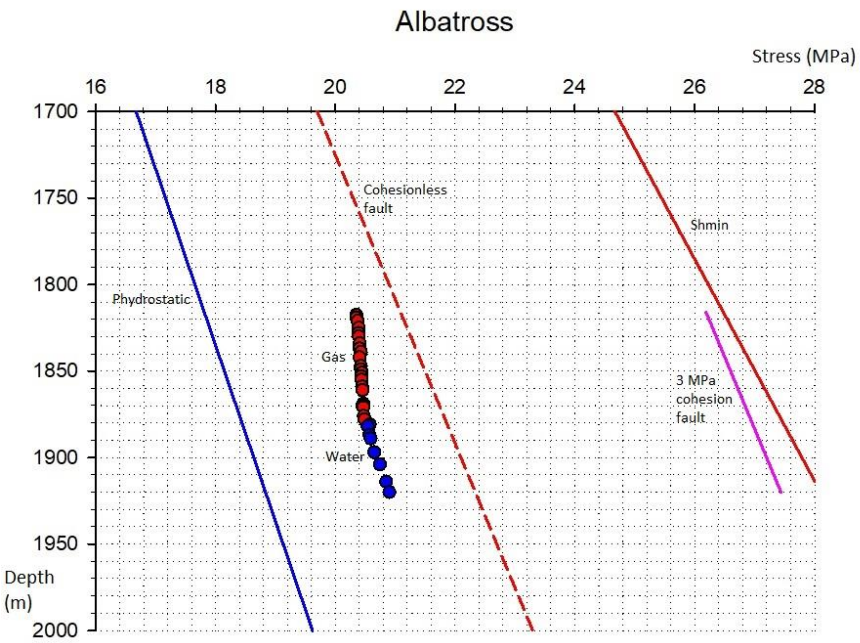

Figure 26: (previous page) RFT plot of Albatross

15.6 MPa/km, and a water column of 320 m on the spot; a hydraulic fracture limit of 26.55 MPa can be assumed at the top of the gas column. This gives an RC of around 6 MPa, with an OpF (overpressure factor) of 0.28. Meanwhile P_{pcrit} without a cohesion at this depth can be assumed to be around 21 MPa, which is within 1 MPa from the observed pore pressure. Meanwhile the P_{pcrit} for a fracture with 3 MPa cohesion would be around 26.2 MPa at this depth.

In the SH160_Sh case faults 2, 3, 4 and 7 on the western side of the structure seem to be closer to failure with critical pressures reaching below 2 MPa (Figure 27). Meanwhile, the three on the eastern part remain with a moderate critical pressure. Increasing the S^{Hmax} will lead to a considerable increase in fault stability in this scenario resulting in critical pressures in excess of 10 MPa on most of the fault surfaces (Figure 28 & 29).

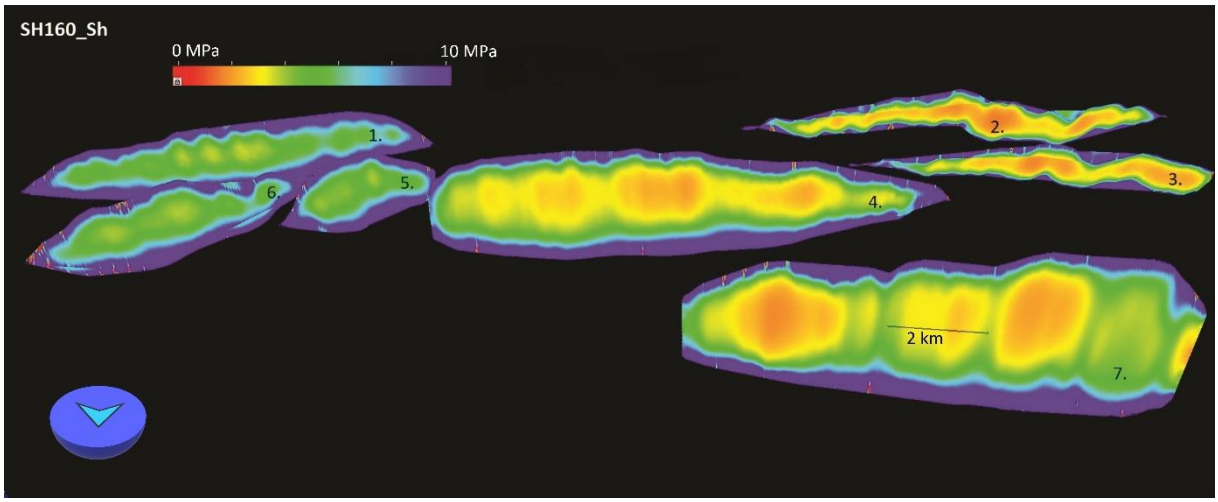

Figure 27: Slip stabilities at SH160_Sh on Albatross

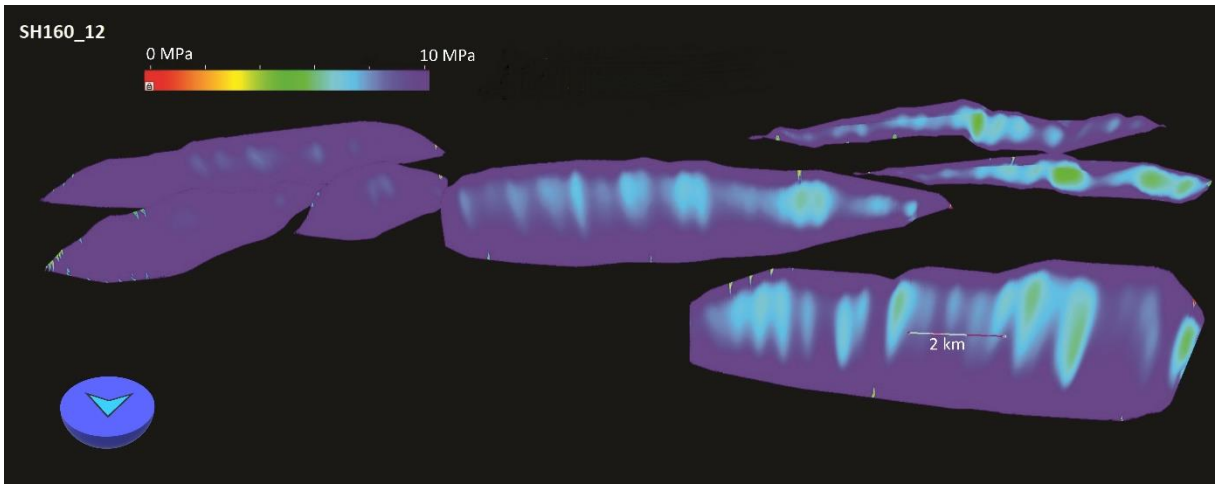

Figure 28: Slip stabilities at SH160_12 on Albatross

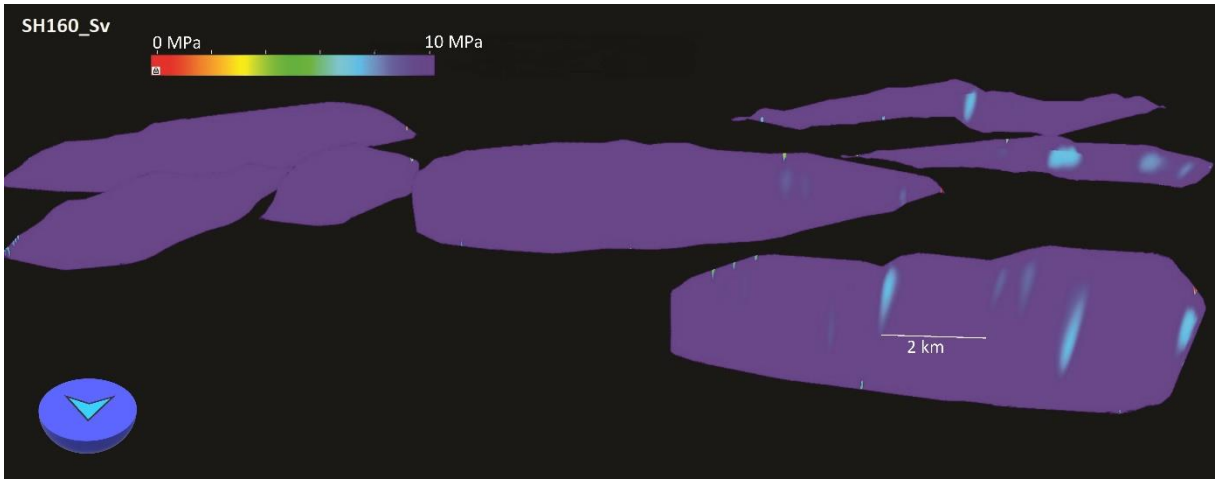

Figure 29: Slip stabilities at SH160_Sv

In the SHmax180 stress scenarios the very same pattern can be observed.

Albatross Sør

Albatross Sør is situated south of Albatross (Figure 25). Both structures can be found in the shallowest part of the survey area; where north dipping fault blocks dominate. Both Albatross discoveries are towards the axis of the basin, where these fault blocks become the shallowest. Albatross Sør is delineated by one major north dipping fault towards the north; while towards the south the gas column tapers off to zero before reaching the next fault zone.

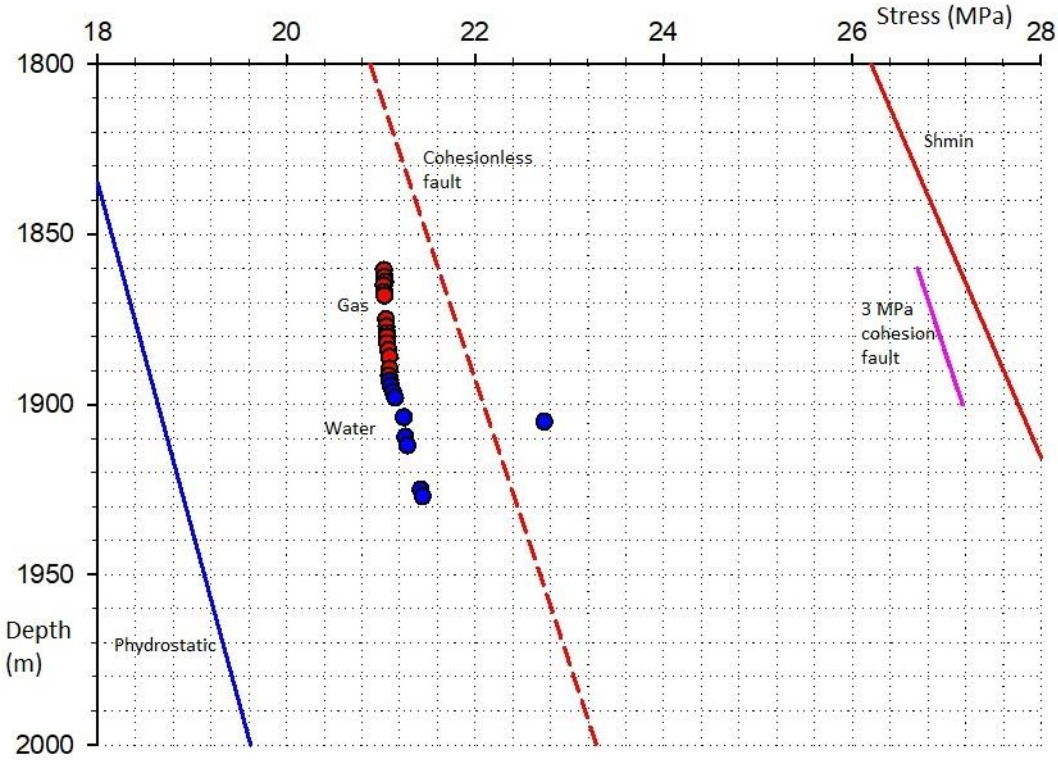

Figure 30: RFT plot of Albatross Sør from well 7121/7-2

Discovery well 7121/7-2 hit the top reservoir at 1860 m below sea level. Based on RFT measurements the GWC was recognized at 1892 m. Pressure at the top of the gas reaches to 21 MPa, while at the GWC it gets close to 22 MPa (Figure 30). The hydrostatic pressure at this depth can be expected around 18.2 MPa, which gives a slight overpressure of 2.8 MPa. The hydraulic fracture limit is around 27.2 MPa, which means RC is around 6.2 MPa. OpF is at 0.31. Similarly, to Albatross however the dynamic capacity seems to be much lower if we consider P_{pcrit} for shear failure in cohesionless fractures: at this depth it can be expected to be around 21.7 MPa, which is within 1 MPa away from the actual pore pressure.

In the SH160_Sh scenario slip stability is lowest on fault 2 at the west of the structure. Similarly to the ones on Albatross, the critical pressure here comes within 2 MPa. On fault number 1 and on the smaller fault segment to the south (number 3) critical pressures rarely go below 4 MPa (Figure 31). With an increase in S_{Hmax} gradient, the fault planes become more stable until S_v is reached (Figure 32 & 33). Again, the orientation of S_{Hmax} does not affect the critical pressures in the different scenarios: SH180 scenarios came out with the same results.

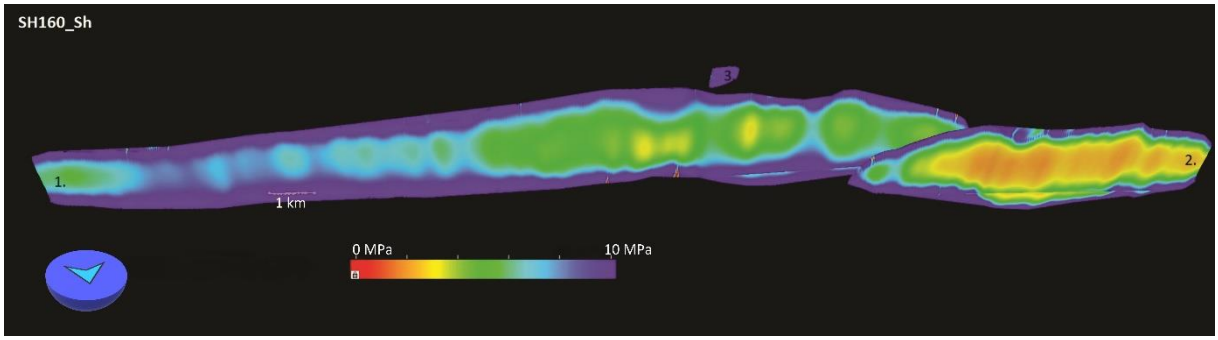

Figure 31: Slip stabilities at SH160_Sh on Albatross Sør

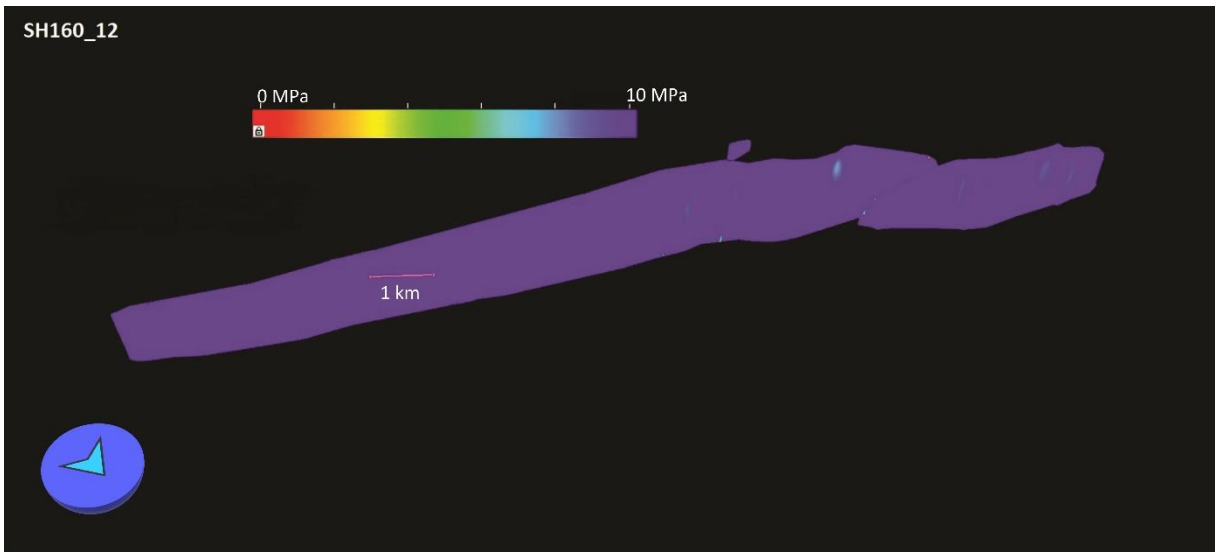

Figure 32: Slip stabilities at SH160_12 on Albatross Sør

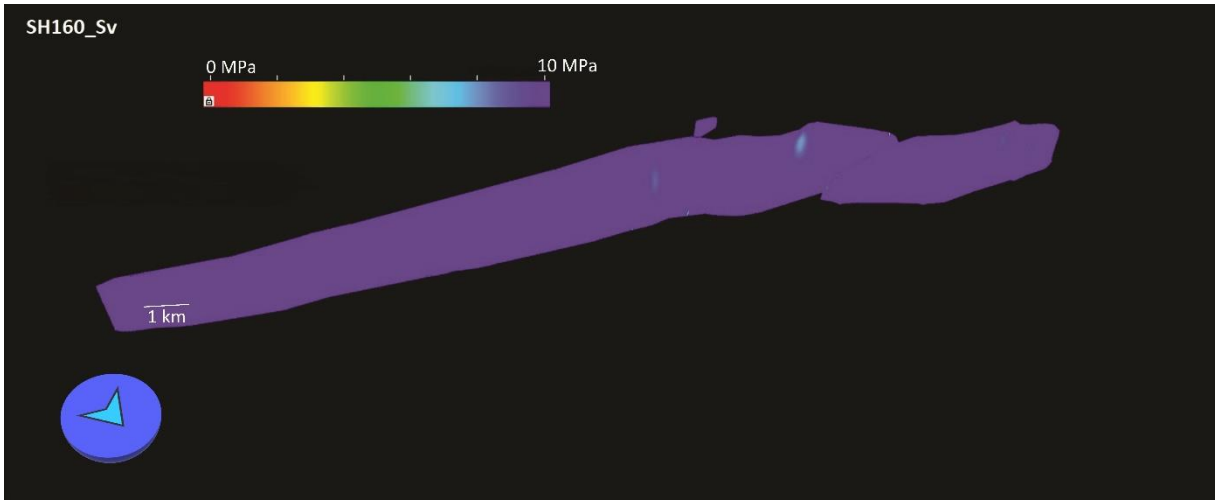

Figure 33: Slip stabilities at SH160_Sv on Albatross Sør

Snøhvit

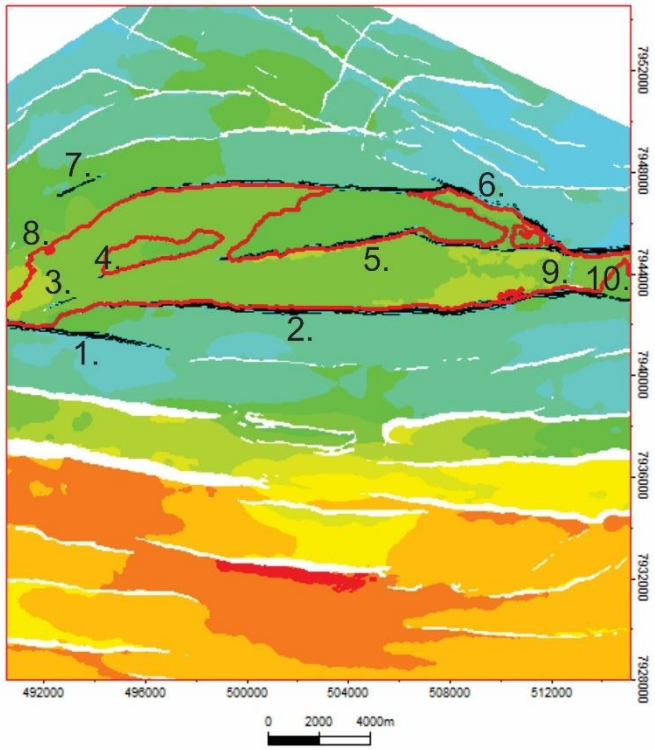

Figure 34: Faults and HWC at Snøhvit. See figure 18 for color code.

Snøhvit is an oil and gas discovery lying in the northern, deeper half of the basin characterized by horst-graben structures. The E-W trending structure is delineated by E-W normal faults on the northern and

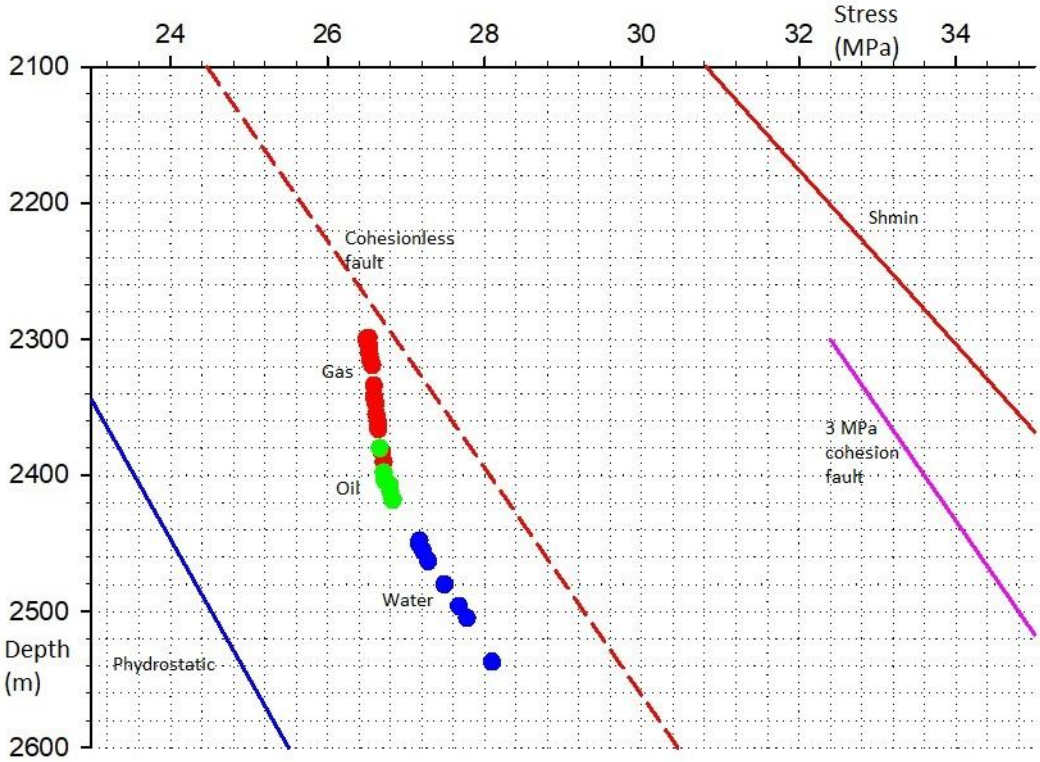

Figure 35: RFT pressure plot of Snøhvit from well 7121/4-1

southern edge, and SW-NE and SE-NW fault segments on the eastern and western edges (Figure 34).

Similarly to Albatross, the seismic data is degraded by a zone of acoustic masking to the west, while another masking zone can be observed close to the NE corner of the structure.

Figure 36: Slip stabilities at SH160_Sh at the southern edge of Snøhvit

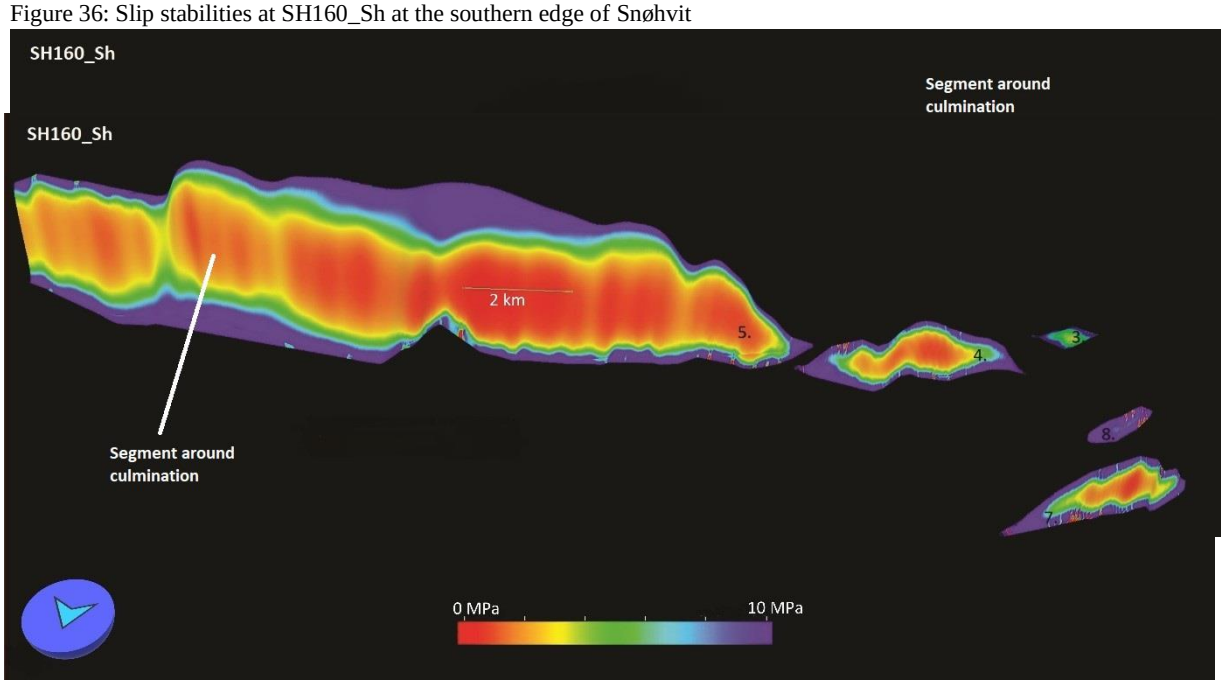

Figure 37: (previous page) Slip stabilities at SH160_Sh on fault 5

Discovery well 7121/4-1 encountered gas in the Stø and Nordmela formations from 2296 m. A GOC was identified at 2403 m, while the OWC at 2420 m. RFT pressures show a gas gradient of 0.09 psi/ft or about 2 MPa/km; and an oil gradient of 0.32 psi/ft (7.23 MPa/km) (Figure 35). At the top of the hydrocarbon column in the well the pressure reaches 26.52 MPa, while at the bottom the water phase pressure is at 27.17 MPa. S_{hmin} at depth can be expected at 33.94 MPa, while hydrostatic pore pressure would be at 22,92 MPa. This gives an RC of 7.44 MPa, with an OpF of 0.33. P_{pcrit} at the top of the HC column can be assumed at 26.64 MPa.

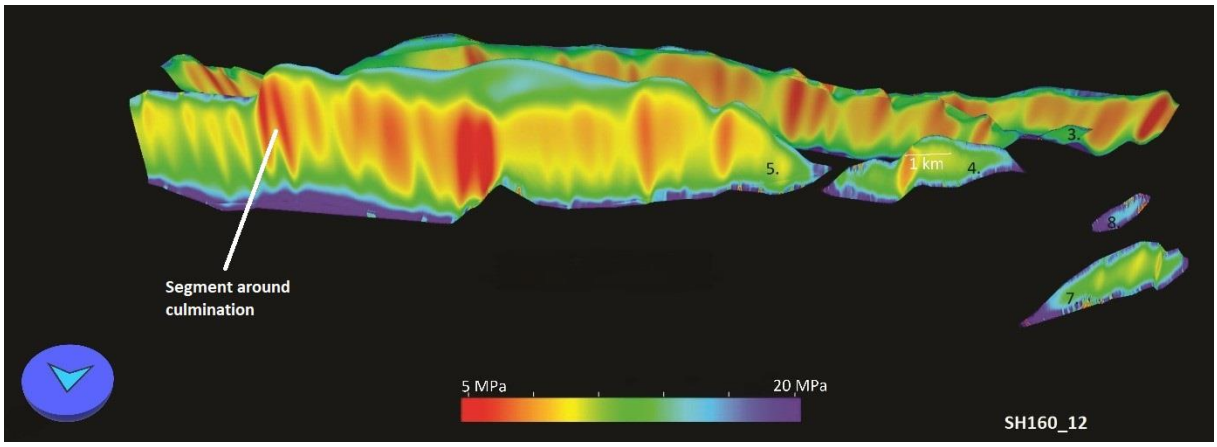

Figure 38: Slip stabilities at SH160_12 from the north side of Snøhvit

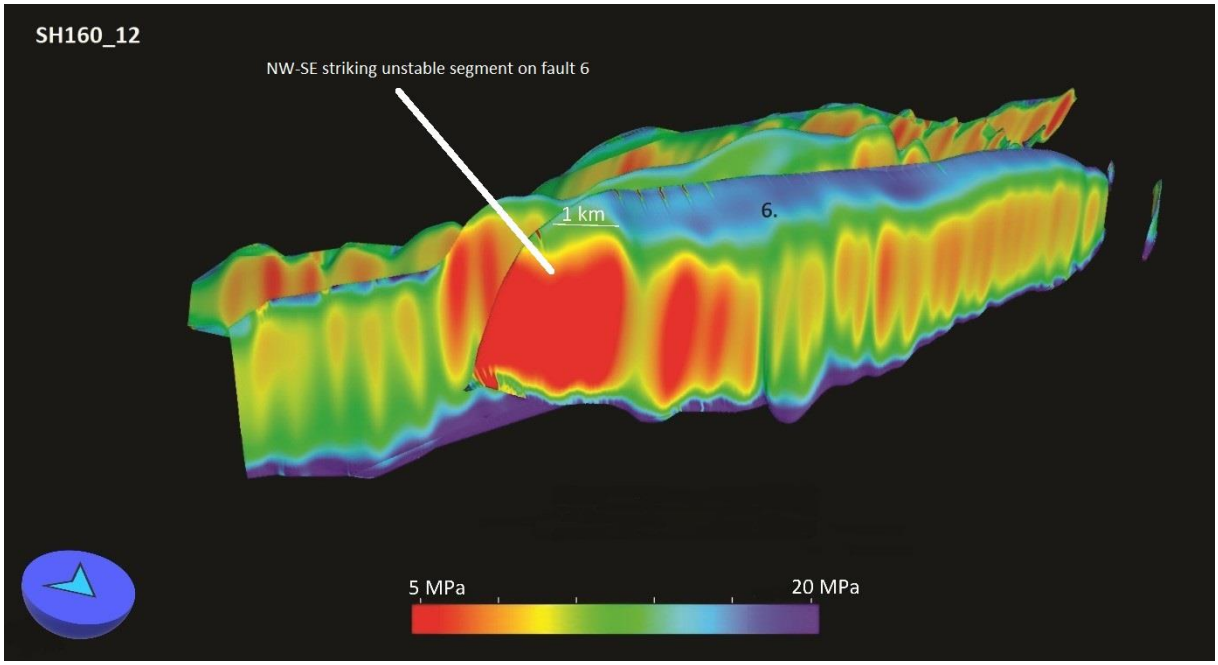

Figure 39: Slip stabilities at stress scenario SH160_12 on fault 6

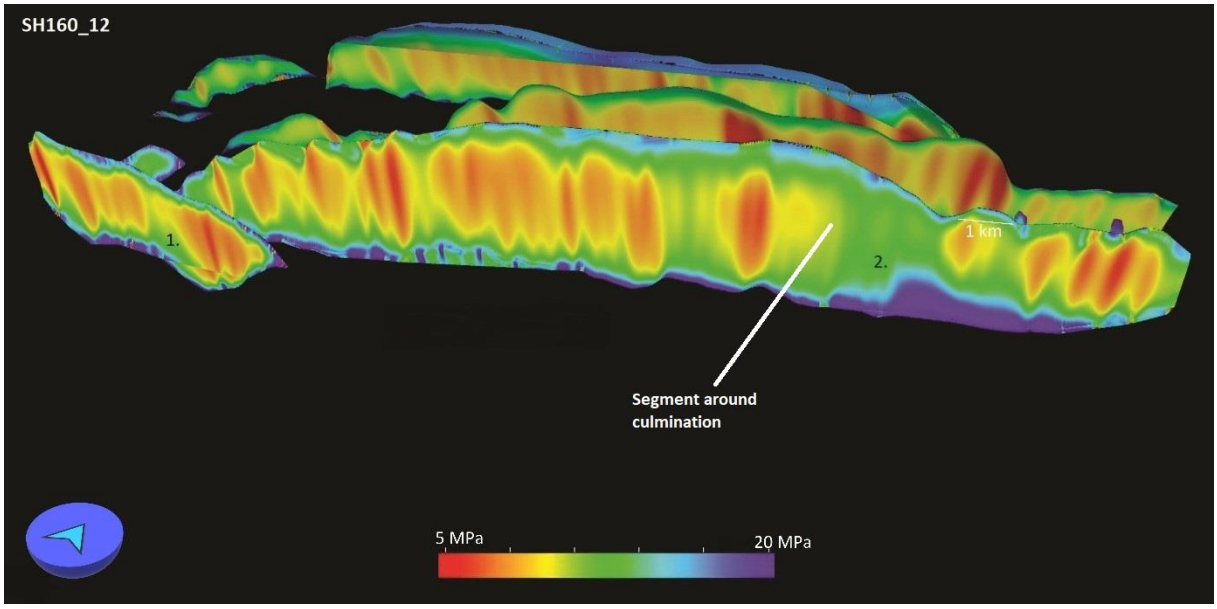

Figure 40. Slip stabilities at SH160_12 on the southern faults at Snøhvit

In the SH160_Sh case all the major faults delineating and crosscutting the structure show low critical pressures. With the exception of fault 8, 3, 9 and 10 all faults have segments where the critical pressure goes below 2 MPa (Figure 36 & 37). Major critical areas extend along the strikes of these faults, resulting in an overall high risk on the whole structure. With an increasing S_{Hmax} gradient two things happen: fault segments with higher risk become more localized, but at the same the absolute magnitude of critical pressure increases. As a result, these localized critical segments do not pose as big of a risk to fault leakage as in the case of a 2D stress field. Nevertheless, the spatial distribution of critical segments in these stress fields can still correlate with the ones in the SH160_Sh scenario. Hence, it is still worth emphasizing that in the SH160_12 and SH160_Sv scenarios the middle parts of fault 5 and the more NW-SE striking segments of fault 6 seem to have lower critical pressures (Figure 38, 39, 41, 42). Both of these segments can be found on the Eastern, Northeastern parts of the structure.

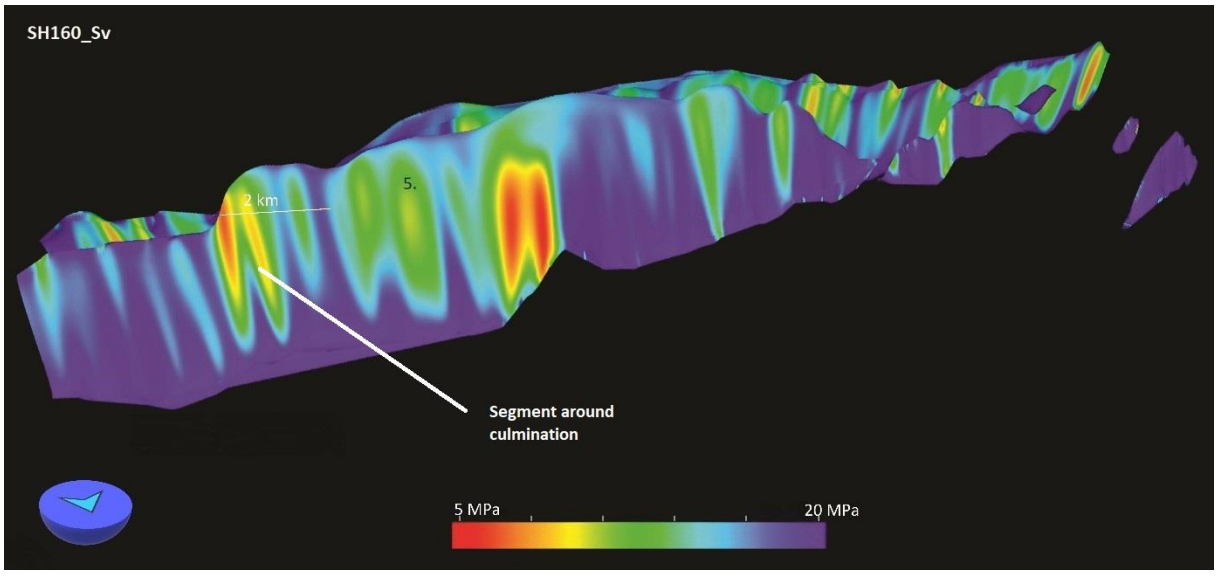

Figure 41 (previous page): Slip stabilities at SH160_Sv on fault 5

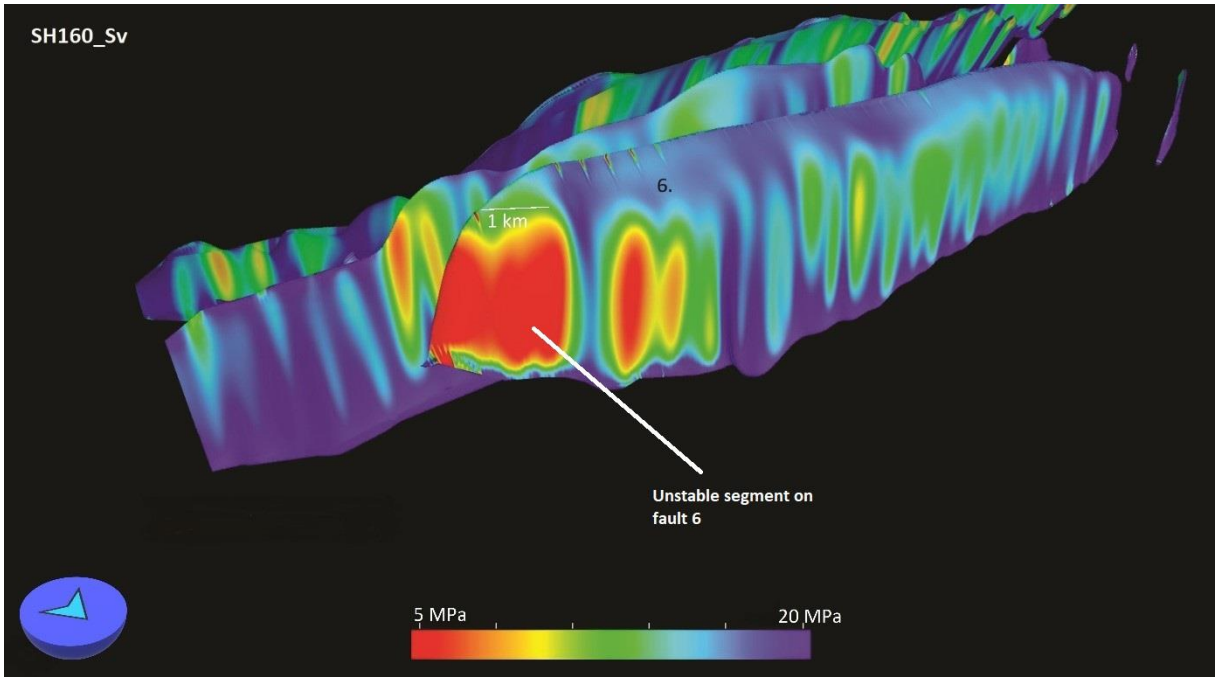

Figure 42. Slip stabilities at SH160_Sv on fault 6

In the SH180 scenarios the same trend can be observed. Naturally, some difference appears in the locations of the critical segments that is due to the different horizontal stress orientations. The NE-SW striking smaller faults (3,7,8) and the two N-S segments at the Eastern edge of the field (9, 10) also become favorably oriented in SH180_12 and SH180_Sv (Figure 43, 44, 45).

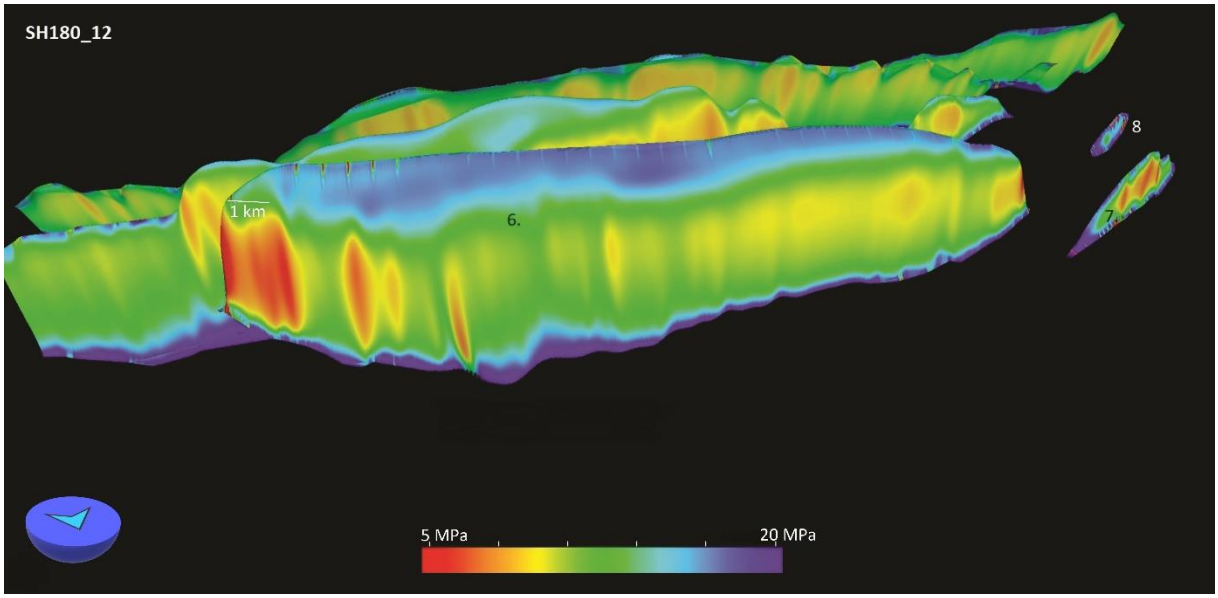

Figure 43. Slip stabilities on the north side of Snøhvit at SH180_12

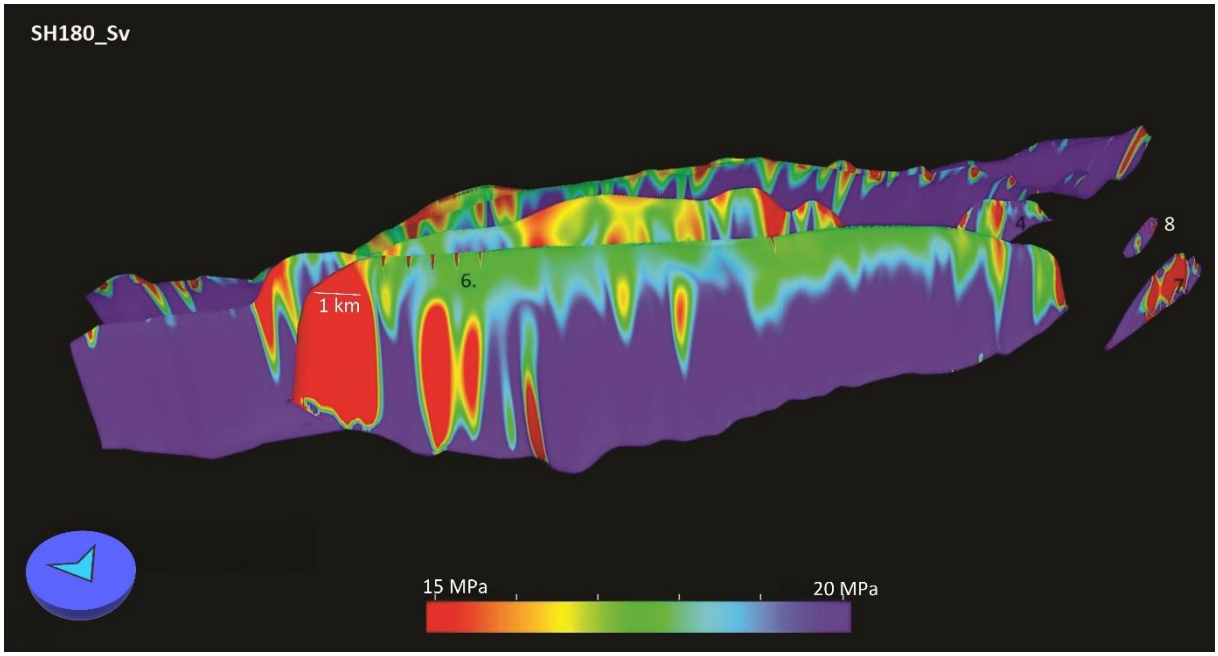

Figure 44. Slip stabilities on the north side of Snøhvit at SH180_Sv

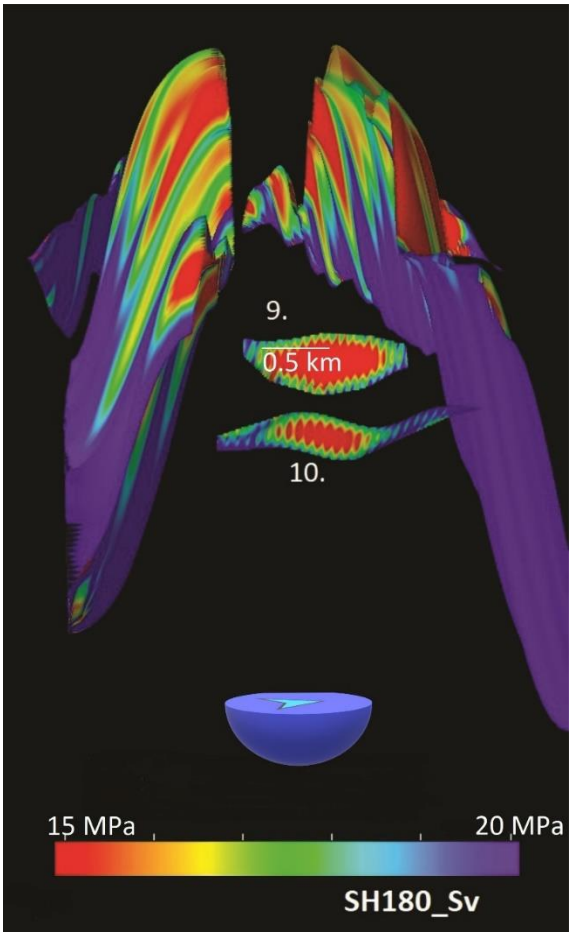

Figure 45. Slip stabilities on faults 9 and 10 at SH180_Sv.

Snøhvit-Nord

Wildcat well 7121/4-2 hit Snøhvit Nord in a horst just north of Snøhvit. The southern edge of the prospect is delineated by southerly dipping normal faults. Towards the north a gentle antiform creates closure in a different fault block (Figure 46).

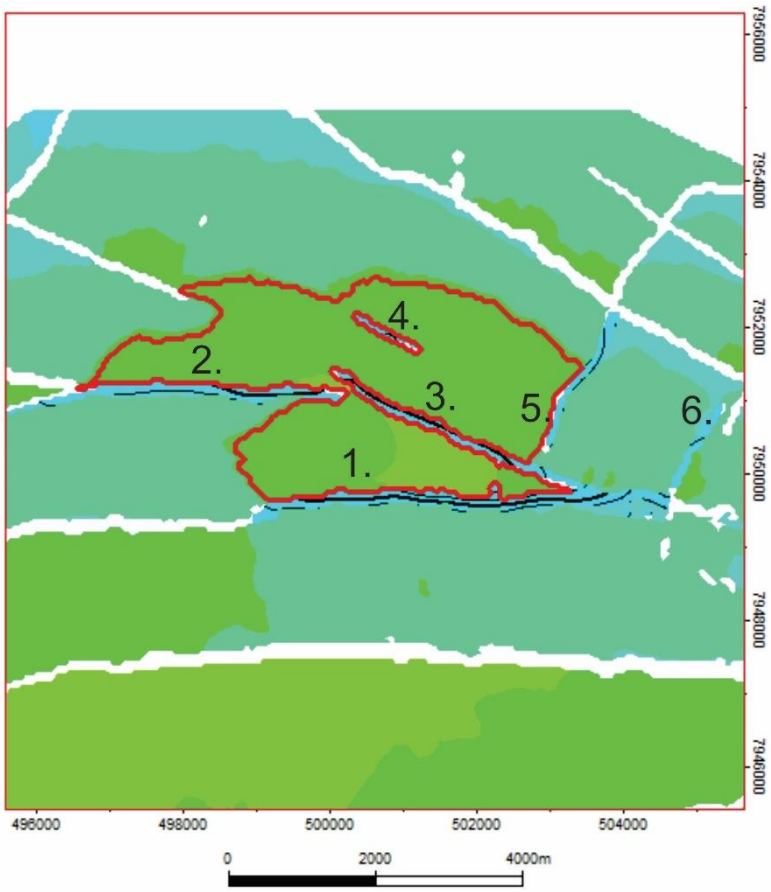

Figure 46. Faults and GWC at Snøhvit Nord. See figure 18 for color code.

The gas bearing Stø formation was hit at 2458 m below sea level, and the GWC was found to be at 2495 m. At the top of the gas pressure reaches 27.37 MPa, while at the GWC 27.67 MPa was measured (Figure 47). This means that the reservoir is only slightly overpressured, with approximately 2.8 MPa over hydrostatic pressure. A LOT just before hitting the reservoir has been performed in this well at 2460 m RKB. Leak-off occurred at a pressure equivalent to a mud weight of 1.86 g/cm3 corresponding to 38.7 MPa. The regional Shmin gradient of 15.6 MPa gives an Shmin value of 35.7 MPa. That is a difference of 3 MPa, but for the RC and OpF calculations the latter value will be used for conservative calculations. That still gives an RC of 8.3 MPa-a huge margin when taking into account the average natural gas densities. The OpF value from this is around 0.25; showing that despite the high absolute value of RC; the trap is probably much closer to its dynamic capacity thanks to a narrow mud window.

This is even more true to the critical pressure associated with cohesionless faults; which at this depth would be around 28.9 MPa; or less than 2 MPa away from the actual recorded pressure.

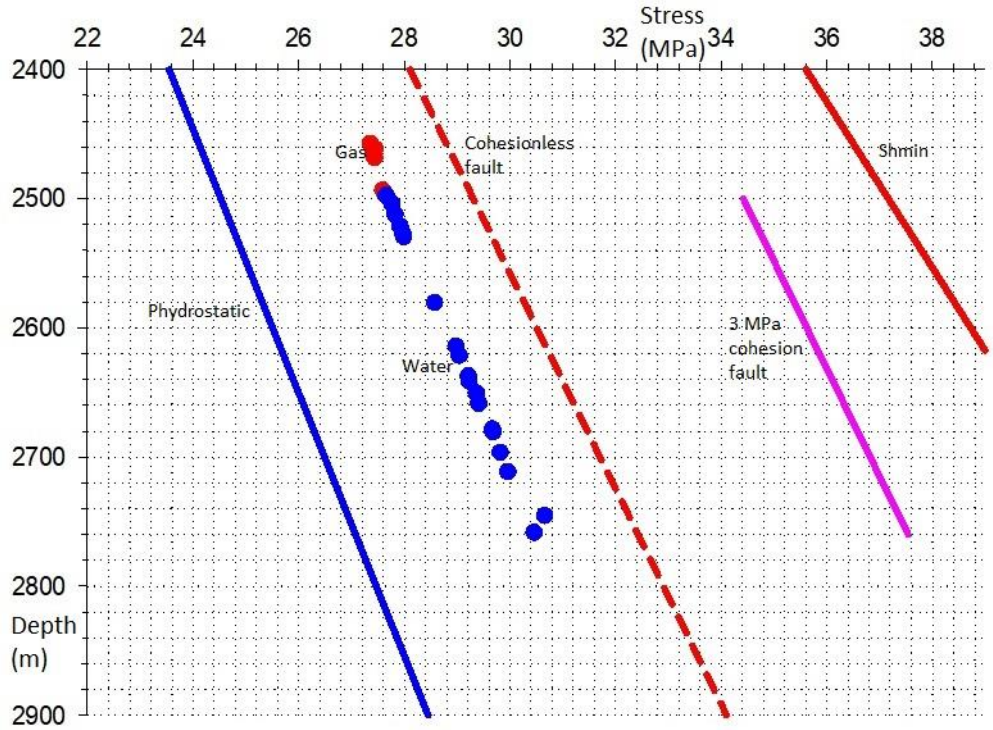

Figure 47. RFT plot for Snøhvit Nord from well 7121/4-2

When it comes to slip stability on faults; fault 1 is the most unstable in SH160_Sh scenario. This is the only fault plane that has considerably large segments with critical pressure perturbations of less than 2 MPa (Figure 48). Faults 2, 3 and 5 have critical pressures mostly between 4 and 6 MPa, while faults 4 and 7 have 10 MPa and above. Increasing S_{Hmax} will again increase slip stability as well, however different fault planes will be favorably oriented. In SH160_12 scenario all faults become more favorably oriented for failure except for faults 4 and 7; while in SH160_Sv scenario faults 3 and 5 would slip most easily (Figure 49).

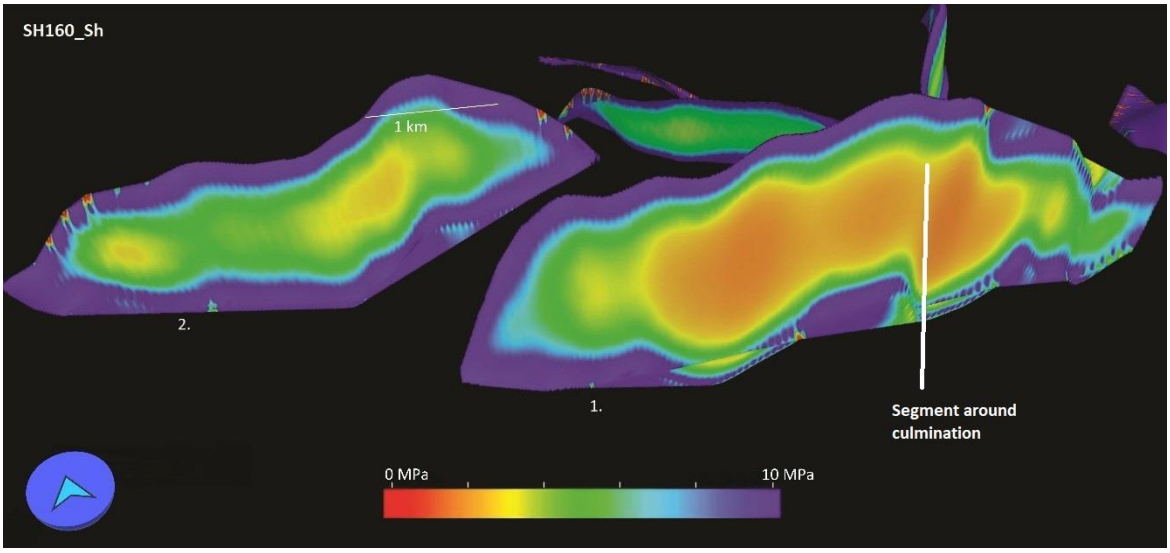

Figure 48 (previous page): Slip stabilities on the south side of Snøhvit Nord at SH160_Sh

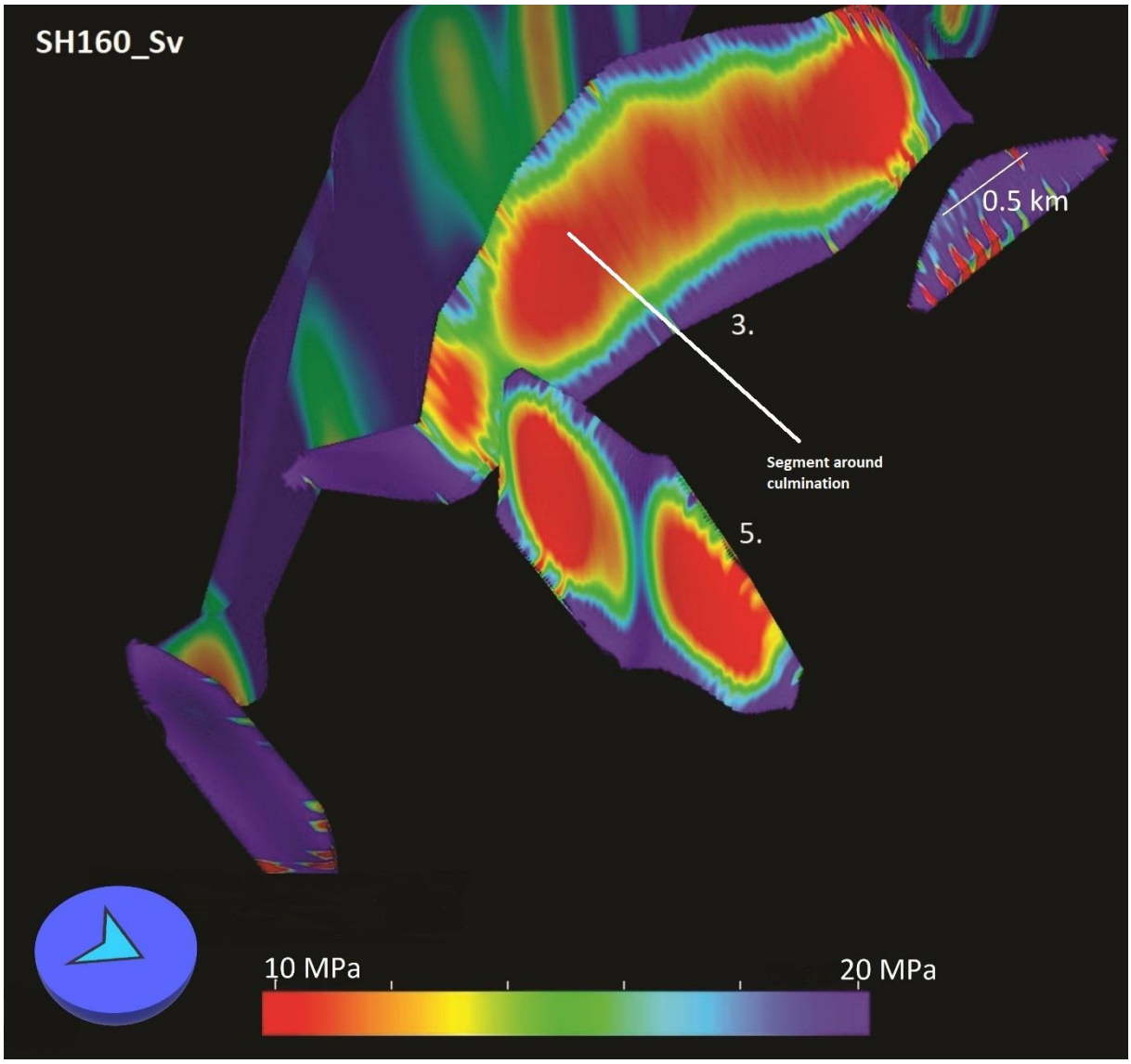

Figure 49. Slip stabilities on fault 3 and 5 at SH160_Sv

By nature a stress field that is isotropic in the horizontal plane is insensitive to horizontal stress orientations. Hence as usual SH180_Sh scenario produces identical slip tendencies as its SH160_Sh counterpart (Figure 50). Increasing S_{Hmax} in the SH180_12 scenario will lead to an increase in absolute slip stability. The most unstable fault in this scenario is fault 5 (Figure 51). The situation is very similar in scenario SH180_Sv with the difference that the role of fault 5 becomes even more pronounced as slip stabilities increase further on all the other faults (Figure 52).

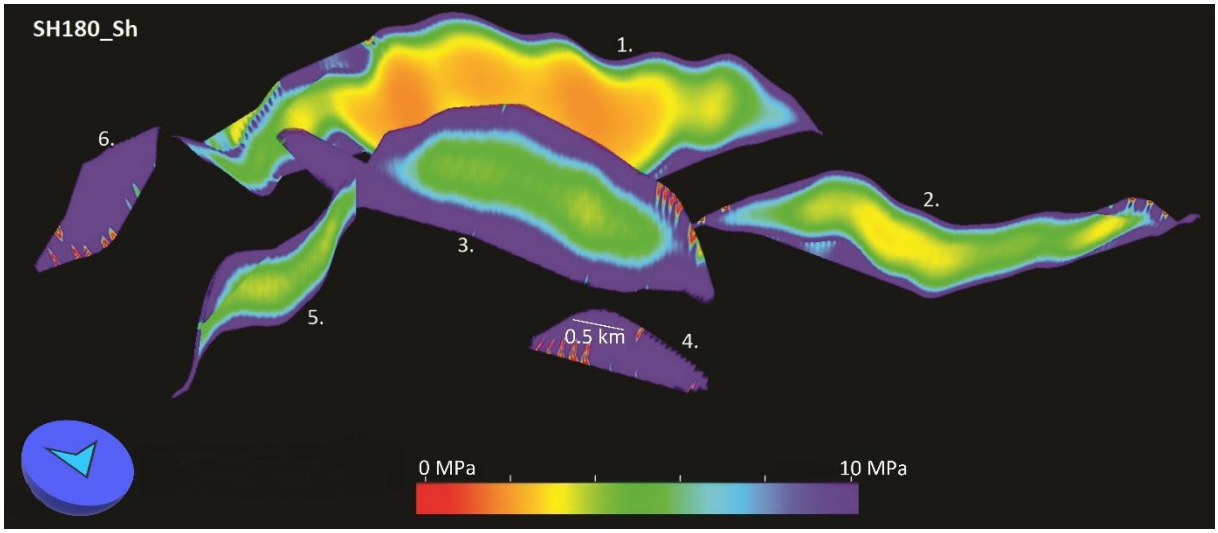

Figure 50. Slip stabilities at Snøhvit Nord at SH180_Sh viewed from the north

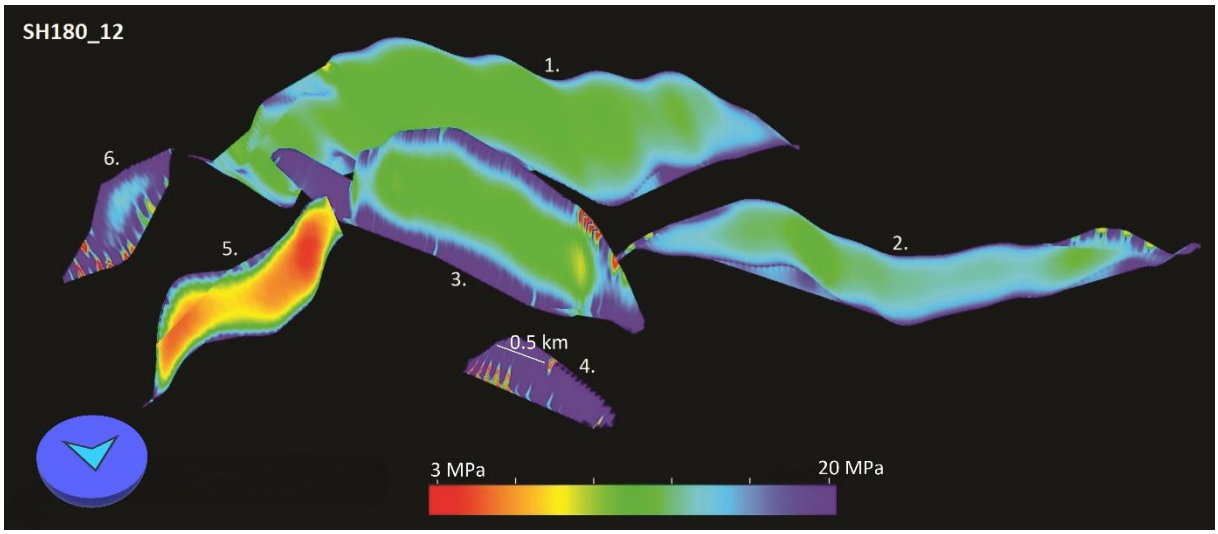

Figure 51. Fault 5 is the most unstable at SH180_12 scenario

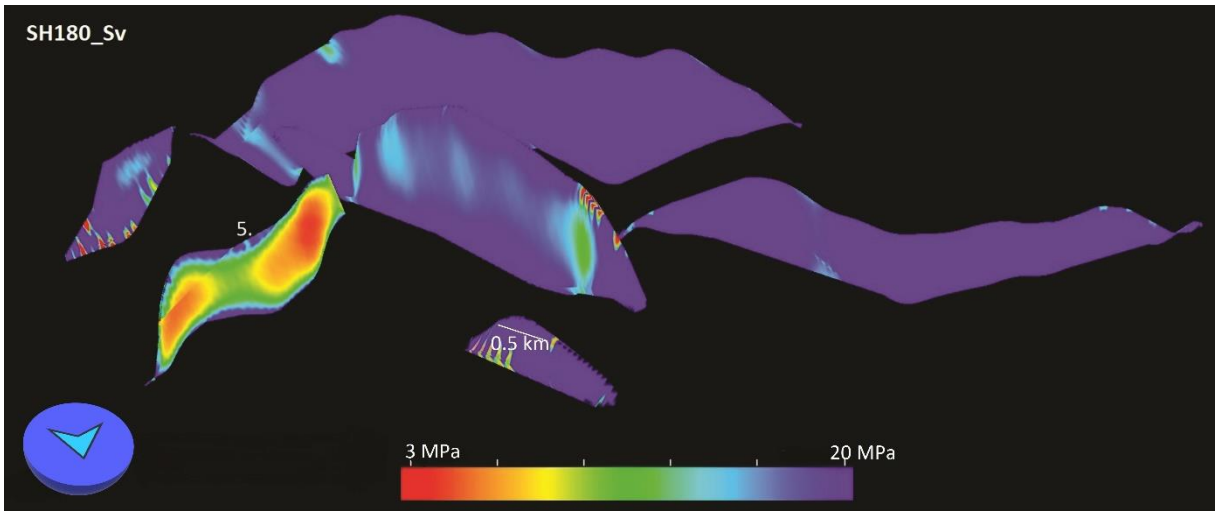

Figure 52. Fault 5 is still the main risk at SH180_Sv

Askeladd

The Askeladd structure is the easternmost one of a group of gas fields sitting on terraces that are separated by N-S trending normal faults of the RLFC. The biggest fault delineating this structure to the west also belongs to this fault complex. In the northernmost part of the structure this fault starts to rotate into a more NW-SE strike. The northern edge of Askeladd is delineated by a NE-SW trending fault; while to the east the GWC mostly follows the structural relief. Some exceptions from this can be seen as some smaller E-W striking faults seem to affect the GWC in this area (Figure 53).

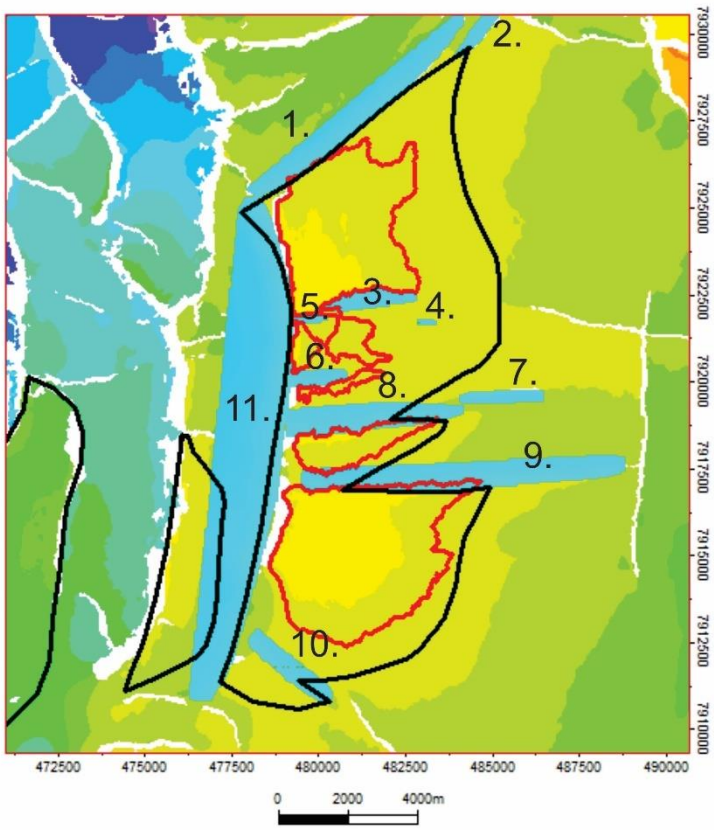

Figure 53. Faults and GWC at Askeladd

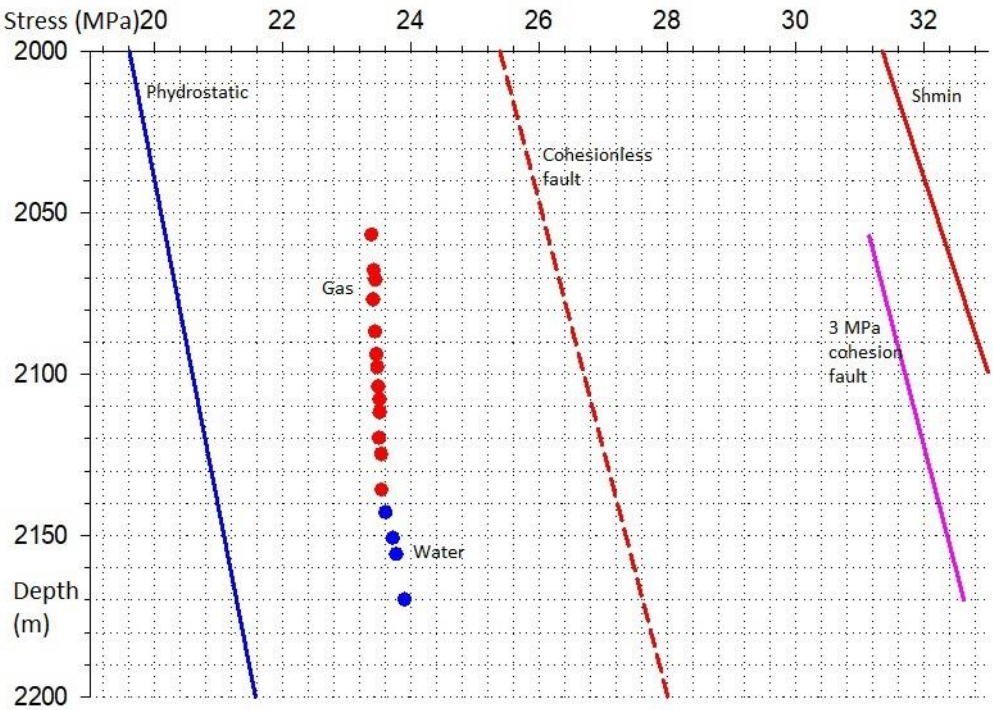

Figure 54. RFT profile of Askeladd from well 7120/8-2

The Stø formation in Askeladd was first spudded by well 7120/8-2, which hit the top reservoir at 2056 m below sea level. The GWC was recognized at 2136 m from the RFT pressure profile; which gave a pressure of 23.4 MPa at the top of the gas column and 23.56 MPa at the bottom (Figure 54). This means, that the pressure at the top of the gas column is around 2.8 MPa above hydrostatic pressure. Regional S_{hmin} gradient gives a minimum stress of 32.3 MPa for this depth considering a water depth of 245 m. This gives a retention capacity of almost 9 MPa. OpF is 0.24. If we consider shear failure along cohesionless fault surfaces to be the dynamic control, then a critical pressure of around 26.2 MPa can be expected at this depth. The actual pressure at the top of the gas column is only 2.8 MPa away from this value.

Faults in the SH160_Sh case show moderate slip stability. None of the fault planes have extensive areas with less than 2 MPa critical pressure. The lowest slip stabilities are shown by fault 1, 9 and 11, where critical pressure perturbations of 5 MPa can be observed (Figure 55(A)). With the increase of S_{Hmax} the effect of fault strike becomes more pronounced. Hence, in the SH160_12 scenario it can be observed that the faults most favorably oriented for failure are 10 and 11 (Figure 55(B)). On fault 11 areas with smaller than 2 MPa slip stability can be seen, while fault 10 stays around 5 MPa. With S_{Hmax} reaching the magnitude of S_v in

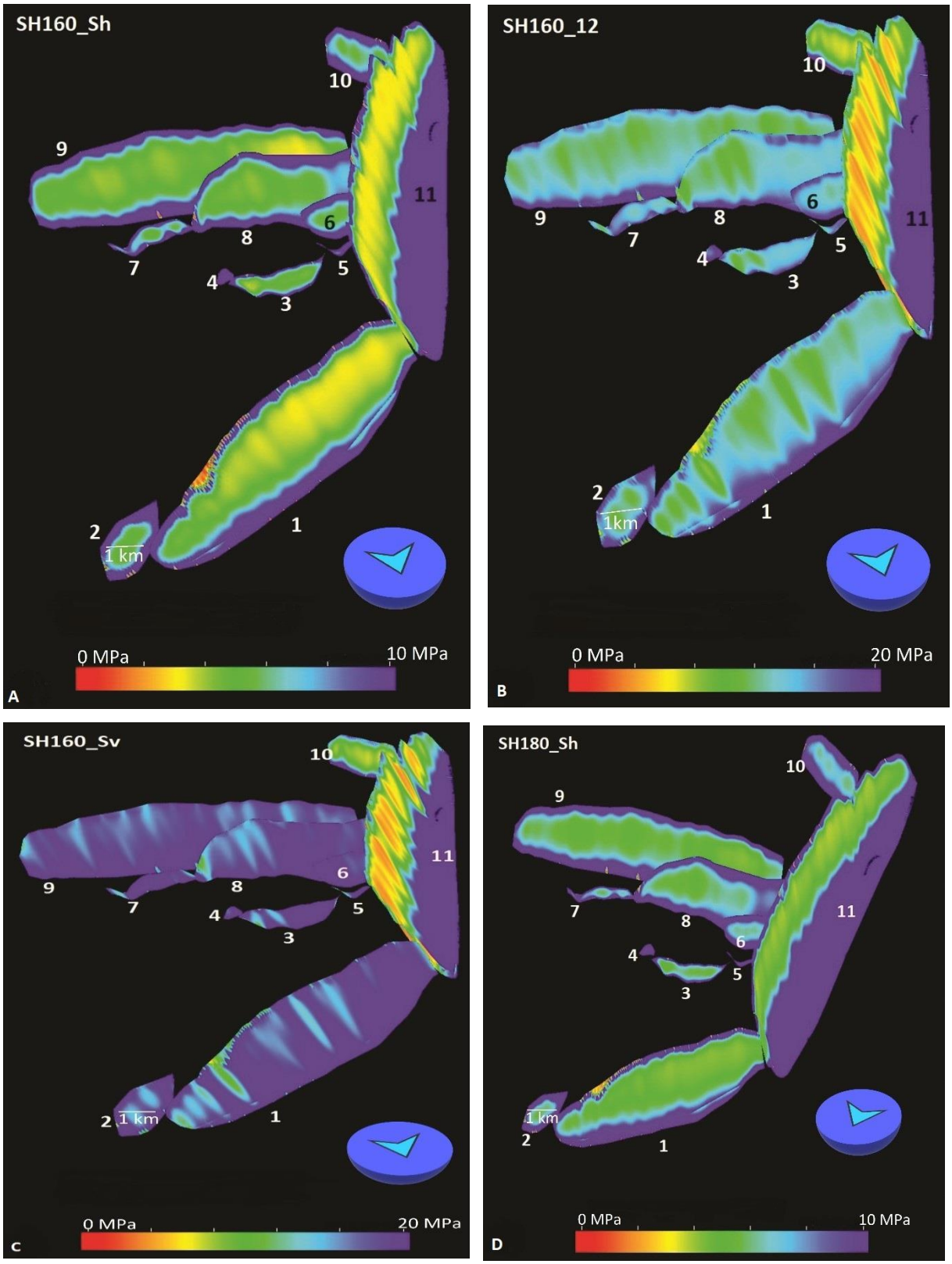

Figure 55. Slip stabilities on Askeladd at SH160_Sh (A), at SH160_12 (B), SH160_Sv (C) at SH180_Sh (D)

SH160_Sv the importance of these to fault planes becomes even more highlighted, while other fault planes become more stable both in absolute and relative terms (Figure 55(C)).

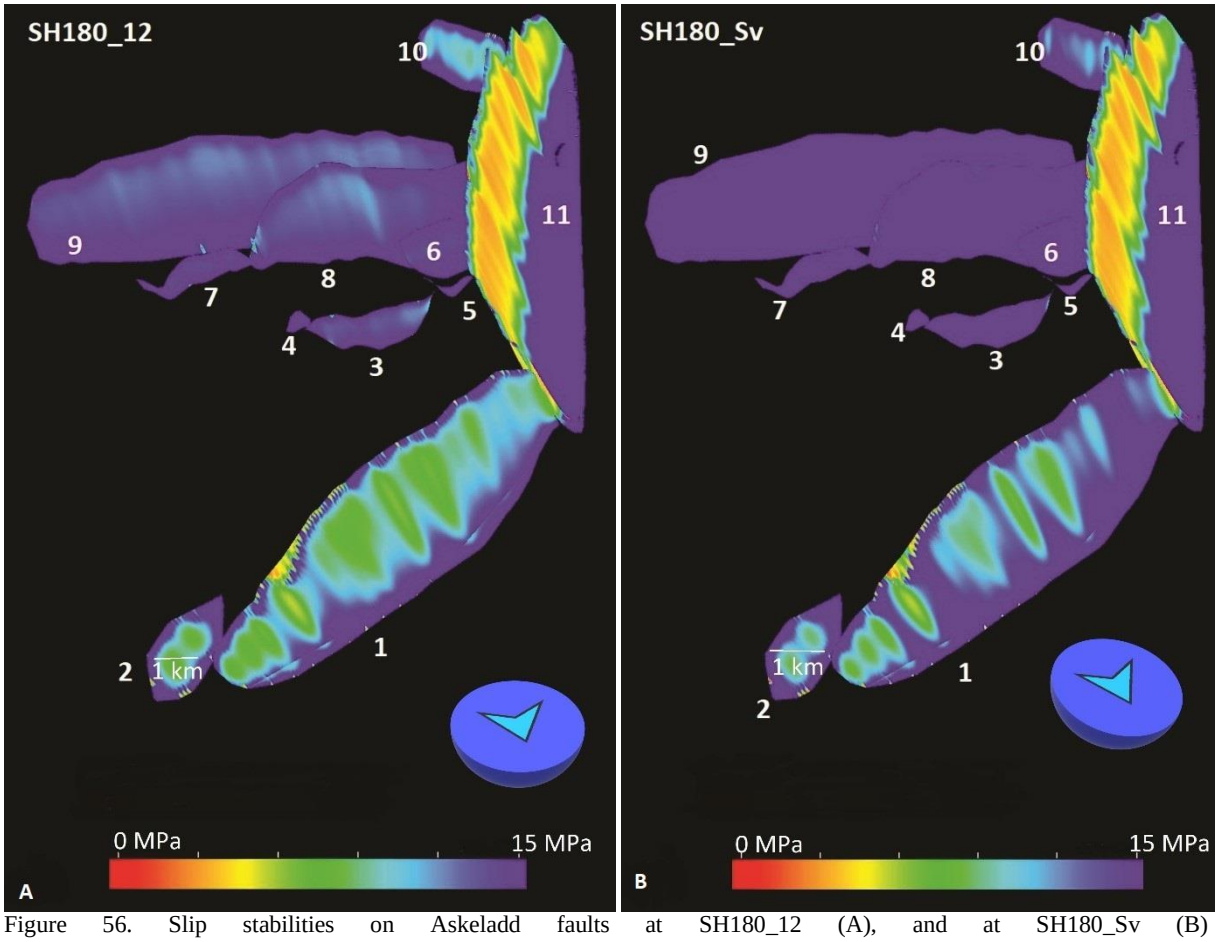

Figure 56. Slip stabilities on Askeladd faults at SH180_12 (A), and at SH180_Sv (B)

In SH180_Sh scenario critical pressures are even lower than for its SH160_Sh counterpart (Figure 55(D)). Increasing S_{Hmax} will destabilize fault 11 in the same manner as in the stress fields with 160 degree S_{Hmax} orientations (Figure 56 (A)). Fault 10 will also become a bit more unstable, but faults 1 and 2 on the northern edge of the structure also show lower relative stability. This lower relative stability however is still somewhere between 3 and 6 MPa. Only fault 11 shows critical pressures less than 3 MPa. Further increasing S_{Hmax} will lead to fault 11 being the only fault with considerable risk (Figure 56(B)).

Askeladd Gamma

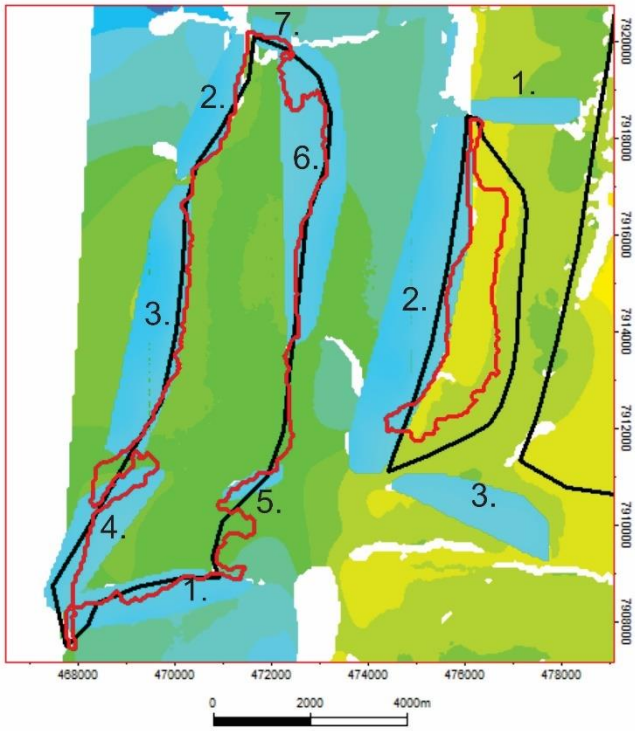

Figure 57. Faults and GWC at Askeladd Gamma (to the right) and Askeladd Vest (to the left). See figure 18 for color code.

Askeladd Gamma lies just west of the main Askeladd structure. It is located on a deeper terrace formed by faults of the RLFC. The structure is also bounded by an E-W and a NW-SE striking fault (Figure 57).

This gas accumulation was discovered by wildcat well 7120/7-2 that hit top Stø at a depth 2127.5 m below sea level. The GWC was recognized from RFT plots at 2206 m (Figure 58). Pressure at the top of the gas column reaches 24.15 MPa, while 24.4 MPa was measured at the top of the water leg. This means that pressure in the reservoir is just over 3 MPa over hydrostatic pressure. The stress field model for the Askeladd area predicts an S_{hmin} of around 33.5 MPa. This means a retention capacity of 9.3 MPa and an OpF of 0.24. P_{pcrit} at this depth is expected to be 27.1 MPa which is only 3 MPa away from actual pore pressure.

In the SH160_Sh case only moderate critical pressures can be observed mostly on fault 2 delineating the structure to the east (Figure 59 (A)). Increasing S_{Hmax} will result in slip stabilities lower than 4 MPa on the same fault surface, however the fault still seems relatively stable overall (Figure 59 (B)). The same can be said until increasing S_{Hmax} to the magnitude of S_v (Figure 60 (A)). In the case of Askeladd

Gamma the stress models with N-S S_{Hmax} orientations seem to produce very similar results (Figure 60 (B)-(D)).

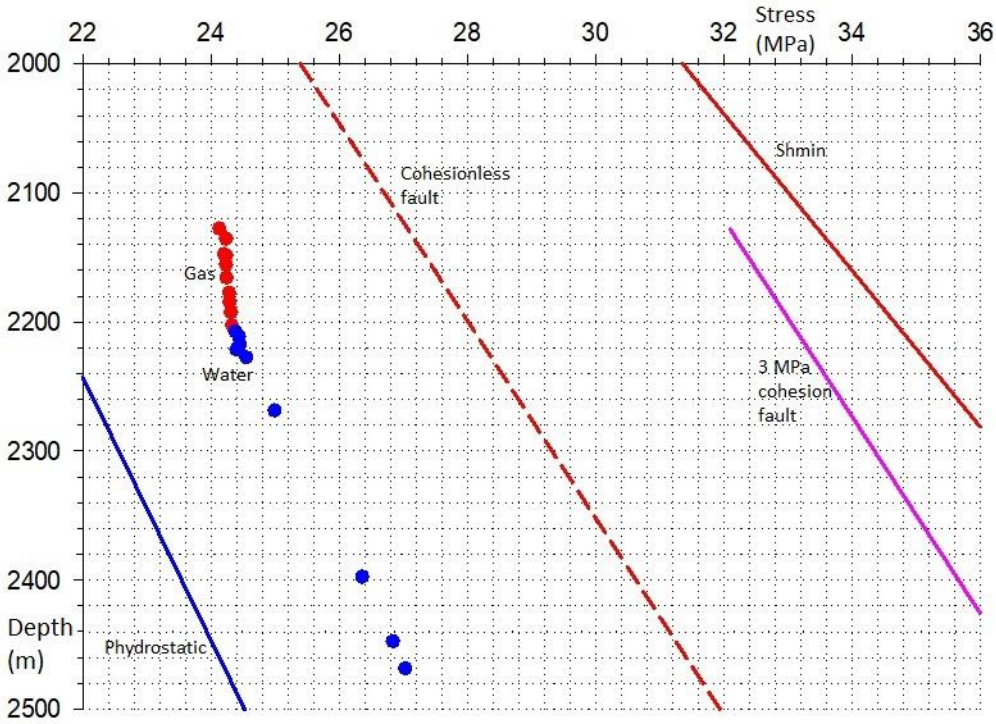

Figure 58. RFT plot of Askeladd Gamma from well 7120/7-2

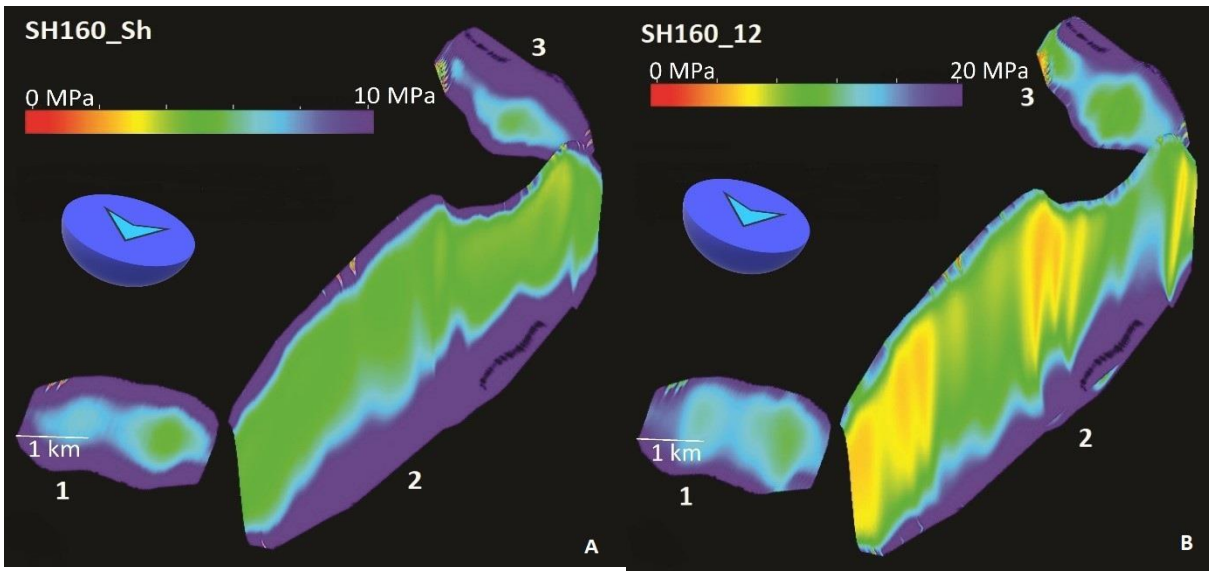

Figure 59. Slip stabilities on Askeladd Gamma at SH160_Sh (A), and SH160_12 (B)

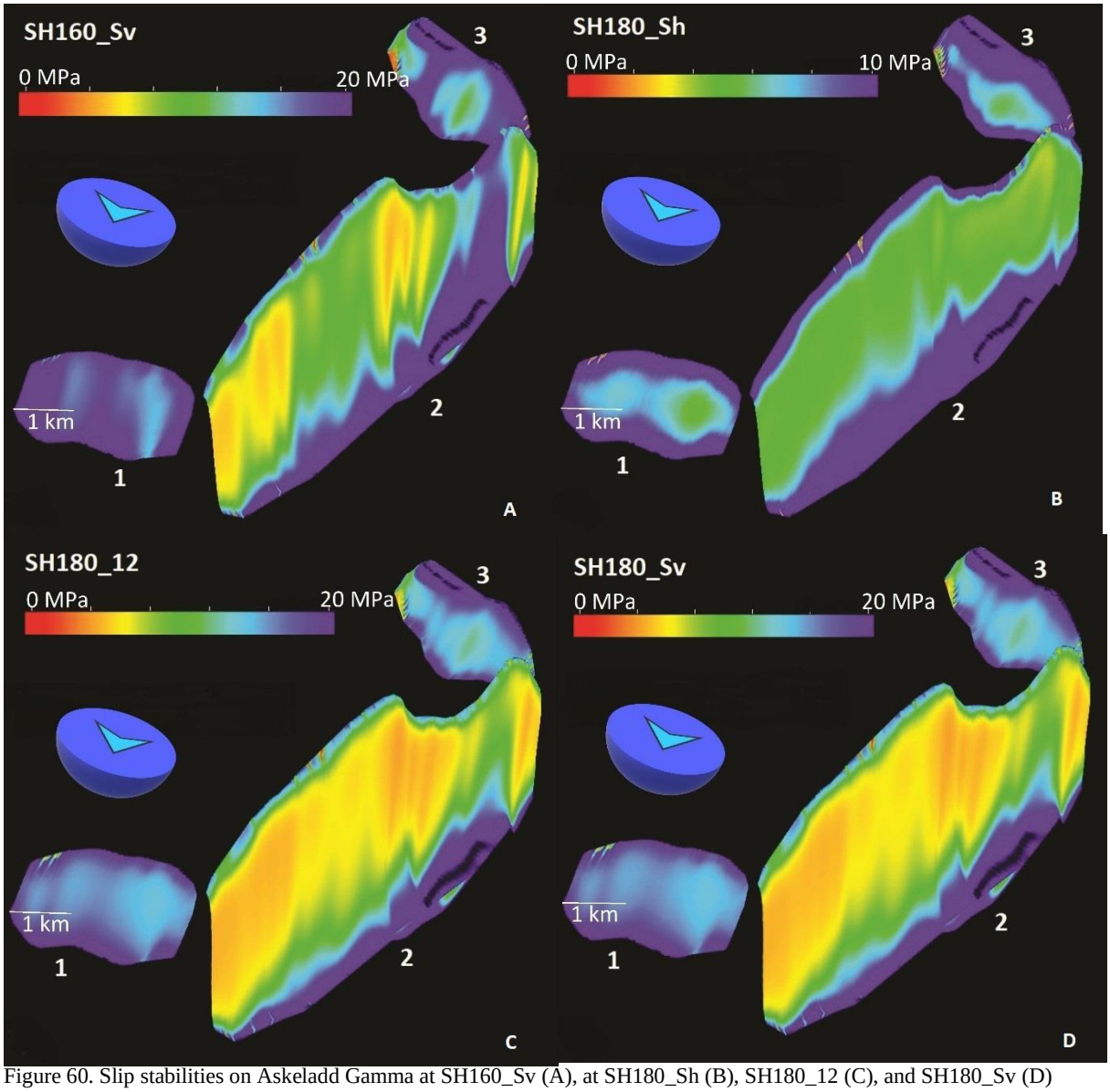

Figure 60. Slip stabilities on Askeladd Gamma at SH160_Sv (A), at SH180_Sh (B), SH180_12 (C), and SH180_Sv (D)

Askeladden Vest

Askeladd Vest is the westernmost of all the Askeladd structures also situated on a N-S trending terrace (Figure 57). It is bounded by several faults with mostly NNE-SSW, N-S, E-W and WNE-ESW orientations. For the most part the reservoir is delineated by faults, however on the SE corner of the structure the GWC is defined by depth contour.

The structure was hit by well 7120/7-1, that reached top Stø at a depth of 2383 m below sea level. The GWC in the well was recorded at 2448 m. Pressure at the top of the gas column was 26.6 MPa, or 2.8 MPa above hydrostatic pressure. S_{hmin} at this depth can be expected around 37.8 MPa, while P_{pcrit} can be at 30.5 MPa. This means the dynamic capacities in this structure are above average with a retention

capacity of 11.2 MPa and an OpF of 0.2. Even P_{pcrit} is around 4 MPa away from the recorded pore pressure, which is significant compared to numbers from other fields.

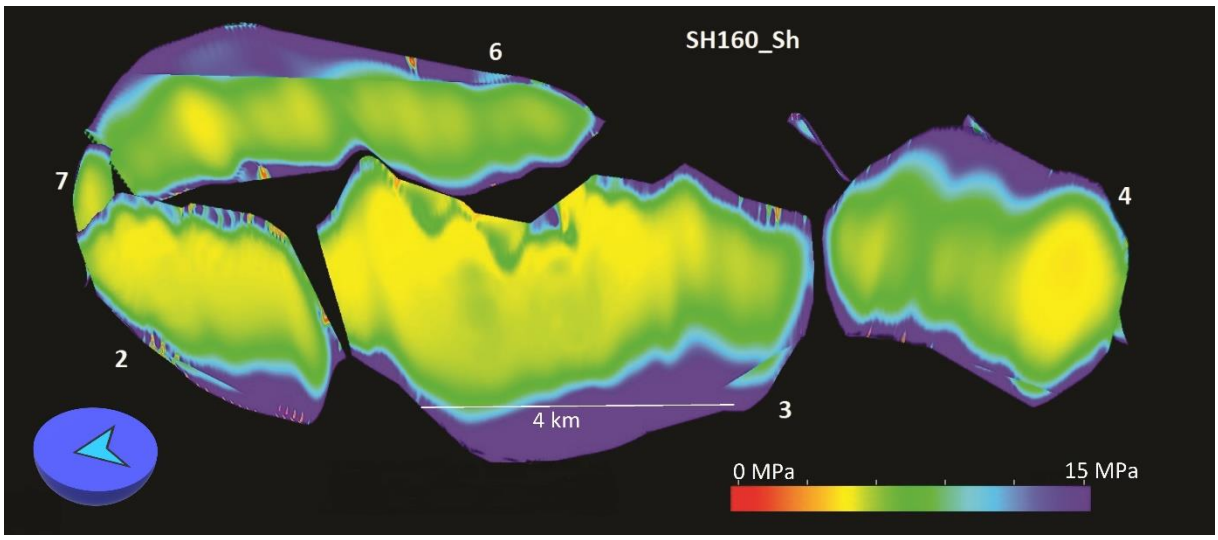

Figure 61. Slip stabilities at Askeladd Vest at SH160_Sh

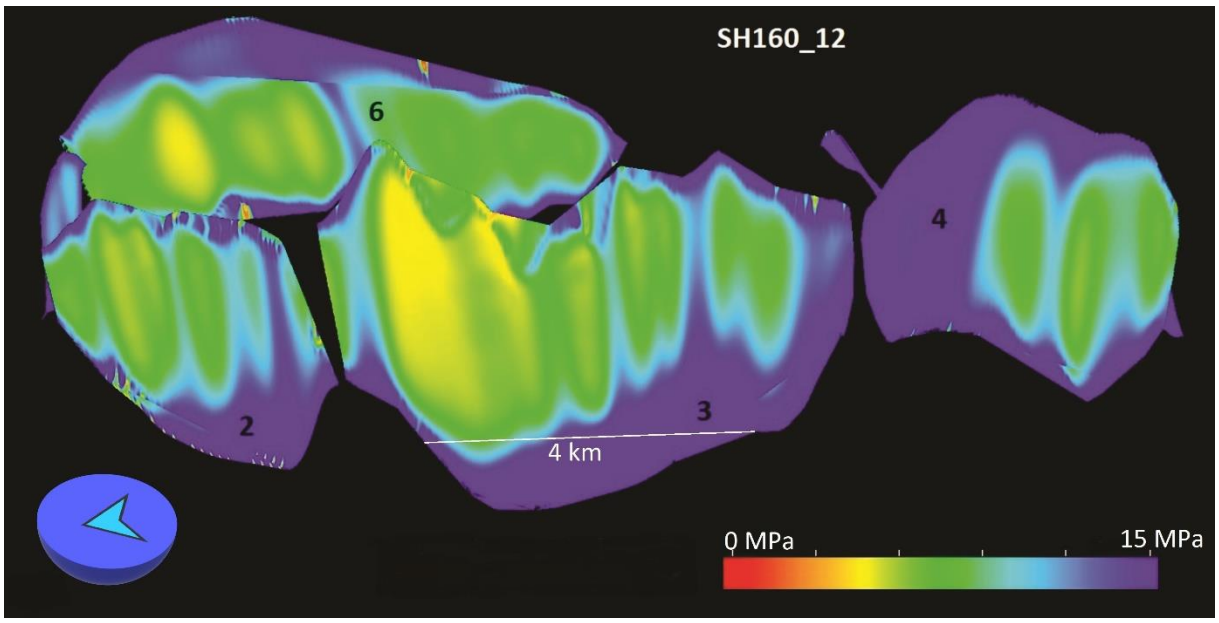

Figure 62. Slip stabilities at Askeladd Vest at SH160_12 stress scenario.

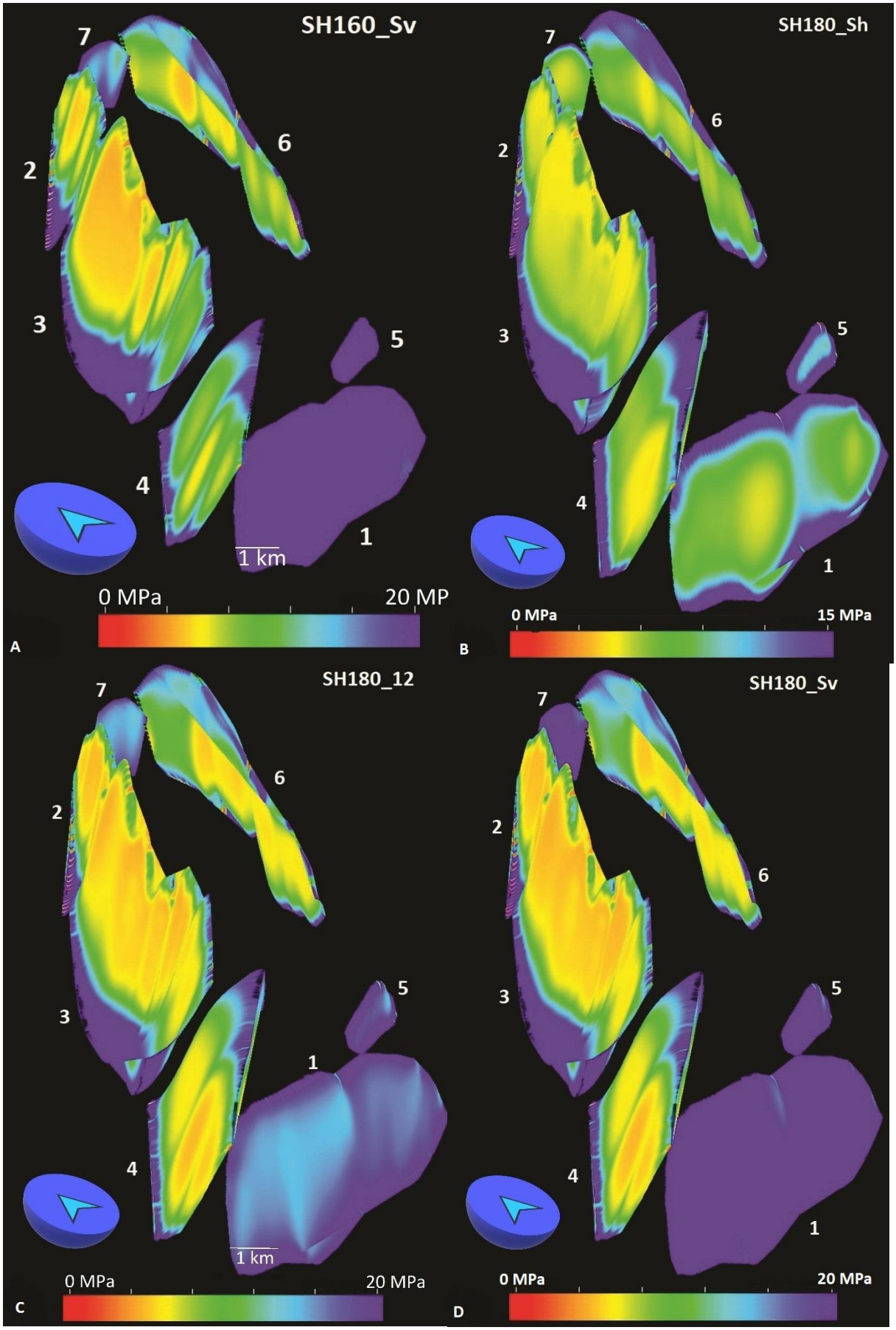

Figure 63. Slip stabilities at Askeladd Vest at SH160_Sv (A), at SH180_Sh (B), at SH180_12 (C) and at SH180_Sv (D)

The SH160_Sh scenario produces very similar outcomes to that of Askeladd Gamma (Figure 61). Not one fault plane has slip stabilities lower than 2 MPa, and for the most part they stay between the 5-8 MPa range. Not much change can be observed in the SH160_12 case (Figure 62). Notable observation is that faults 1 and 5 stayed very "cold" while the other fault planes have retained their moderate slip stabilities. Further increasing S_{Hmax}, it becomes clear that the more unstable faults surrounding the structure are the ones roughly N-S oriented (faults 2, 3, 4, 6). Absolute critical pressures however are still high, rarely going below 4 MPa (Figure 63 (A)).

The situation is very similar in the SH180 models: with the increase of S_{Hmax} it seems like the more or less N-S oriented faults are the most unstable ones (Figure 63 (B)-(D)).

Delta Vest

Delta Vest is a horst structure at the NW corner of the survey area. Its main NW-SE trend is defined by two similarly trending normal faults which intersect each other at the SE termination of the structure. The NW-SE trending main structure is dissected into two smaller horsts and a graben by two NE-SW faults (Figure 64).

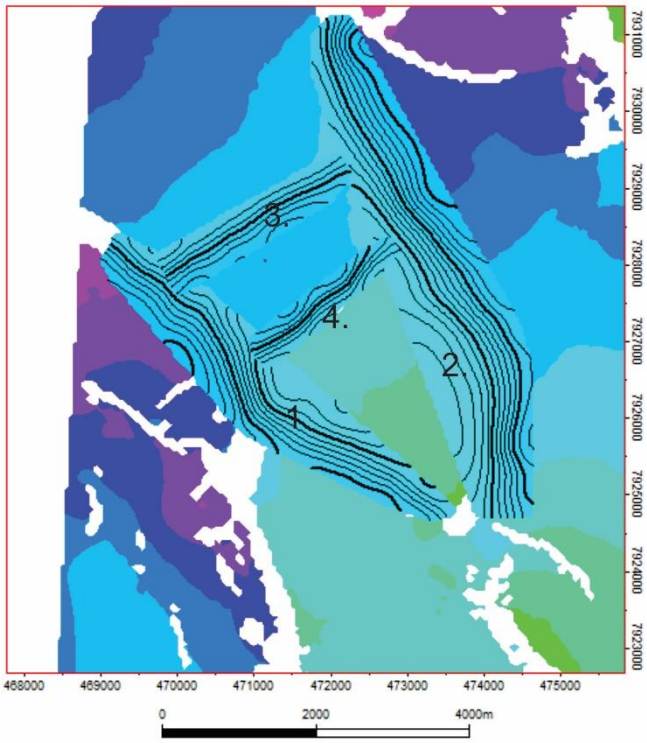

Figure 64. Fault around Delta Vest. See figure 18 for color code.

The structure was drilled by well 7120/7-3 at the culmination of the northwesternmost fault block. The closure of this block is created to the southeast by the first SW-NE trending normal fault. Towards the northwest this block progressively deepens towards the Tromsø Basin. On the survey area there is no mappable fault in this direction, meaning that this block has the most direct connection to the source areas. The well has hit top Stø in this block at a depth of 2867 m. Here, they have recorded a pressure

of around 31.5 MPa, that is 2.8 MPa over the hydrostatic pressure. Retention capacity is around 14.1 MPa with an OpF of 0.165 assuming an S_{hmin} of 45.6 MPa.

Figure 65. Slip stabilities at Delta Vest at SH160_Sh (A) and SH160_12 (B)

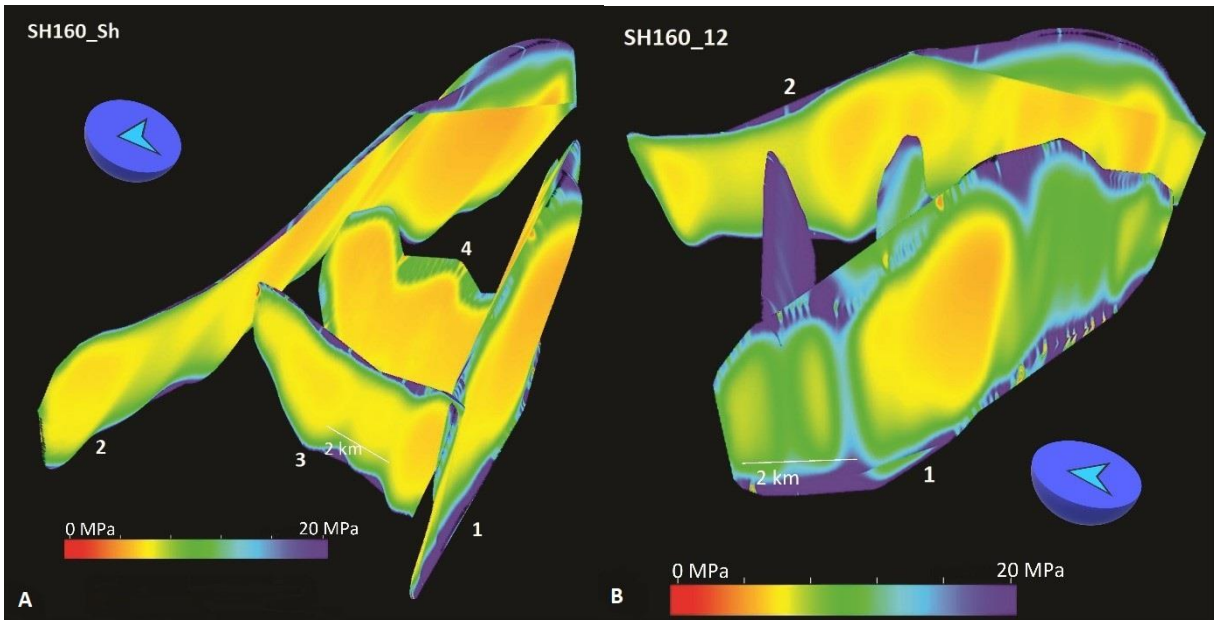

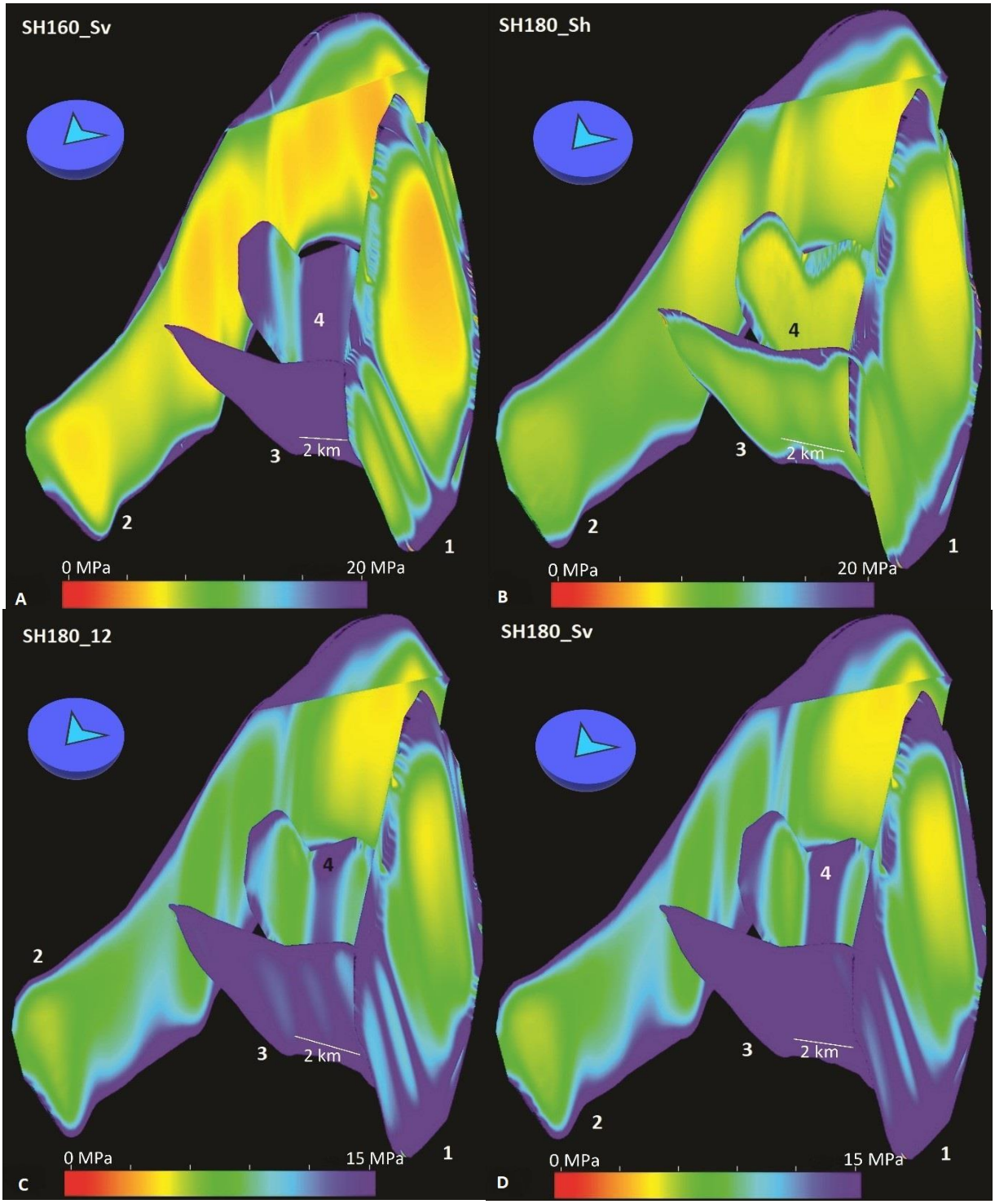

Figure 66. Slip stabilities at Delta Vest at SH160_Sv (A), at SH180_Sh (B), at SH180_12 (C) and SH180_Sv

In the SH160_Sh case there is no considerable variation in the slip tendencies of the different fault planes (Figure 65 (A)). All of them show intermediate critical pressures ranging between 4 and 8 MPa. Increasing the S_{Hmax} to 1.2x S_{hmin} will make faults 3 and 4 cold; while critical pressures stay the same on faults 1 and 2 (Figure 65 (B)). This trend will continue until SHmax=Sv (Figure 66 (A)). The same trends can be observed under the SH180 stress models, with the small differences that faults 1 and 2 seem to remain a bit more stable than in SH160 models (Figure 66 (B)-(D)).

Askeladden-Beta

Askeladden Beta is a dry structure located just just to the north of the main Askeladden discoveries. To the west it is delineated by a fault of the RLFC. Two E-W faults intersect this larger fault; both of which rotate to a NE-SW strike towards the NE end of the structure. The NE termination of the structure is defined by a fault segment striking approximately E-W. Here; close to 90 degree fault intersections also become common.

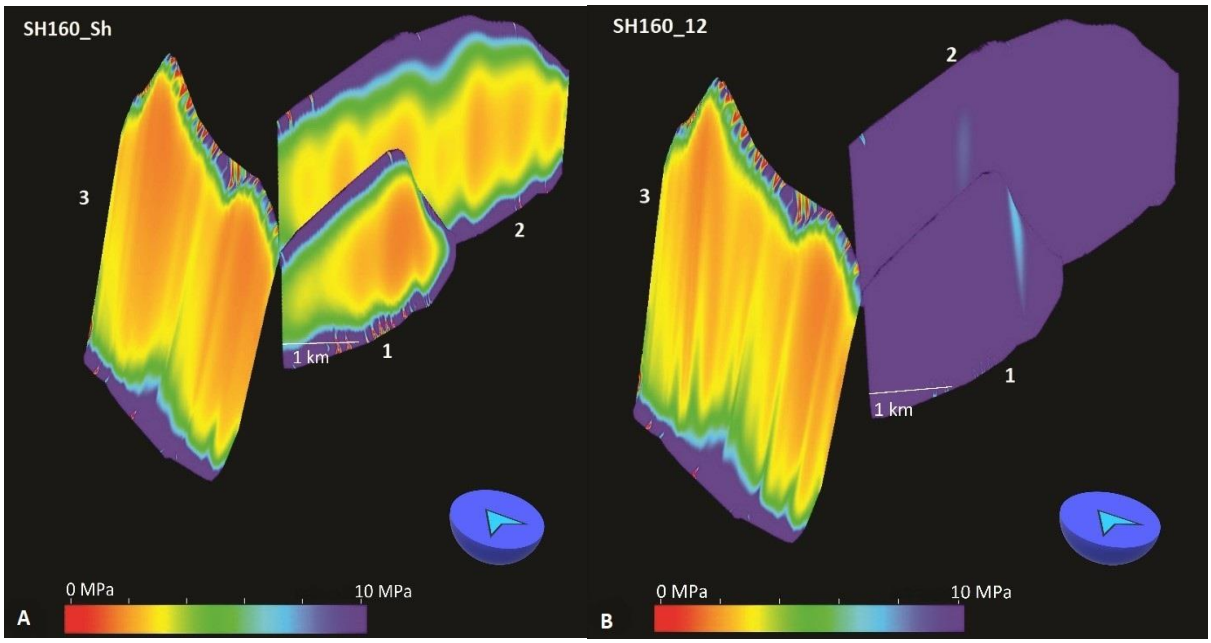

Figure 67. Slip stabilities at Askeladd Beta at SH160_Sh (A) and SH160_12 (B)

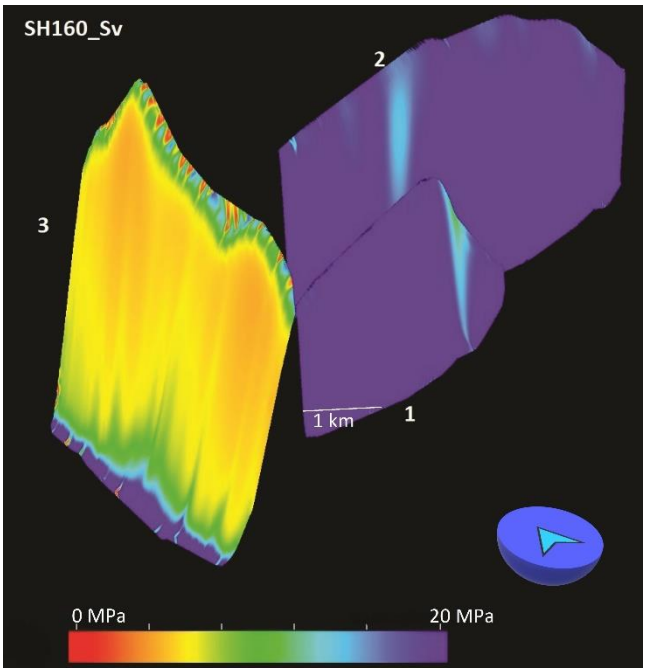

Figure 68. Slip stabilities at Delta Vest at SH160_Sv

The structure was drilled by wildcat well 7120/8-4, which reached the Stø Formation at 2240.8 m below sea level. The main Jurassic reservoirs were found to be dry, however substantial residual oil and gas shows that this structure was also formerly hydrocarbon bearing. Pressure points recorded after hitting the Stø formation scatter around 27 MPa. This means that pressure in the empty reservoir is around 4.5 MPa over the hydrostatic pressure. The regional S_{hmin} gradient used in the geomechanical model for the Askeladd area gives an S_{hmin} of around 35.2 MPa considering a water depth of 275 m. This means an RC of around 8.2 MPa and an OpF of 0.35. The regional gradient of P_{pcrit} means that the critical pressure at this depth will be around 28.5 MPa; or less than 2 MPa over the recorded pressures.

In the SH160_Sh larger spots of around 2 MPa critical pressure can be observed on faults 1 and 3, while fault 2 remains more between 2 and 4 MPa (Figure 67 (A)). Increasing S_{Hmax} until S_v it becomes quite clear that the main dynamic control is emplaced by fault 3 Figure 68. Not much difference can be seen in the SH180 models, except maybe that faults 1 and 2 do not become cold as rapidly with an increase in S_{Hmax}; however the overall role of fault 3 is still unquestionable.

6. Discussion

6.1. Failure mechanisms controlling HC columns

Based on data from Hermanrud (2014) about the underfilling of the traps; it is quite clear that the hydrocarbon column heights in the studied structures are not controlled by their spillpoints. According to Hermanrud (2014) two structures are possible exceptions from this; the main Askeladd structure and Albatross Sør. In these cases the HWC is too close to the spillpoint to establish without uncertainty if the traps are underfilled or not. This however does not invalidate the point that a simple geometric fill-spill scenario is not the dominant controlling factor on HC column heights in the area. Hence, the first question to be asked is whether it is possible to pick a dynamic controlling mechanism that can give an explanation to the observed HC column heights. The most simple tool for this analysis is by plotting the reservoir pressures on stress plots together with the estimated principal stress gradients, and failure gradients as done in the previous chapter.

This method helps visualizing the different dynamic capacities through the horizontal distance between the RFT pressure plot from the reservoir and the different stress and failure gradients. It also provides a good visual/graphical method for estimating HC column heights given that the failure gradient of the controlling factor is known. This could be the case when pressure plots seem to align themselves along a given gradient. In this case pressure buildup in the reservoir would be Støpped at a pressure equivalent to the stress determined by the failure gradient for that given depth. Graphically, the pressure increase can happen in two ways: increasing the height of the RFT plot, or increasing the height of a lower density phase, essentially pushing the plot to the right. An example to the former would be a simple filling of the trap via secondary or tertiary migration, while for the latter gas dissolution and expansion would be a common cause. The method can also be used in reverse: empirically determining a failure

gradient by choosing a best fit line to several pressure plots from different prospects would allow to speculate on the possible dynamic mechanism controlling the HC heights in these traps.

The main issue however, is that this method completely disregards the spatial orientation of the structural elements that might be conduits of leakage (incl. fault planes) with regards to the stress field. Assuming that if a given RFT plot aligns itself with a failure gradient then that gradient is the controlling factor is only true when favorably oriented structural elements exist. This means fractures or faults that are perpendicular to S_{hmin} in case of tensile failure or oriented 30 degrees away from the largest principal stress in case of (most) shear failure(s) (according to Mohr-Coulomb failure criteria). The further away the real orientations are from this ideal orientation, the larger pore pressure increase is needed to induce failure. This also means that the RFT plot on a pressure vs depth diagram can pass the failure line.

For this discussion and study, this comes with an important consequence. The failure line for the cohesionless tensile failure of the cap rock is represented by the S_{hmin} gradient in this study. The other two failure gradients were constructed by determining the amount of pressure increase needed to induce a shear failure at different depths on a cohesionless plane with a frictional coefficient of 0.6 and on a plane with the same friction but with a cohesion of 3 MPa; in both cases assuming the failure of an ideally oriented fault segment. Hence, these failure models do not account for the cases where ideally oriented fault segments do not exist; and so less favorably oriented segments can become the weak point in the structure through a different failure mechanism.

Nevertheless, the sequence of the dynamic controlling mechanisms is generally in agreement with what we can see on the stress plots: a cohesionless fault is naturally relatively weak. With the increase of cohesion, the pressure needed to induce slip also increases. Finally, this is followed by tensile failure of cap rock. Although not a topic of the thesis, but capillary leakage through the seal is generally the dynamic process requiring the largest critical pressure. An exception from this rule can often be the tensile failure of seal. The tensile failure of seal or a fault plane can happen before shear failure of fault plane especially in more isotropic stress fields (Figure 17). The stress gradients used in the base models (especially that of S_v and S_{hmin} since these are the ones affecting stress anisotropy in a normal faulting setting) do not suggest that this is a very likely scenario; however uncertainties around stress field heterogenity in the study area would bring us not to rule out the possibility of such failures becoming controlling mechanisms locally.

In the cases of this study, RFT pressure plots from all the fields seem to well align themselves with the failure gradient of a cohesionless shear failure. This result is even more compelling when we consider that this is the case in both base stress models (in the Snøhvit model this gradient is 12 Mpa/km, while in the Askeladd model it is 13.1 Mpa/km). On some structures the measured pressures come within 2 MPa from P_{pcrit}. Some variation can be observed in the critical pressures among the different structures, but some of that could also be explained by well position. The RFT plots were taken from wildcat wells,

which are generally drilled close to the culmination of a trap, but some of the wells hit the top reservoir downdip from this point. This would mean that the recorded pressures at the top of the gas column could be a bit further away from the failure gradient than at the top of the structure. Hence, the further away the well is from the culmination, the more inaccurate the estimations on critical pressure can be. This inaccuracy however can easily be handled if the slope of the gas gradient and the vertical distance between the top reservoir at the well and the top reservoir at the culmination are known.

The larger issue is posed by reservoir compartmentalization. The pressure recorded in the wildcat wells of the structures were uniformly extrapolated to the whole structure. This way, the present study does not account for reservoir compartmentalization. This means, that in theory parts of the investigated structures can have considerably different pore pressures than what was incorporated in the stress models. This can affect the results, bringing P_{pcrit} down in case of higher than anticipated pressures, or brining it up in the opposite case. A few studies have written about reservoir compartmentalization mainly on the Snøhvit structure with regards to pressure increase in injection wells (L. Chiaramonte et al., 2011), (Laura Chiaramonte et al., 2015). Based on these it does seem that some parts of the reservoir are not in pressure communication with each other. However, the amount of overpressure seems to be stable across the different structures, so it does not seem likely that compartmentalization would seriously affect the results.

A simple way of risking a prospect based on its reservoir pore pressure is by calculating the retention capacity. A low RC can indicate a high geomechanical risk (high risk of mechanical failure). At the same time, a low RC can also indicate a low risk from an exploration point of view. The reason for this is that RC is calculated by subtracting the pore pressure from the least principal stress at the given depth. Since failure and leakage that happen around pore pressures equaling S_{hmin} are usually associated with extensional failure; a low RC is an indication that 1, the reservoir pressure is around dynamic equlibrium and 2, the controlling dynamic mechanism is hydrofracturing. This is a preferable condition during exploration, since shear failure along preferably oriented fault planes usually limits pore pressures and HC columns at a lower pressure, i.e. smaller HC columns.

The result of this is that large retention capacities do not necessarily mean that those traps are able to fill further up to the level of S3, but rather that there is another dynamic process that controls the pressures at a lower equilibrium. As discussed above, this could be shear failure along fault planes. Shear failure can limit the magnitude of pressure in the reservoir at different levels depending on a number of factors. These factors include fault plane orientation, stress anisotropy and fault cohesion. The further away a fault plane is oriented from the ideal orientation for failure (according to Anderson`s faulting theory), the harder it reactivates, hence it allows a higher pressure. An increase in fault cohesion affects the dynamic capacity in a similar manner. Finally, the lower the stress anisotropy, the higher

pressure increase is possible without the Mohr circle touching a failure envelope. Hence, a low stress anisotropy generally promotes HC column preservation.

Stress anisotropy and fault plane orientations can also affect the shear failure`s limiting ability relative to extensional failure (related to S3). In some cases extensional failure can happen at a lower pressure than shear failure, and so becoming the main dynamic control (Figure 17).

As discussed in data & methods chapter, failure lines were calculated for the stress vs depth diagrams. Since stress anisotropy affects failure, separate failure gradients were established for the two base stress models that are both based on shear failure on cohesionless surfaces. Since failure envelopes with cohesion are not linear; a linear stress gradient cannot be given. Instead, the required pore pressures for shear failure on these planes were calculated for each of the structures at the HC column`s depth interval. A cohesion of 3 MPa was chosen.

The most obvious observation is that in all structures both shear failure lines are lower than S3, meaning that in theory shear failure is the main dynamic controlling factor. In some cases (Albatross, Albatross Sør, Askeladd, Askeladd Gamma) the failure line with cohesion gets within 1 MPa of the S3 gradient. However, these two failure gradients do not seem to affect pore pressure in any way, since RFT pressure points seem to well align themselves with the failure gradient for the cohesionless shear failure. The two Albatross structures and Snøhvit all had pore pressures within 1 MPa from the estimated P_{pcrit}. Meanwhile, their retention capacities are around 6-7 MPa, and with overpressure factors of only around 0.25-0.3. Albatross Sør`s OpF of 0.31 is the second largest from all the structures; which is most likely a result of a relatively narrow mud window due to its shallow depth. Looking at the commonly used RC and OpF values of these two structures points to a common misunderstanding during exploration already discussed above. Taking these two values as an indication of dynamic capacity (and ignoring other failure mechanisms than hydrofracturing); could lead us to believe that the pressures are not in dynamic equilibrium. In the case of an overfilled petroleum basin (like the Hammerfest Basin), where hydrocarbon supply was enough to fill the trap, this can lead to a false conclusion that the traps could be filled to spill. The thought behind such conclusion would be that the traps` closure is relatively small compared how strong the seal is. The controlling factors for HC column heights in this case would be geometric features (closure, reservoir-reservoir juxtaposition) since the traps can fill up before any failure occurs.

However, when we consider other failure mechanisms it becomes apparent that the pressures encountered in the reservoir can still be the results of a dynamic equilibrium. Instead of simply equaling seal strength to S3, this approach acknowledges that seal strength can be subjected to variability that is influenced by a number of factors discussed above. Since a lot of the fields on the NCS are in faulted traps; only using RC and OpF as indexes for dynamic capacity ignores the role of fault planes in leakage and puts all the emphasis on the hydrofracturing of seal. Albatross, Albatross Sør and Snøhvit are all 1

MPa away from P_{pcrit} while showing a relatively high RC. Examining both factors can mean the difference between a filled to spill and an underfilled interpretation. This is especially important in the case of the Hammerfest Basin where no fluid contacts have been recognized on seismic data.

It is interesting to note; that these three structures that have similarly low P_{pcrit} values, have significantly different underfilling. While Albatross has the biggest distance between the deepest HC shows and its spillpoint, and Snøhvit is also approximately 150 m underfilled; Albatross Sør is almost filled to spill (Figure 2). This observation is taken as evidence that even if similar controlling mechanisms limit the HC column heights in the traps; the degree of underfilling can be affected by several factors. From these factors this thesis will examine the spatial distribution of potentially leaky fault planes and their relative position to the structures` culminations.

The highest P_{pcrit} with over 5 MPa was observed at Delta Vest, one of the empty structures. The other empty trap, Askeladd Beta has around 1.5 MPa, however it is important to note that for the wildcat well of this latter trap a well completion log was not available, so the pressure value from here might be inaccurate. The evidence for this comes from the amount of overpressure; which in every other structure in the survey seems to be relatively stable between 2.5-3 MPa, while it is 4.5 MPa for Askeladd Beta. Hence, the pressure inside this reservoir might have been overestimated, which would cause the real P_{pcrit} to be larger as well.

It is important to emphasize, that the different P_{pcrit} values across the structures do not necessarily differences in dynamic control mechanisms. The highest observed P_{pcrit} from Delta Vest belongs to the Askeladd base stress model. The structures belonging in this base model on average exhibit higher P_{pcrit} values than those in the Snøhvit area. This can be explained by the lower anisotropy of the Askeladd stress model which resulted in a higher failure gradient. Moreover, Delta Vest is also the deepest structure, so it is not surprising that it has the highest P_{pcrit}, considering that the gradients diverge with depth.

To summarize the experiences from the pressure records it can be said that the introduction of P_{pcrit} as the pressure increase necessary to induce shear failure on incohesive fault planes showed that the structures can be in fact in dynamic equlibrium and high retention capacities do not guarantee that they are filled to spill or that they are able to refill. In order to further understand the possible role of P_{pcrit} in HC column heights, a fault slip stability analysis was carried out, where the spatial variation of P_{pcrit} was visualized on the fault planes in different stress regimes.

6.2. The effect of P_{pcrit} on HC column preservation

Albatross

Albatross is a gently south dipping structure with mostly E-W trending faults. Faults 5 and 6 at the Eastern edge of the structure also go into more NE-SW orientations. Most of the faults are north dipping, the exception from this are faults 2 and 3 at the SW corner of the structure. The culmination of the trap can be found at the center of structure in the footwall of fault 4. The top reservoir gets shallower towards the north, until fault 4 displaces it into a graben creating a closure that reaches a depth of 1756 m below sea level at its shallowest (Figure 69 (B)). To the east, faults 5 and 6 maintain this closure; but to the west the top Stø becomes shallower again in the hanging wall, dipping SE and creating another, deeper closure with fault 7 (Figure 69 (A)). This closure to the NW is connected to the main central closure via a fault relay ramp between fault 3 and 4.

Figure 69. View of top Stø at Albatross with faults and the GWC in red (A) cross section of Albatross (shown by yellow line on A) (B).

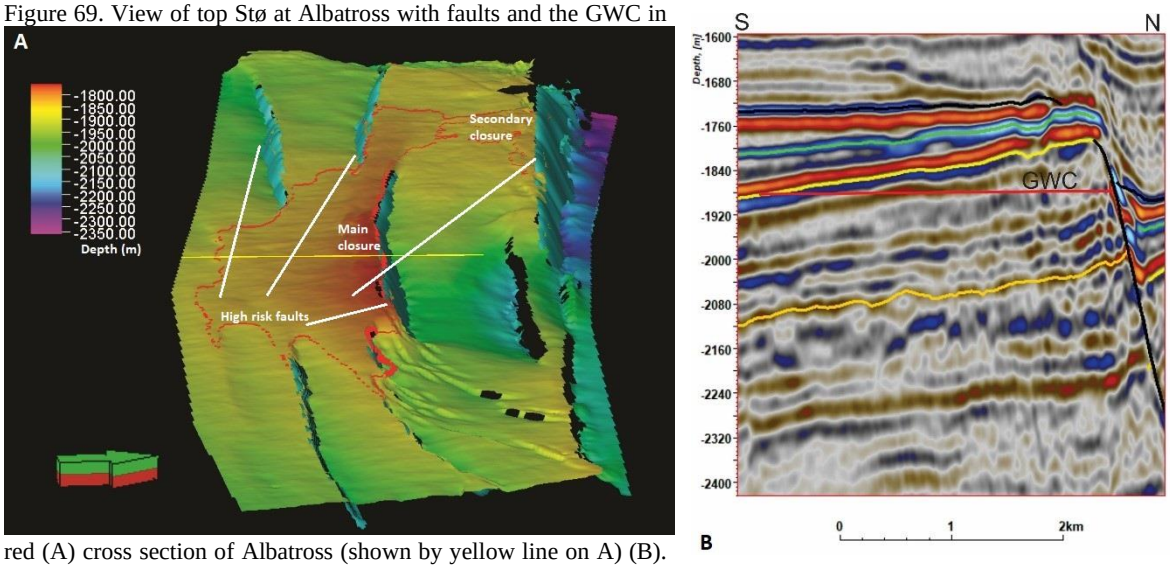

Dark yellow is top Fruholmen, light yellow top Stø, green is top Hekkingen and black is top Knurr

As seen in the results, the faults on the western side of the structure seem to have larger risk of leakage in every stress scenario. This larger risk is retained even when increasing S_{hmax}, even though in absolute terms the fault planes become more stable. It is interesting to note that the relatively large change in strike of fault 5 and 6 do not seem to affect their slip stabilities. Based on these observations it can be concluded that Albatross is definitely a high risk structure when it comes to fault assisted leakage. This is because the most unstable faults around the structure are the ones closest to the shallowest parts of the top reservoir. Fault 4 is the one directly at the culmination of the structure, while faults 3 and 7 also have a major role in creating a secondary closure to the NW. Among the structures investigated by Christian; Hermanrud et al. (2014); Albatross is the most underfilled one. However, with around 300 m, Albatross also has the largest closure.

Albatross Sør

Albatross Sør has a very similar structure to Albatross. Across much of the structure, the top reservoir is dipping gently to the S-SW. Here, the GWC does not come into direct contact with any fault planes. The closure is created by faults 1 and 2; two north dipping, E-W striking normal faults (Figure 70). The culmination of the structure is around 1850 m deep in the hanging wall of fault 1.

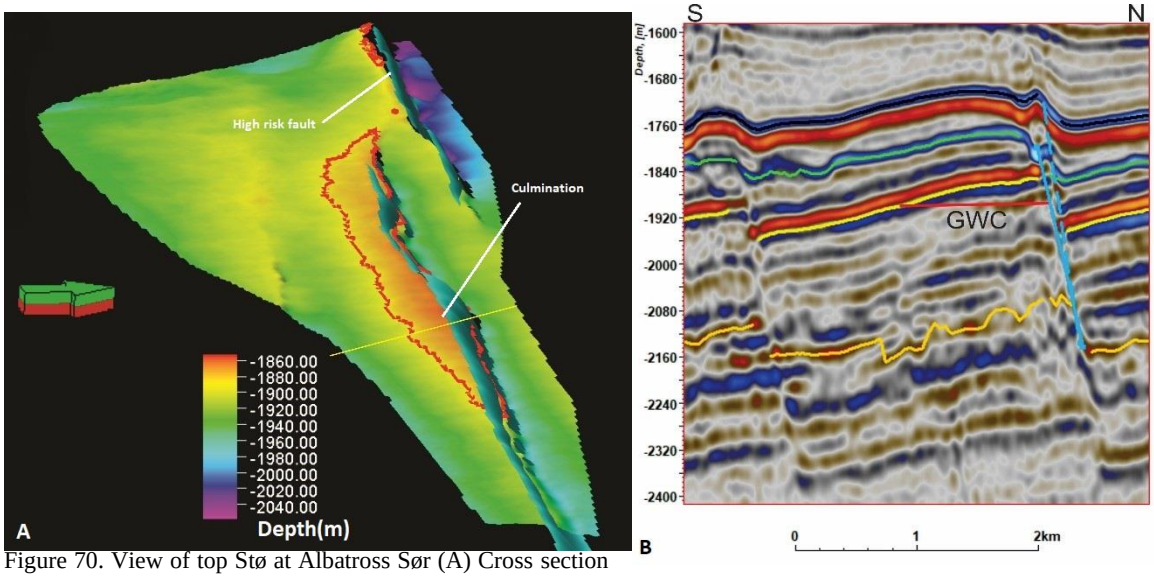

Figure 70. View of top Stø at Albatross Sør (A) Cross section at Albatross Sør (B)

The faults of Albatross Sør had very similar patterns of slip tendency in both SH160 and SH180 stress scenarios. It is obvious that with the increase of S_{Hmax}, absolute slip stability increases and there is no real threat of fault assisted leakage. At lower values of S_{hmax} however, both fault 1 and 2 register lower slip stabilities. The bigger risk seem to be posed by fault 2 with major areas of the fault plane showing less than 2 MPa of P_{pcrit}. This fault however, does not intersect the top reservoir at the culmination. Fault 1 around the structure`s culmination shows rather moderate values of P_{pcrit} (4-6 MPa). Based on this observation, Albatross Sør is a lower risk structure. According to Christian; Hermanrud et al. (2014) Albatross Sør is one of the structures that can be potentially filled to spill. On the top reservoir and fault interpretation used in this study; the shallowest intersection between fault 2 and top Stø is around a depth of 1885 m, which is only 7 m shallower from the GWC as recorded from the RFT plot of well 7121/7-2. It is worth mentioning however, that while Albatross Sør could be filled to spill, it also has a small closure of around 70 m.

Snøhvit

Snøhvit is a very complex structure, where the HWC for the most part abuts against fault surfaces. Faults 4 and 5 separate the structure into a northern and a southern part (Figure 72). The southern block is a shallower westerly dipping horst that contains the culmination at the eastern edge. Here, the top Stø reaches up to around 2270 m below sea level. The other shallow area that can be observed on the top Stø interpretation at the southwestern edge of the structure is probably the result of an area of major acoustic masking and is not a real structural element. The main faults delineating the structure from the

north and south are E-W striking normal faults (faults 1, 2, 5, 6). Fault 6 has a NW-SE striking segment to the east, while there are a number of NE-SW oriented faults to the west (faults 3, 4, 7, 8). Faults 9 and 10 are N-S striking, the former intersects the southern block around the culmination.

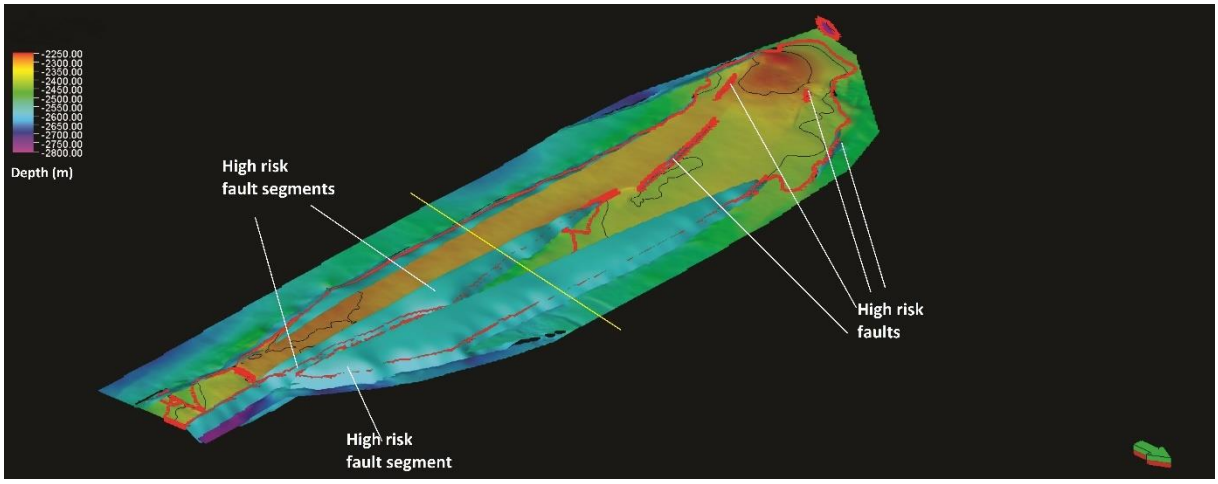

Figure 71. High risk faults at Snøhvit

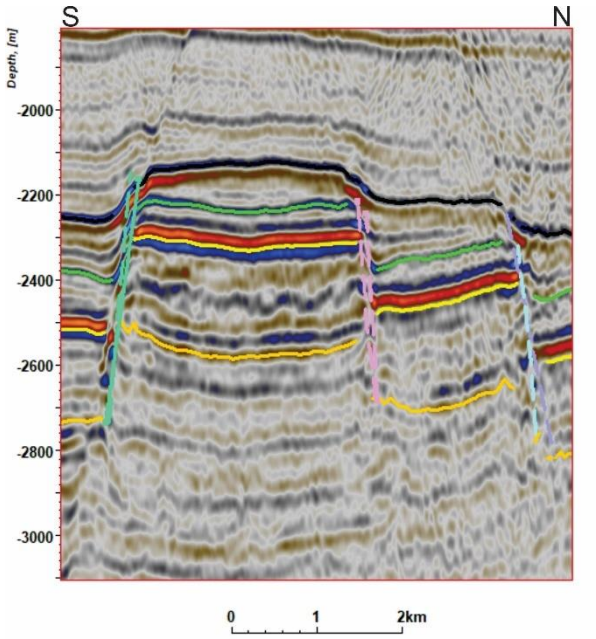

Figure 72. Cross section at Snøhvit shown by the yellow line on figure 71.

The risk areas here show much variation with strike and S_{hmax} orientation. In the case of an S_{hmax} oriented at 160 degrees fault 5 and 6 (especially the NW-SE striking parts) become high risk, with faults 4 and 7 also having P_{pcrit} of less than 2 MPa. The same is true faults 1 and 2 at the southern edge of the structure. Increasing S_{hmax} will concentrate the risk areas around the central and eastern parts of fault 5

and at the NW-SE segment of fault 6. This would be less favorable for HC preservation, since fault 5 at the eastern parts is close the culmination of the southern block. In the case of N-S S_{hmax} the NE-SW striking faults at the western edge of the field would pose a higher risk; as it has been concluded by previous studies (Linjordet & Skarpnes, 1992), . Of these faults, fault 7 has its shallowest intersection with the top reservoir exactly at GWC. Fault 8 with similar orientation intersects the top Stø at a shallower level, but it is difficult to establish where exactly, due to acoustic masking. Another risk area in this scenario is still the NW-SE segment of fault 6. Also faults 9 and 10 have a higher slip potential when S_{hmax} is increased to S_v, but their absolute significance seems low.

In summary, the Snøhvit structure would be classified as high risk based on fault slip tendency. This is due to the large variety of strikes that can be observed on faults in and around the structure. Fault 2 intersects the top reservoir around the culmination. This fault would only pose major risk around there in the SH160_Sh scenario. However, fault 5 and 6 have segments that seem to be consistently among the riskiest areas. These come close to the culmination of the trap at the eastern edge (Figure 71).

Snøhvit Nord

Snøhvit Nord is a heavily faulted horst just north of Snøhvit. The structure has two main culminations: in the southern part a horst wedging out to the east, delineated by faults 1 and 3; and in the northern delineated by faults 2 and 3. This latter culmination is situated at a fault relay ramp created by fault 2 and 3. The GWC also seems to be controlled by fault intersections at the western and southeastern edges of the structure (Figure 73).

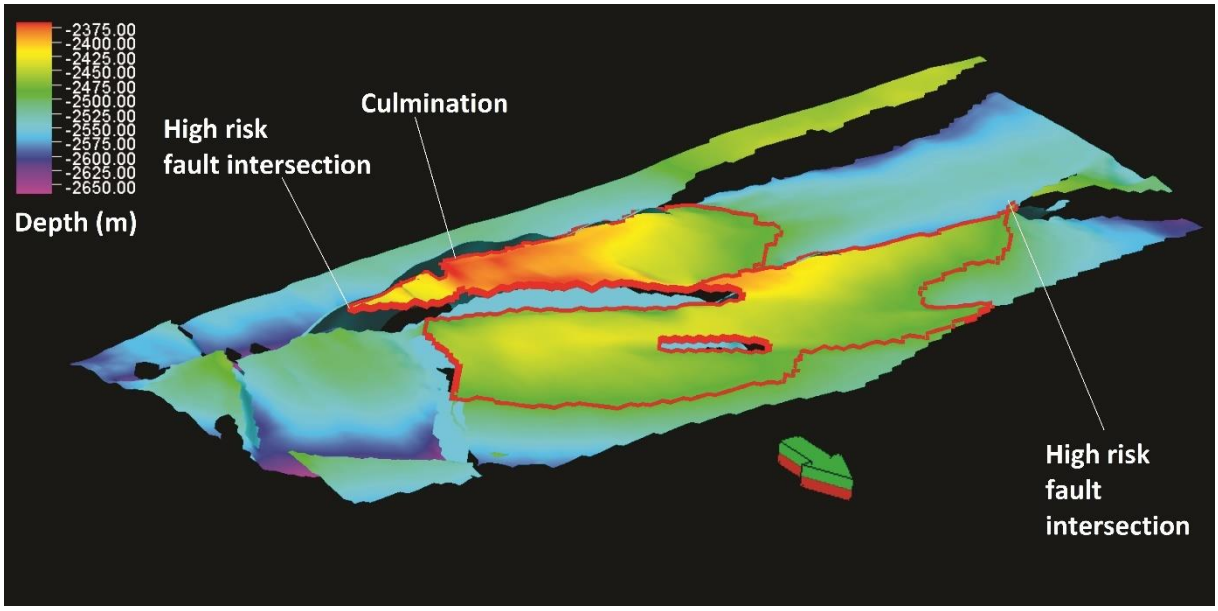

Figure 73. View of top Stø at Snøhvit Nord

At low S_{hmax}=S_{hmin} the only fault plane with considerable risk fault 1. With an increase of S_{hmax} in the SH160 scenario fault 3, while in SH180 scenario fault 3 and 5 stand out. These two faults also have an

intersection, which intersects the top reservoir around the GWC. The same thing can be said about the fault intersection at the western edge of the field (Figure 73).

Askeladd

The Askeladd structure lies at the western edge of a terrace separating the Hammerfest Basin from the deeper Tromsø Basin. The most obvious feature is the N-S trending normal fault delineating the structure from the west and creating a closure for the gently S-SE dipping top Stø. The structure can be dealt up into at least four smaller parts each with its own closure. From north to south these smaller blocks are separated by roughly E-W trending normal faults.

Based on the slip stability modeling it can be concluded that the Askeladd structure shows only moderate levels of risk when it comes to fault assisted leakage. Even in the S_{hmax}=S_{hmin} stress scenarios, where P_{pcrit} is generally the lowest; the fault planes only show moderate levels of critical pressure. It is obvious that fault 11 to the west and faults 1, 2, 9 and 10 have the biggest risk of failure depending on the different stress models; but even their critical pressures remain above 2 MPa. It is interesting to note that according to Christian; Hermanrud et al. (2014) Askeladd is yet another structure that is potentially filled to spill.

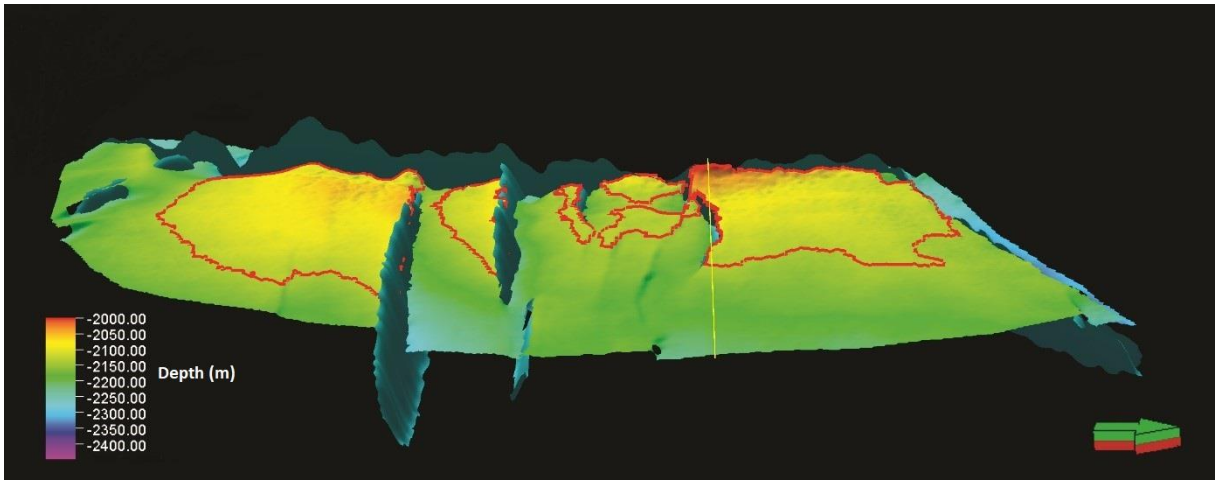

Figure 74. View of Askeladd

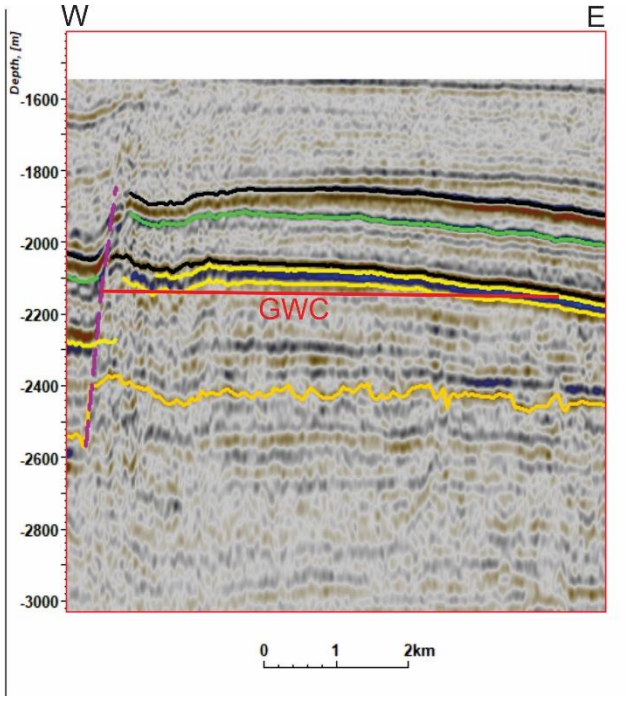

Figure 75. Cross section at Askeladd

Askeladd Gamma

Askeladd Gamma lies on the next terrace west from Askeladd. The top Stø here gently dips towards the east (Figure 76), southeast and the main closure is created by a large N-S trending normal fault to the west. Two E-W trending faults delineate the structure to the north and south. The main culmination of the structure can be found in the middle of the terrace, just east from the main fault in the form of an antiform, probably related to fault drag. On the interpretation the top Stø forms an east dipping monocline just before fault that seems to reach a shallower depth than the antiform. It is difficult to tell which of these is the real culmination of the structure, but the fact that the top reservoir has a closure

that is not in direct contact with any fault plane, would already reduce the exploration risk of this prospect.

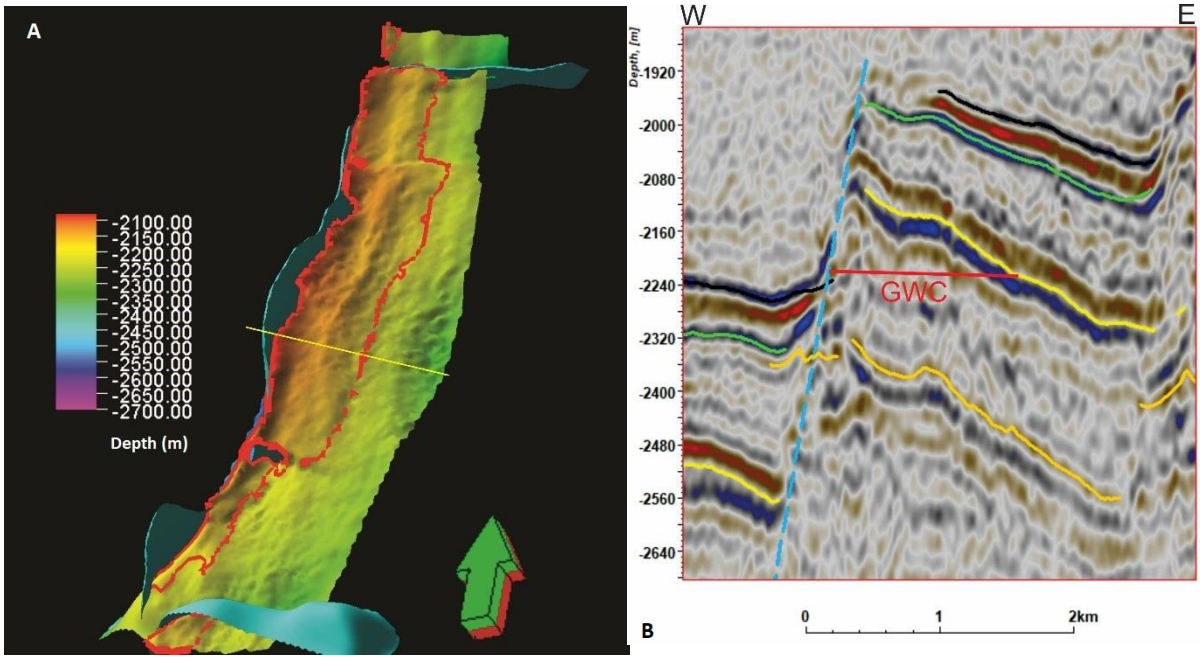

Figure 76. View of top Stø and Askeladd Gamma (A), cross section of Askeladd Gamma (B)

This is especially important, since the fault with the main leakage risk seems to be fault 2, the main fault creating the closure itself. And although the absolute critical pressures do not seem to reach below 2 MPa on the fault surface; it does seem like that fault and the anticline plays a major role in the level of GWC. This is based on the observation that the projection of the GWC on the top Stø interpretation seems to follow the axis of the antiform.

Askeladd Vest

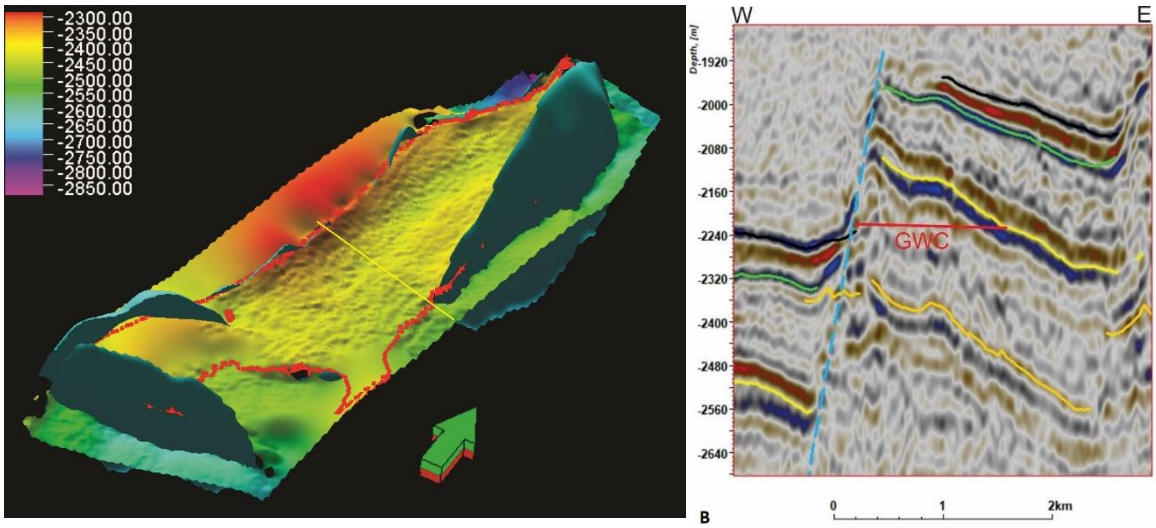

Figure 77. View of top Stø at Askeladd Vest (A), cross section of Askeladd Vest (B)

Askeladd Vest is the deepest structure sitting on the terraces towards the Tromsø Basin (Figure 77). The shallowest points on the structure can be found at the western and eastern edges of the field, right next to faults 2, 3, 4 and 6.

These are also the faults that seemed to be the most unstable in all of the stress scenarios. Faults 1 and 5 but also 7 remain relatively cold during all stress scenarios. As with the other Askeladd fields so far, the overall risk of fault failure and fault assisted leakage seem to be lower than that of the Snøhvit and Albatross structures.

Delta Vest

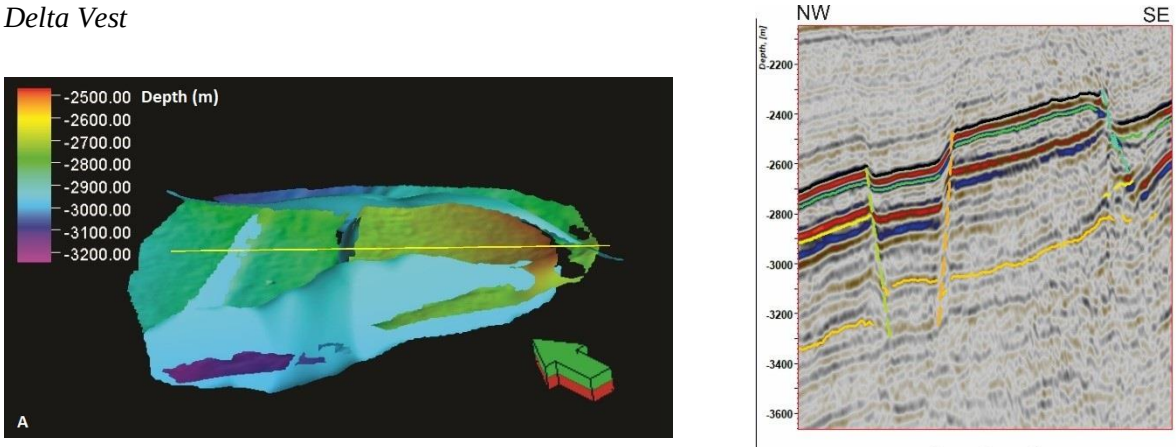

Figure 78. View of top Stø and faults at Delta Vest (A), cross section of Delta Vest (B)

The culmination of Delta Vest can be found in the southeasternmost block at the intersection of faults 1 and 2 (Figure 78). Faults 1 and 2 seem to be the fault planes involving the most risk in this structure. Since their intersection can be found updip and close to the culmination, it is obvious that this structure would be associated with a large exploration risk.

Askeladd Beta

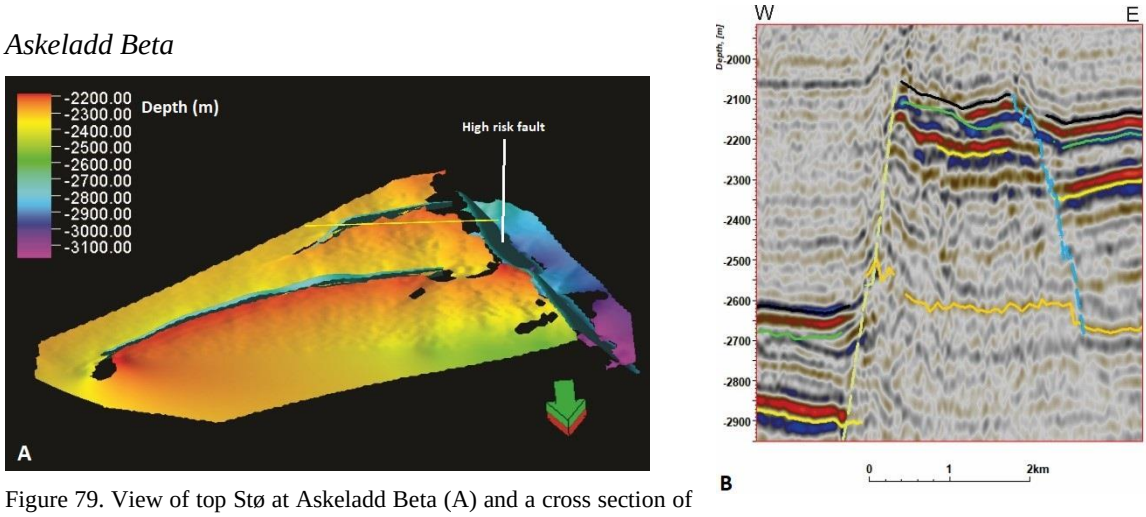

Figure 79. View of top Stø at Askeladd Beta (A) and a cross section of Askeladd Beta (B)

This structure has its culmination against fault 3 which is the main fault delineating the structure to the west. This fault is a part of the RLFC. The main strike in that fault complex changes from a N-S

dominating around the other Askeladd structures to a more NW-SE orientation around Askeladd Beta. This has made it more favorably oriented in the SH160 scenario, but its also the main risk on the structure when S_{hmax} is N-S oriented.

Edmundson et al. (2019) has conducted a study into possible leakage mechanisms covering Albatross, Snøhvit and the main Askeladd structures. The study investigated the theoretical hydrocarbon column heights in the traps in different controlling mechanisms; assuming a charge that is able to fill the traps. The different controlling mechanisms considered were capillary leakage through cap rock, capillary leakage through fault planes, hydrofracturing of cap rock and fault reactivation. The study concludes that fault reactivation is the one leakage process that best explains the underfilling of the structures; and with the help of throw-depth profiles along fault surfaces it also identified faults that were reactivated after charge and would pose the main risk. These faults would be fault 2 on Albatross south, 3 and 4 on Albatross, 1, 2 and 6 on Snøhvit and 1, 8, 9 and 11 on Askeladd.

7. Conclusions

- The Hammerfest Basin is a well explored, mature hydrocarbon basin located in the SE Barents Sea, offshore Norway. The basin contains a number of different petroleum plays with source rocks and reservoir rocks at several stratigraphic levels. The most well explored play is the one associated with the Middle Jurassic sandStønes of the Realgrunnen subgroup. It consists of fault bounded traps that were created by the Late Jurassic-Early Cretaceous Cimmerian rifting phase. The resulting low porosity shale formations such as Fuglen and Hekkingen form the seal for the Middle Jurassic plays; and while the latter is also a high quality source rock, it probably had minor role in charging these traps besides the Triassic sources of Klappmyss and Steinkobbe formations.

- The Snøhvit field complex can be found in the western part of the Hammerfest Basin; consisting of a number of structures that include Snøhvit, Snøhvit Nord, Albatross, Albatross Sør, Askeladd, Askeladd Gamma and Askeladd Vest. These structures have all presented the issues that pose as the biggest exploration risk in the area: underfilled and gas prone traps. With a number of dry structures also drilled in the area and hydrocarbon shows down to the spillpoints of the underfilled traps as well; it became obvious that the reason behind dry and underfilled traps is not insufficient hydrocarbon charge.

- A number of different mechanisms and processes have been named in various studies as the main reason behind spill and leakage from these traps. These inculde: differential tiliting of traps, gas exsolution and expansion realated to erosion and uplift, stress and pore pressure perturbations related to glacial erosion and cylic loading and unloading from glaciers, seal

breach via hydrofracturing and fault assisted leakage to name a few. These processes are often related and connected to each other as well.

- Evidence has been accumulating for the role of faults in vertical leakage in the area in the form of bright spots, amplitude anomalies around fault planes, and gas chimneys and pockmarks at fault tips. Establishing which fault planes are prone to leakage can be one of the main ways of risking prospects in the area. However the issue of fault permeability is extremely complex with many different variables such as fault gouge(?) ratio, fault juxtaposition, fault throw, degree of cementation, orientation relative to stress field etc. Hermanrud et al (2014) looked at the relative positions of fault-top reservoir intersections and the HWC in traps of the Snøhvit field complex. That study emphasized the importance of fault intersections in controlling the hydrocarbon column heights in these traps. There is however also evidence for the reactivation of some of the faults in the study area after filling of the traps. This has led to interpretations where reactivated faults formed the primary pathways for migration out of the traps. This resulted in studies investiagting the throw vs depth profiles of the fault planes to find out about the active phases of these faults.

- The approach used by this thesis to find fault planes prone for reactivation was the critically stressed fault theory. The method incorporates stress field models, the relative orientation of fault planes to the principal stresses and reservoir pore pressure to find the slip stabilities of fault planes. Slip stabilities give a delta pressure (referred to as Ppcrit), or critical pressure. This is the amount of pressure increase that is needed to cause slip on the fault surface, and make it a poterntial leakage pathway.

- After establishing the principal stress gradients for the two main stress models used in the study; the RFT pressure plots from the wildcat wells of the different structures were plotted on a pressure vs depth plot against hydrostatic pressure gradient, and the principal stress gradients. Failure gradients for cohesionless faults with a coefficient of friction of 0.6 were also calculated for the two stress models, by bringing the representative Mohr circles to a shear failure with the failure envelope. From these, retention capacities (RC) and critical pressures (Ppcrit) were calculated for close to the culmination of the traps. The results showed that for all of the traps in the study area the RC is much higher than Ppcrit. A high RC however does not necessairily mean that the traps are not in dynamic equlibrium since RC only accounts for one specific failure mechanism; that is hydrofracturing (tensile opening of cohesionless fractures oriented prependicular to minimum prinicpal stress) of the seal. Instead, based on the proximity of the RFT plots to the fault shear failure gradients on the

pressure vs depth plots; and the low Ppcrit values it is much more likely that these traps are in fact dynamic equlibrium that is controlled by fault reactivation.

- In the next step the critical pressures were plotted on the fault planes. These were done in different stress scenarios to account for the uncertainties in the stress models. Also, each of the input parameters at the different stress scenarios were calibrated for the water depth for each of the structures. High risk fault planes and fault segments were identified as the ones that consistently showed low critical pressures in the various stress scenarios.

- The results showed that in general the Askeladd structures have lower risk associated with them when it comes to fault assisted leakage. Structural factors (like an antiform downdip from the culmination of the trap like in the case of Askeladd Gamma) also play a factor in this; but the absolute slip stabilities of the faults on the Askeladd traps seems a bit higher than on the other structures to the east. The exception from this is Askeladd Beta which shows critical pressures below 2 MPa on the main fault at the SW corner of the trap around the culmination. This is also one of the dry structures. The other dry structure Delta Vest does not have anomalously low slip stabilities compared to the underfilled Askeladd structures; however two of its faults associated with the highest risk intersect each other at the top of the structure. Lying in the eastern part of the survey area, Albatross is the most underfilled structure; and with high risk faults around the highest points of the trap. Snøhvit and Snøhvit Nord also have high risk faults close to the culminations, with the latter field also having fault intersections around the GWC. While Albatross and the two Snøhvit structures show high risk of fault assisted leakage; the exception here is Albatross Sør. This trap has a fault to the west that shows low slip stabilities; however this fault does not intersect the top reservoir around the culmination. In fact; the highest point of intersection between this fault and the top reservoir coincides with the GWC in the trap.

- Uncertainties with the results mainly come from the stress models. Some of that uncertainty has been incorporated with the use of different stress scenarios, but local stress field perturbations are still a possibility. Having more reliable information on the stress field could improve the reliability of the results greatly. Also, there was no available data on the mechanical properties of the faults in this area. Cohesionless faults were used to model slip stabilities since the failure line for such a fault fit the reservoir pressures quite well. It is important to mention however, that it is highly unlikely that these fault surfaces would be cohesionless in reality as well. Since it seems like that dynamic controls are in fact affecting

the hydrocarbon column heights in the area, it could be beneficial to focus on collecting more reliable data on the stress field for future exploration efforts in the Barents Sea.

References

Berglund, L. T., Augustson, J., Farseth, R., Gjelberg, J., & Ramberg-Moe, H. (1986). The evolution of the Hammerfest Basin. *Habitat of Hydrocarbons on the Norwegian Continental Shelf*, 319-338.

Bird, K. J., Charpentier, R. R., Gautier, D. L., Houseknecht, D. W., Klett, T. R., Pitman, J. K., et al. (2008). Circum-Arctic resource appraisal; estimates of undiscovered oil and gas north of the Arctic Circle. *U.S. Geological Survey Fact Sheet*.

Brekke, H., & Riis, F. (1987). Tectonics and basin evolution of the Norwegian shelf between 62°N and 72°N. *Norsk Geologisk Tidsskrift, 67*, 295-321.

Chiaramonte, L., White, J., & Trainor-Guitton, W. (2015). Probabilistic geomechanical analysis of compartmentalization at the Snøhvit CO2 sequestration project. *J. Geophys. Res. Solid Earth, 120*, 1195-1209.

Chiaramonte, L., White, J. A., & Johnson, S. (2011). Preliminary geomechanical analysis of CO2 injection at Snøhvit, Norway. *45th US Rock Mechanics / Geomechanics Symposium, 2011*.

Doré, A. G. (1995). Barents Sea Geology, Petroleum Resources and Commercial Potential. *Arctic, 48*, 207-221.

Edmundson, I., Rotevatn, A., Davies, R., Yielding, G., & Broberg, K. (2019). Key controls on hydrocarbon retention and leakage from structural traps in the Hammerfest Basin, SW Barents Sea: implications for prospect analysis and risk assessment. *Preprint*.

Faleide, J. I., Gudlaugsson, V., & Gudlaugsson, S. T. (1993). Late Mesozoic-Cenozoic evolution of the south-western Barents Sea in a regional rift-shear tectonic setting. *Marine and Petroleum Geology, 10*, 186-214.

Finkbeiner, T., Zoback, M., & Flemings, P. (2001). Stress, Pore Pressure, and Dynamically Constrained Hydrocarbon Columns in the South Eugene Island 330 Field, Northern Gulf of Mexico. *AAPG Bulletin, 85*, 1007-1031.

Fristad, T., Groth, A., Yielding, G., & Freeman, B. (1997). Quantitative fault seal prediction: a case study from Oseberg Syd *Norwegian Petroleum Society Special Publications, 7*, 107-124.

Gaarenstroom, L., Tromp, R. A. J., De Jong, M. C., & Brandenburg, A. M. (1993). Overpressures in the Central North Sea: implications for trap integrity and drilling safety. *Petroleum Geology of Northwest Europe: Proceedings of the 4th Conference Geological Society, London, 2*, 1305-1313.

Gabrielsen, R. H. (1984). Long-lived fault zones and their influence on the tectonic development of the southwestern Barents Sea. *J. geol. Soc. London, 141*, 651-662.

Gabrielsen, R. H., Farseth, R. B., Jensen, L. N., Kalheim, J. E., & Riis, F. (1990). Strucutral Elements of the Norwegian Continental Shelf: Part 1: The Barents Sea Region. *NPD-Bulletin No. 6*.

Gartrell, A., Zhang, Y., Lisk, M., & Dewhurst, D. (2003). Enhanced hydrocarbon leakage at fault intersections: an example from the Timor Sea, Northwest Shelf, Australia. *Journal of Geochemical Exploration, 78-79*, 361-365.

Gernigon, L., Brönner, M., Roberts, D., Olesen, O., Nasuti, A., & Yamasaki, T. (2014). Crustal and basin evolution of the southwestern Barents Sea: From Caledonian orogeny to continental breakup. *Tectonics, 33*, 347-373.

Gölke, M., & Brudy, M. (1996). Orientation of crustal stresses in the North Sea and Barents Sea inferred from borehole breakouts. *Tectonophysics, 266*, 25-32.

Gudlaugsson, S. T., Faleide, J. I., Johansen, S. E., & Breivik, A. J. (1998). Late Palaeozoic structural development of the south-western Barents Sea. *Marine and Petroleum Geology, 15*, 73-102.

Harper, T. R., & Lundin, L. R. (1997). Fault seal analysis: reducing our dependence on empiricism *Norwegian Petroleum Society Special Publications, 7*, 149-165.

Henriksen, E., Bjornseth, H. M., Hals, T. K., Heide, T., Kiriyukhina, O. S., Klovjan, G. B., et al. (2011). Uplift and erosion of the greater Barents Sea: impact on prospectivity and petroleum systems. *Arctic Petroleum Geology, 35*, 271-281.

Hermanrud, C., Halkjelsvik, M., Kristiansen, K., Bernal, A., & Strömback, A. C. (2014). Petroleum column-height controls in the western Hammerfest Basin, Barents Sea. *Petroleum Geoscience, 20*, 227-240.

Hermanrud, C., Nordgard Bolas, H. M., & Teige, G. M. G. (2005). Seal Failure Related to Basin-scale Processes. *Evaluating fault and cap rock seals: AAPG Hedberg Series, 2*, 13-22.

Hillis, R. R., & Nelson, E. J. (2005a). *In situ stresses in the North Sea and their applications: petroleum geomechanics from exploration to development in: Petroleum Geology: North-West Europe and Global Perspectives.* Paper presented at the 6th Petroleum Geology Conference.

Hillis, R. R., & Nelson, E. J. (2005b). In situ stresses in the North Sea and their applications: petroleum geomechanics from exploration to development. *Petroleum Geology: North-West Europe and Global Perspectives—Proceedings of the 6th Petroleum Geology Conference*, 551-564.

Hoshino, K. (1972). Mechanical Properties of Japanese Tertiary Sedimentary Rocks under High Confining Pressures. *Geological Survey of Japan, 244*.

Hubbert, M., & Willis, D. (1957). Mechanics of hydraulic fracturing. *Transactions of Society of Petroleum Engineers of AIME, 210*, 153-163.

Jakobsson, K. H. (2018). A hiStøry of exploration offshore Norway: the Barents Sea from HiStøry of the European Oil and Gas Industry. 465.

Knipe, R. J., Fisher, Q. J., Jones, G., Clennel, M. R., Farmer, A. B., Harrison, A., et al. (1997). Fault seal analysis: successful methodologies, application and future directions *Norwegian Petroleum Society Special Publications, 7*, 15-40.

Linjordet, A., & Grung Olsen, R. (1992). The Jurassic Snøhvit Gas Field, Hammerfest Basin, Offshore Northern Norway. *AAPG Special Volumes*, 349-370.

Linjordet, A., & Skarpnes, O. (1992). Application of horizontal stress directions interpreted from borehole breakouts recorded by four-arm dipmeter tools. *Norwegian Petroleum Society Special Publications, 2*, 681-690.

Mildren, S. D., Hillis, R. R., Lyon, P. J., Meyer, J. J., Dewhurst, D., & Boult, P. (2005). A New Technique for Geomechanical Assessment of the Risk of Reactivation-related Breach of Fault Seals. *AAPG Hedberg Series, 2*, 73-85.

Mohammedyasin, S. M. (2017). Two-Dimensional Seismic Interpretation and Petroleum System Modelling in the Hammerfest Basin, SW Barents Sea. *Journal of Geology & Geophysics, 6*.

Mohammedyasin, S. M., Lippard, S. J., Omosanya, K. O., Johansen, S. E., & Harishidayat, D. (2016). Deep-seated faults and hydrocarbon leakage in the Snovhit Gas Field, Hammerfest Basin, Southwestern Barents Sea. *Marine and Petroleum Geology, 77*, 160-178.

Morris, A., Ferrill, D. A., & Henderson, D. B. (1996). Slip tendency analysis and fault reactivation. *Geology, 23*, 275-278.

Nordgard Bolas, H. M., & Hermanrud, C. (2002). Rock stress in sedimentary basins-implications for trap integrity. *Norwegian Petroleum Society Special Publications, 11*, 17-35.

Nordgard Bolas, H. M., & Hermanrud, C. (2003). Hydrocarbon leakage processes and trap retention capacities offshore Norway. *Petroleum Geoscience, 9*, 321-332.

Nordgard Bolas, H. M., Hermanrud, C., & Teige, G. M. G. (2005). The Influence of Stress Regimes on Hydrocarbon Leakage. *Evaluating fault and cap rock seals: AAPG Hedberg Series, 2*, 109-123.

NPD. (2018). *Resource report 2018*. Retrieved from Stavanger:

Ohm, S. E., Karlsen, D. A., & Austin, T. J. F. (2008). Geochemically driven exploration models in uplifted areas: Examples from the Norwegian Barents Sea. *AAPG Bulletin, 92*.

Ostanin, I., Anka, Z., & di Primio, R. (2017). Role of Faults in Hydrocarbon Leakage in the Hammerfest Basin, SW Barents Sea: Insights from Seismic Data and Numerical Modelling. *Geosciences, 7*.

Ostanin, I., Anka, Z., di Primio, R., & Bernal, A. (2012). Identification of a large Upper Cretaceous polygonal fault network in the Hammerfest basin: Implications on the reactivation of regional faulting and gas leakage dynamics, SW Barents Sea. *Marine Geology, 332-334*, 109-125.

Raaen, A. M., Horsrud, P., Kjorholt, H., & Okland, D. (2006). Improved routine estimation of the minimum horizontal stress component from extended leak-off tests. *International Journal of Rock Mechanics and Mining Sciences, 43*, 37-48.

Rodrigues Duran, E., di Primio, R., Anka, Z., Støddart, D., & Horsfield, B. (2013). '3D basin modelling of the Hammerfest Basin (southwestern Barents Sea): A quantitative assessment of petroleum generation, migration and leakage'. *Marine and Petroleum Geology, 45*, 281-303.

Selley, R., & Sonnenberg, S. (2015). *Elements of Petroleum Geology, Third Edition*: Elsevier.

Sibson, R. (1996). Structural permeability of fluid-driven fault-fracture meshes. *Journal of Structural Geology, 18*, 1031-1042.

Sibson, R. (2000). Fluid involvment in normal faulting. *Journal of Geodynamics, 29*, 469-499.

Smelror, M., Petrov, O., Birger Larssen, G., & Werner, S. (Eds.). (2009). *Geological HiStøry of the Barents Sea*. Trondheim: Geological Survey of Norway.

Sund, T., Skarpnes, O., Nordgard Jensen, L., & Larsen, L. M. (1986). *Tectonic Development and Hydrocarbon Potential Offshore Troms, Northern Norway in Future Petroleum Provinces of the World*.

Sverdrup, E., & Bjorlykke, K. (1997). Fault properties and the development of cemented fault zones in sedimentary basins: field examples and predictive models *Norwegian Petroleum Society Special Publications, 7*, 91-106.

Tasianas, A., Martens, I., Bünz, S., & Meinert, J. (2016). Mechanisms initiating fluid migration at Snøhvit and Albatross fields, Barents Sea. *Arktos, 26*.

Vaddakepuliyambatta, S., Bünz, S., Meinert, J., & Chand, S. (2013). Distribution of subsurface fluid-flow systems in the SW Barents Sea. *Marine and Petroleum Geology, 43*, 208-221.

Vorren, T. O., Richardsen, G., Knutsen, S.-M., & Henriksen, E. (1991). Cenozoic erosion and sedimentation in the western Barents Sea. *Marine and Petroleum Geology, 8*, 317-340.

Welbon, A. I., Beach, A., Brockbank, P. J., Fjeld, O., Knott, S. D., Pedersen, D., & Thomas, S. (1997). Fault seal analysis in hydrocarbon exploration and appraisal- examples from offshore mid-Norway. *Norwegian Petroleum Society Special Publications, 7*, 125-138.

Wiprut, D., & Zoback, M. D. (2002). Fault reactivation, leakage potential, and hydrocarbon column heights in the northern North Sea. *Norwegian Petroleum Society Special Publications, 11*, 203-219.

Worsley, D. (2008). The post-Caledonian development of Svalbard andthe western Barents Sea. *Polar Research, 27*, 298-317.

Zoback, M. D. (2007). *Reservoir geomechanics*: Cambridge University Press.

Zoback, M. L., Zoback, M. D., Adams, J., Assumpcao, M., Bell, S., Bergman, E. A., et al. (1989). Global patterns of tectonic stress. *Nature, 341*, 291-298.